ROLES OF PANX1 CHANNELS IN LARVAL ZEBRAFISH: FROM GENES TO VISUAL-MOTOR BEHAVIOR

NICKIE SAFARIAN

A DISSERTATION SUBMITTED TO

THE FACULTY OF GRADUATE STUDIES

IN PARTIAL FULFILLMENT OF THE REQUIREMENTS FOR THE DEGREE OF

DOCTOR OF PHILOSOPHY

GRADUATE PROGRAM IN BIOLOGY

YORK UNIVERSITY

TORONTO, ONTARIO

APRIL 2021

ABSTRACT

Pannexin1 (Panx1) forms ATP-permeable single membrane channels that play a role in the (patho)physiology of the nervous system. Two independent copies of *panx1* (i.e., *panx1a* and *panx1b*) have been identified in the zebrafish. To evaluate each *panx1* copy's role in the visual system, we developed zebrafish *panx1* knockout models (i.e., *panx1a*$^{-/-}$, *panx1b*$^{-/-}$, and *panx1a*$^{-/-}$/*panx1b*$^{-/-}$ double knockout; DKO) using TALEN technology. The RNA-seq analysis of 6 days post-fertilization larvae was confirmed by Real-Time PCR and paired with testing visual-motor behaviors. Results demonstrated that both Panx1s contribute to the retinal OFF pathways function, though through different signaling pathways. Panx1a proteins specifically affect the expression of gene classes representing the development of the visual system and visual processing. The molecular and behavioral findings also provide for the first-time evidence that the ablation of *panx1a* alters dopaminergic signaling and that adenosine signaling links Panx1a proteins to the dopaminergic pathway. Indeed, altered visuomotor behavior in the absence of functional *panx1a* was simulated through D1/D2 receptor agonist treatment, and rescued applying either D2 receptor antagonist, haloperidol, or adenosine receptor agonist, adenosine. The Panx1b protein emerged as a modulator of the circadian clock system; thereby, affecting diverse biological processes from metabolic pathways to cognition. In terms of vision, loss of *panx1b* disrupted the retinal response to the abrupt loss of illumination and decreased visual acuity in the dark. Also, it led to cognitive dysfunction, anxiety-related behavior, and difficulty forming visual memory. Interestingly, loss of both *panx1* copies in a double knockout resulted in specific transcriptome changes in which biological processes related to the circadian clock were regulated opposite to the changes observed in *panx1b*$^{-/-}$ larvae. However, these changes did not translate into morphological and behavioral defects in DKO larvae. We concluded that *panx1a* and *panx1b* functions are relevant to the retinal OFF-pathways, which support visual-motor functions underlying complex behaviors of freely swimming fish.

DEDICATION

I would like to dedicate this dissertation to my mother and father, for their undying love and encouragement to fulfill my dreams.

ACKNOWLEDGEMENTS

The intellectual journey I have taken from the infancy of my doctoral studies to the completion of this dissertation was not accomplished on my lonesome. This work could not have been completed without the guide of innumerable supporters to whom I offer sincere appreciation.

I am utterly indebted to my supervisor, Dr. Georg Zoidl, for giving me the opportunity to study and do research under his guidance. Over the years, his dynamism, vision, sincerity, and motivation have deeply inspired me. Thank you, Dr. Zoidl, for dedicating your time and energy to make me a stronger intellectual and support me to sharpen my thinking, expand my skills, and succeed throughout this research. I will forever admire you for your determination in expanding your knowledge and the knowledge of your students and for your friendship, empathy, and sense of humor.

I would also like to thank my supervisory committee (past and present): Dr. Thilo Womelsdorf, Dr. Logan Donaldson, and Dr. Joseph De-Souza for serving on my advisory committee and for supporting my intellectual development throughout my doctoral studies. Their advice, critiques, and suggestions were invaluable in bringing the project to higher levels.

My sincere thanks also go to Dr. Xiao-Yan Wen (Zebrafish Centre for Advanced Drug Discovery, St. Michael's Hospital, Toronto, ON) for conducting the *panx1b* TALENS' microinjection experiment and training me on this technique.

A most gracious thank you is owed to Christiane Zoidl for sharing her knowledge and technical expertise. My words of thanks will never be truly sufficient to express to you my deepest gratitude for your time and support in helping to complete the story of my work.

To the talented group of scientists in the Zoidl lab, I thank you for the stimulating discussions, friendship, support, and all the fun we have had together.

I would like to express my sincere gratitude to my dearest friend Daantje and her father for their insights as well as happy distractions to rest my mind outside of my research. Thank you for believing in me, even when I didn't believe in myself.

Last but not least, I have to thank my family.

Dad, you set me down the science path before I can even remember and enlightened my journey with your wise counsel. How could I have got through any of this without you? I sincerely thank you for all you have done for me.

Mom, thank you for always taking good care of me and for your sympathetic ear. There are not enough words in me to express how grateful I am for your infinite love and support. You have been the most encouraging and supportive influence in my life.

My sisters and brothers, thank you for all the prayers and support. You have always been there for me, and I will always be there for you. I love you all and forever will.

Daniel, my one and only, you served as my inspiration to pursue this undertaking. Your daily encouragement gave me the strength to carry on to the next day despite innumerable challenges and frustrations. Thank you for being my cheerleader. This achievement is a small part of the woman you have made me be.

TABLE OF CONTENTS

LIST OF TABLES

LIST OF FIGURES

LIST OF SUPPLEMENTARY FIGURES

LIST OF SUPPLEMENTARY TABLES

LIST OF ABBREVIATIONS

Symbol	***Definition***
AC	Amacrine cell
AMPAR	α-amino-3-hydroxy-5-methyl-4-isoxazolepropionic acid receptor
AR	Adenosine receptor
ATP	adenosine-5'-triphosphate
BC	Bipolar cell
BSA	Bovine serum albumin
$Ca2^{+}$	Calcium ion
cAMP	3'-5'-cyclic adenosine monophosphate
CL	Cytoplasmic loop
CT	Carboxy terminus
Cl^{-}	Chloride ion
CNS	Central nervous sytem
Cx	Connexin
DMSO	Dimethyl sulfoxide
DR	Dopamine receptor
EGFP	Enhanced green fluorescent protein
EL	Extracellular loop
ER	Endoplasmic reticulum
ERG	Electroretinogram
EtBr	Ethidium bromide
GABA	Gama amino butyric acid
HC	Horizontal cell
IHC	Immunohistochemistry
INL	Inner nuclear layer
Inx	Innexin
IP3	Inositol trisphosphate
IPL	Inner plexiform layer
ipRGC	Intrinsically photosensitive retinal ganglion cell
K^{+}	Potassium ion
kDa	Kilodaltons
KO	Knockout
mL	Mililitre
mM	Millimolar
N2a	Neuroblastoma 2a or Neuro2a

Na^+	Sodium ion
NGS	Normal goat serum
nl	Nanolitre
NMDAR	N-methyl-D-aspartate receptor
ON	Over night
ONL	Outer nuclear layer
OPL	Outer plexiform layer
P2XR	P2X receptor
P2YR	P2Y receptor
Panx	Pannexin
PBS	Phosphate buffered saline
PCR	Polymerase chain reaction
PE	Pigmented epithelium
pg	Picogram
PKA	Protein kinase A or cAMP-dependent protein kinase
PKC	Protein kinase C
PR	Photoreceptor
RGC	Retinal ganglion cell
ROI	Region of interest
s	Second
SEM	Standard error of the mean
TALEN	Transcription activator-like effector technology
TL	Topfel longfin
WT	Wild-type
μL	Microlitre
μM	Micromolar
μm	Micrometer

Chapter 1. Introduction

1.1. Background

Life has passed through four major phases, or eras, during evolution (Bonner, 2019). The first era started with the emergence of eukaryotic single cells that multiply asexually. The second era was accompanied by the invention of sexual reproduction, meiosis, which allows for more diverse offspring. The third era began with the emergence of multicellularity, an easy way to become larger and dominant. In the fourth era, a radical innovation, the nervous system, changed everything again, and this only occurred in animals (Bonner, 2013a, 2013b). Animals, as motile multicellular organisms, needed a coordinated fast response system between their several sensing and mobility-generating organs in order to forage rapidly, respond to danger and survive in the environment. For example, transduction of the sensing of a predator in the environment through the visual system allowed for a rapid avoidance motor response (Mattson and Bruce-Keller, 1999; Fields, Bischof and Levin, 2020). This stimulus-response coordination relies on tight communications among neuronal communities (Potolicchio et al., 2012; Marijuán, del Moral and Navarro, 2013). With evolution, such communication mechanisms have diversified to become integrated into a complex regulatory network, whereby the activity level of individual neuronal cells can be sensed and regulated according to the immediate condition (Potolicchio et al., 2012). An evolutionary-conserved feature of this regulatory network is the expression of membrane channels made of Pannexins, a group of transmembrane proteins that mediate intracellular communication in the nervous system (Panchin, 2005).

Developmental, structural, and functional studies of Pannexins provide a comprehensive framework of how a common intra-cellular mechanism can subserve unique physiological functions in the nervous system. An even more daunting task is to uncover how Pannexins signaling pathways might be altered, which could potentially lead to more effective treatment strategies for associated neuro-pathologies (Yeung, Patil and Jackson, 2020). Primarily, the Pannexin research relied on fairly unspecific pharmacological tools and siRNAs to silence pannexins. Recently, targeted deletions of rodent and fish pannexin genes have made it possible to re-evaluate and explore their (patho)physiological functions in vivo (Bargiotas et al., 2012). This thesis investigated the role of Pannexin1 in the zebrafish visual system. Generating a knockout zebrafish model allowed for unraveling the net of the Pannexin1 signalome, which is a key for understanding the depth and breadth of its tissue-specific functions and is also critically important for Pannexin1-based drug development.

1.2. Neuronal communication in the nervous system

The central nervous system (CNS) is composed of a heterogeneous population of cells that can be classified into three distinct groups, namely neuronal, glial and vascular cells (Decrock et al., 2015). Dynamic communication and tight relationships amongst these cellular groups are essential for proper development and normal functioning of the CNS, allowing integration and processing of information originating from inside or outside the body as well as responding accordingly to situations (Decrock et al., 2015). The integration of neuron-glial-vascular cells into functional units occurs via two main mechanisms: direct cell-to-cell communication and indirect autocrine/paracrine

communication (Hawkins and Davis, 2005; De Bock et al., 2014; Decrock et al., 2015). While direct intercellular interactions are facilitated through gap junction channels made of connexin (Cx) proteins, paracrine communication through extracellular compartments is mediated in part via pannexin (Panx) membrane channels. Over the last decades, extensive studies have revealed multiple aspects of Cxs channels' contribution to the neuro-glial-vascular communication and, therefore, to CNS physiology and pathology (Decrock et al., 2015). However, pannexins are rather newcomers to the field. Below, a summary of the pannexin protein family will first be given. Then, their multifaceted role in paracrine signaling in both physiological and pathological conditions in the CNS will be summarized.

1.3. Pannexin

Pannexin (Panx) is a family of three integral membrane glycoproteins (i.e., Panx1, Panx2, and Panx3) that Panchin and colleagues identified as vertebrate gene sequences that bear homology to the invertebrate innexin (Inx) gap junction proteins (Panchina et al., 2000). While no sequence homology exists between pannexins and the vertebrate gap junction proteins, connexins, they share topological commonalities (Boassa et al., 2007; Penuela et al., 2007). Individual Panxs (***Figure 1.1***) have four α-helical transmembrane (TM) domains, two extracellular loops (ECL), a single intracellular loop (ICL), and cytoplasmic N- and C-termini (Baranova et al., 2004; Boassa et al., 2007; Yen and Saier, 2007). Panx channels are formed by the oligomerization of these individual Panx subunits.

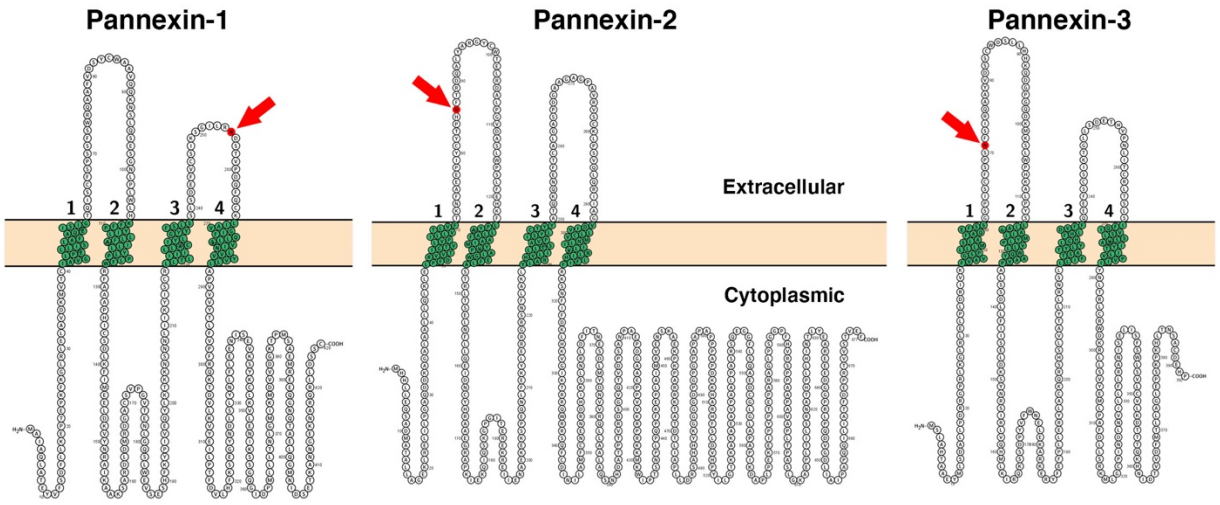

Figure 1.1. Transmembrane topology of pannexin family members. *Panx1 (426), Panx2 (677), and Panx3 (392) of varying amino acid lengths are tetra-spanning integral membrane proteins with N-glycosylation consensus sites (depicted in red) at amino acid 254 (Panx1), 86 (Panx2), and 71 (Panx3). Arrows point to N-glycosylation sites, and numbers indicate the position of transmembrane domains. Panx1 proteins oligomerize to form single-membrane channels, connecting cytoplasmic space into the extracellular milieu. The predicted sequence features of three Panx proteins were visualized using the Protter open-source tool (http://wlab.ethz.ch/protter/start/). (Created by N.S.).*

Although pannexins were initially considered to represent a redundant system to the connexins (Bruzzone et al., 2003; Fushiki et al., 2010), it is now widely accepted that gap junction formation by pannexins is unlikely for several reasons, reviewed in (Sosinsky et al., 2011). Instead of intercellular channels that span the two plasma membranes, pannexins primarily assemble to form unopposed single-membrane channels that expose intracellular space into the extracellular milieu. Panx channels allow the passage of different ions and small molecules in many cell types (Ambrosi et al., 2010). The various modes of activation and mechanisms regulating Panx channels' permeability to different ions and small molecules have been extensively studied and reviewed elsewhere (Penuela, Simek and Thompson, 2014; Boyce et al., 2018). Since Panx1 is the most-studied and the best-characterized family member and the focus of this research, it will be reviewed in further detail in the following sections.

1.4. Pannexin1 overview

1.4.1. Discovery

Using PCR with degenerated primers, Panchin et al. cloned sequences homologous to innexins from mollusk central nervous system (CNS) and flatworm whole-animal cDNA (Panchina et al., 2000). Then, they searched the GeneBank database for homologous sequences using BLAST algorithm tools and revealed similarities to two human proteins: MRS1 (GeneBank accession number AF093239) and MRS1-related protein (Panchina et al., 2000). Given the ubiquitous expression of the innexin-like proteins in the animal kingdom, Panchin proposed a new name, “pannexins” (from the Latin pan meaning ‘complete’ and nexus meaning ‘connection’) for these proteins. However, this term has since been retained for only the vertebrate species. Later, MRS1 and MRS1-related protein were renamed as Panx1 and Panx2, respectively. The third family member, Panx3, was also detected in the human genome soon after (Baranova et al., 2004).

In addition to human, the expression of all three pannexins has now been confirmed in mice, rats, dogs, cows, zebrafish and pufferfish (Yen and Saier, 2007). Experimentation in this thesis have been conducted on the zebrafish *panx1* genes.

In the zebrafish, two independent ohnologues of *panx1* (i.e., *panx1a* and *panx1b*) have been detected (Bond et al., 2012). The extra copy of the *panx1* gene is most likely resulted from the third whole-genome duplication (R3 WGD) event (Bond et al., 2012) occurring between 320 and 350 MYA (Jatllon et al., 2004). Gene duplications occur through 4 major molecular mechanisms: 1) unequal crossing-over (UCO), 2) retrotransposition, 3) duplicative (DNA) transposition, and 4) polyploidization (Magadum et al., 2013). It is

unlikely that the duplication was the result of an UCO event because it produces tandem repeated sequences linked as neighbors on a chromosome (Zhang, 2003; Hahn, 2009), and the two *panx1* genes are located on separate chromosomes. Retrotransposed duplicates result from the reverse transcription of mRNA into cDNA that are then inserted into a new position in the genome. Because they come from fully processed mRNAs, they lack introns and regulatory sequences of a gene and, consequently, are much less likely to be expressed after duplication (Brosius, 1991). The nearly identical architecture between the two *panx1s* makes them unlikely to be generated by a retrotransposition event. If a duplicative (DNA) transposition had caused the current localization of the two *panx1* genes, the spontaneous excision of either one or two extra *panx1* paralogs from the genome was expected (Feschotte and Pritham, 2007). The fourth major mechanism of duplicate gene formation is polyploidization. Although Whole-genome duplications result in new gene copies of every gene in a genome, only 10–30% of all genes are maintained in the genome for very long (Hahn, 2009). In fact, chromosomal neighborhoods of the two zebrafish *panx1* genes contain compelling evidence in favor of the R3 WGD causing this duplication. First, large syntenic regions (which preserve a similar order and orientation of gene blocks in the same relative positions in the genome) between the duplicated chromosomes have been detected. The *panx1a* gene on zebrafish chromosome 15 (Dre15) is flanked by the same set of genes observed on mouse chromosome 9 (Mmu9). Second, a gene interleaving pattern between the duplicated chromosomes relative to the homologous chromosome from a related species that did not undergo WGD is evident. A block of genes adjacent to the

panx1b gene on zebrafish chromosome 5 (Dre5) is many megabases away on both Mmu9 and Dre15; ***Figure 1.2*** (Bond et al., 2012).

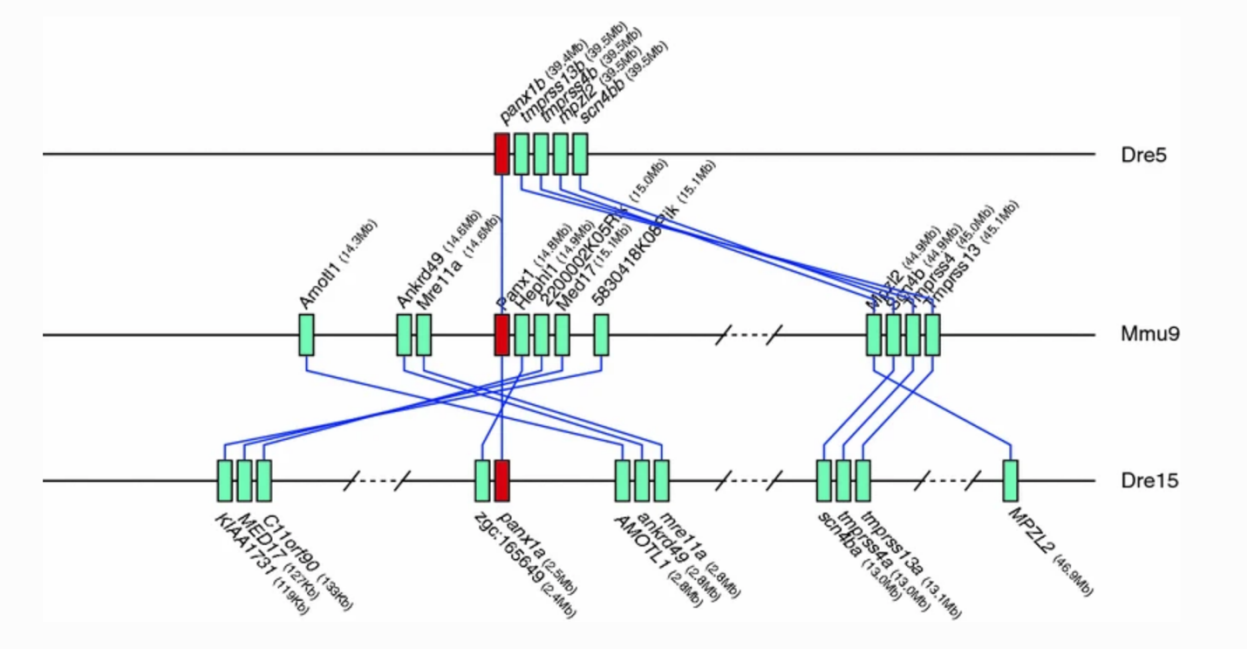

Figure 1.2. Syntenic relationship between zebrafish and mouse chromosomal regions containing panx1 genes. *Solid boxes represent individual genes (panx1 in red, others in green color). Blue lines connect orthologs together. The image is adapted from (Bond et al., 20).*

1.4.2. Structural properties and oligomerization

The main body of research conducted on the Panx1 channels has used frog, murine, or human Panx1 proteins. Herein, we review those papers, and wherever available, the information on the zebrafish Panx1s will be addressed as well.

Initially, structural analyses of Panx1 using bioinformatic tools like TMpred and TopPred programs assigned the amino-acid sequences comprising cytoplasmic and transmembrane domains (Penuela et al., 2007; Spagnol, Sorgen and Spray, 2014). Later, site-directed mutagenesis (Penuela et al., 2008), immunostainings using antibodies against extracellular epitopes (Boyce et al., 2015), and other biochemical assays like

circular dichroism (CD) and NMR (Spagnol, Sorgen and Spray, 2014) confirmed the predicted topologies. Zebrafish Panx1a (411 amino acids, ~46.9 kDa) and Panx1b (422 amino acids, ~47.8 kDa), with an average 55.0 ±6.9 % sequence identity and 67.6 ±7.3 % similarity, share the same predicted membrane topology with all known Panx1 proteins. Panx1 channels are formed by the oligomerization of individual Panx1 proteins (Zoidl *et al.*, 2008; Kurtenbach *et al.*, 2013).

Recently, the Panx1 channel (***Fig 1.3***) was shown to have a unique oligomerization stoichiometry amongst eukaryotic channels, with seven subunits arranged around a large central pore (Deng *et al.*, 2020; Michalski, Johanna L Syrjanen, *et al.*, 2020; Qu *et al.*, 2020; Ruan *et al.*, 2020). This contradicts the previous studies that suggested the Panx1 channel would be hexameric (Boassa et al., 2007; Ambrosi et al., 2010). The tight interactions between subunits establish the heptameric assembly of the channel in which several features resemble that of other large-pore forming channels, including connexin and innexins. For example, the transmembrane (TM) alpha-helices of Panx1, which frame the channels exterior wall, are bundled in a way that the overall helix lengths, angles, and positions strongly resemble that observed in connexins. Also, some features in the Panx1 ECL1 and ECL2 structures, like the two disulfide bonds (Cys66 with Cys267, Cys84 with Cys248) which join the ECL1 and ECL2 together and several ß-strands, are conserved among all large-pore forming channels. The ECL1 also contains an alpha helix that stretches towards the central pore and forms a rigid extracellular entrance ring (Michalski, Johanna L. Syrjanen, *et al.*, 2020; Ruan *et al.*, 2020). The small radius of this constriction site, 4.4 Å, which is about the size of an ATP molecule, suggests that it acts as the main

size-exclusion filter stopping larger molecules from entering the pore (Bao, Locovei and Dahl, 2004; Ma et al., 2012). Unlike the TMs and ECLs, the ICL and C-terminal domain (CTD) show unique structures. Together they assemble into a bundle of helices that contact with the N-terminus. The N-terminal domain lines the interior wall of the Panx1 channel and form an intracellular constriction site, which plays a role in the channel permeability and ion selectivity property (Michalski, Johanna L Syrjanen, *et al.*, 2020; Ruan *et al.*, 2020). Under normal physiological conditions, the CTD blocks the intracellular entrance of the main pore. During apoptosis, the CTD is cleaved by caspase-7, which removes the blockage and allows ATP release through the main pore. Both extracellular and intracellular entrances are positively charged, making the pore favorable for negatively charged cargos like chloride and ATP (Ma *et al.*, 2012; Ruan *et al.*, 2020).

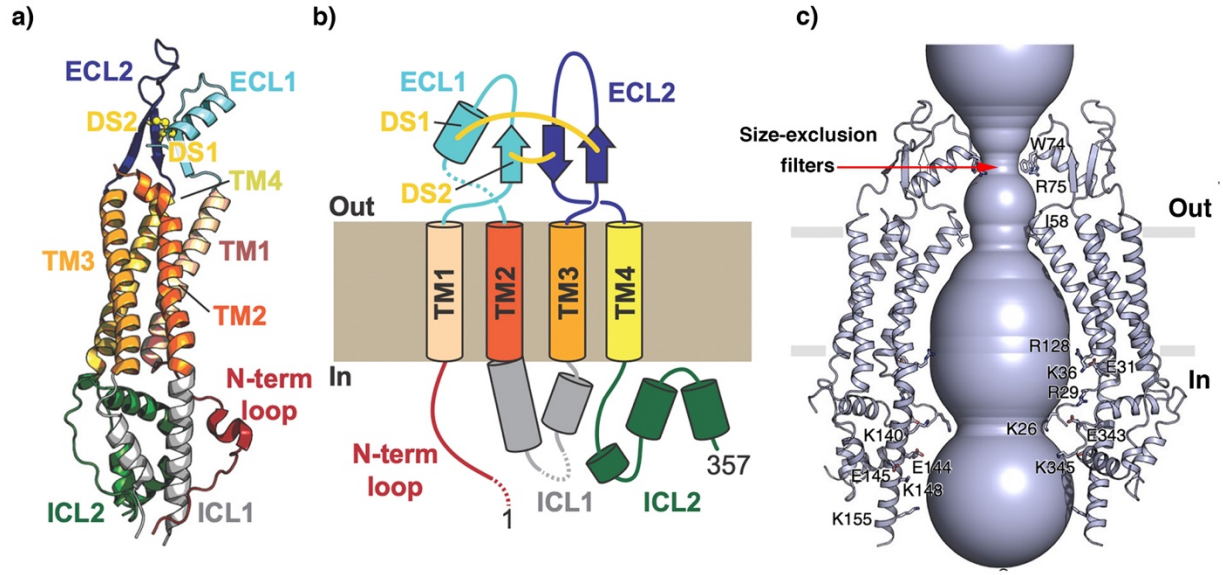

Figure 1.3. Structure of Panx1 channel. *a) Structure of the frog's Panx1 (frPanx1). The domains' colors are in accordance to the cartoon scheme presented in (b). b) Each individual Panx1 protein have four α-helical transmembrane (TM1-4) domains, two extracellular loops (ECL1-2), a single intracellular loop (ICL1), and cytoplasmic N- and C-termini. ICL2 represents the c-terminal domain. c) The pore of PANX1 channel. Selected residues lining the pore are highlighted. The red arrows shows the putative extracellular size-exclusion filter composed of a ring of seven tryptophan amino acids (W74). The seven W74 form a cation-π interaction with R75 from an adjacent subunit which contribute to the anion selectivity of the channel. Parts a and b are adopted from Michalski et al., 2020 and part c is taken from Deng et al., 2020.*

1.4.3. Cell and tissue distribution

Expression of Panx1 transcripts and protein has been extensively studied in various human and murine tissues (Penuela and Laird, 2012). Using in situ hybridization, northern blotting, qPCR, western blots, and immunohistochemistry (IHC), differential levels of Panx1 transcripts were detected in the nervous system, heart, lung, liver, spleen, ovary, placenta, testis, skeletal muscle, and skin (Bruzzone et al., 2003; Penuela, Gehi and Laird, 2013; Cheung, Chever and Rouach, 2014). Notably, the strongest signal for Panx1 mRNA and protein was detected in the murine CNS (Baranova et al., 2004; Penuela et al., 2007). Upon closer inspection within the CNS of rats, neurons and glial cells of different regions such as the cortex, hippocampus, pyramidal cells, amygdala, substantia nigra, thalamus, cerebellum, and spinal cord, as well as sensory systems like the retina, cochlea, and olfactory bulb have shown high Panx1 expression levels (Bruzzone et al., 2003; Weickert et al., 2005; Dvoriantchikova et al., 2006; Zappalà et al., 2006; Boassa et al., 2007).

In the zebrafish, the expression profile of *panx1a* and *panx1b* are distinct. The distribution of *panx1a* follows the ubiquitous expression pattern characteristic of mammalian *panx1* (Zoidl et al. 2008; Prochnow et al. 2009; Bond et al. 2012). On the other hand, the most prominent expression of *panx1b* has been detected in the brain and eyes, while in the other tissues like the heart, kidneys, spleen, skin, and muscles, it's been relatively lower (Bond et al., 2012). In a separate study, Kurtenbach et al. analyzed the relative *panx1s* mRNA levels in seven divisions (i.e., the retina, tectum opticum, tegmentum, brain stem, cerebellum, spinal cord, olfactory bulb) of the adult zebrafish nervous system. They

reported a robust expression of *panx1b* transcripts in the cerebellum, tectum opticum, and spinal cord; whereas, the expression of *panx1a* was lower and less variable in the analyzed CNS tissues (Kurtenbach et al., 2013). In the zebrafish retina, the two *Panx1* proteins have been localized to distinct layers. The *Panx1a* puncta have been localized to the outer plexiform layer (OPL)) in a band-like pattern, representing horizontal cells (N. Prochnow et al., 2009; Kurtenbach et al., 2013). At the same time, the immunoreactivity of Panx1b has been shown to be prominent in the inner nuclear layer (INL) and ganglion cell layer (GCL) (Kurtenbach et al., 2013). The distinct localization pattern of the two Panx1 proteins in the adult zebrafish retina highlights the potentials of their distinct functional implications in vivo.

1.4.4. Post-translational regulation

The process during which proteins can be altered following their translation is known as post-translational modification (PTM). This can include, for example, the attachment of functional groups (like glycosyl, phosphate, ubiquitin, nitric oxide, methyl, etc.) and/or proteolytic cleavage at specific subunits. PTMs alter proteins' conformation, therefore influencing several characteristics of proteins from stability and subcellular localization to function. Here, biochemical characteristics of Panx1 and the impact of PTMs on Panx1 stability, trafficking, and function will be reviewed.

1.4.4.1. Impact on stability and trafficking

Studies on the localization and stability of Panx1 have provided important insights on the putative role(s) of PTMs. Panx1 protein has been detected at different places in the cells, including in the endoplasmic reticulum (ER), endosomal membranes, and the plasma

membrane (Dvoriantchikova et al., 2006; Zoidl et al., 2007; Penuela et al., 2008, 2009; Wang et al., 2009). While Panx1a was mainly found in the cell membrane, Panx1b, like mouse Panx1, has been located in the plasma membrane and perinuclear region (Kurtenbach et al., 2013). Panx1 was reported to have a very long half-life compared to Cx43 (Penuela et al., 2007) and in pulse-chase labeling experiments (Boassa et al., 2007). Blocking protein secretion with brefeldin A (BFA) treatment did not affect the cell surface population of Panx1, which suggests this pannexin was not subject to rapid displacement and renewal. In fact, it took up to 32 h of BFA treatment before some clearing of Panx1 from the cell surface became evident, while clearing of Cx43 from the cell surface was detected about three h after BFA treatment (Penuela et al., 2007). Further evidence that Panx1 is long-lived was provided by pulse-chase fluorescent labeling experiment, which chased Panx1 proteins for 15-18 h before being targeted to lysosomal degradation (Boassa et al., 2007).

The first PTM identified for Panxs was N-glycosylation at an asparagine (Asn, N) residue (Boassa et al., 2007; Penuela et al., 2007). Three distinct molecular weight forms on western blot, sensitive to treatment with N-glycosidase F and endoglycosidase H, were discovered underlying three different N-glycosylated Panx1 species: non-glycosylated core forms – Gly0, high-mannose forms –Gly1 and complex glycosylated forms –Gly2. The three species' subcellular localization is distinct; predominantly, the Gly0 forms are found in the ER, the Gly1 forms in the early Golgi, and the Gly2 forms at the cell surface. Interestingly, these three forms' relative expression levels were cell and tissue-type-specific (Boassa et al., 2007; Penuela et al., 2007).

N-linked glycosylation of Panx1 occurs at a consensus site in its second EL domain (N254 in mice and N246 in zebrafish) and is a pre-requisite for channel insertion into the plasma membrane (Penuela et al., 2007; N. Prochnow et al., 2009; Nora Prochnow et al., 2009). Site-directed mutagenesis or pharmacological blocking of murine Panx1 glycosylation either reduced (Penuela et al., 2007) or abolished (Boassa et al., 2007) its transport to the cell membrane. Nevertheless, N-glycosylation does not interfere with protein ability to form functional channels as the population of N-glycosylation-deficient Panx1 mutants that reach the cell surface are functional in their ability to uptake dye (Penuela et al., 2009).

In zebrafish, Panx1a exhibits the three glycosylated species (Gly0, Gly1, and Gly2) like the murine ortholog. More extensive and higher molecular weight glycosylation forms (associated with the presence of an additional N-glycosylation site in EL1 at N71) have been detected for the Panx1b protein, which was associated with increased cell surface distribution and unique gating properties (Kurtenbach et al., 2013). Recently, two conserved aromatic residues, W123 and Y205, in the transmembrane domains 2 and 3 of the zebrafish Panx1a were identified as amino acids required for proper cell membrane trafficking. Timonina et al. demonstrated that in Neuroblastoma 2a (Neuro 2a) cells, the formation of the complex glycosylation (Gly2) species and thereby the cell membrane distribution of EYFP-tagged Panx1a was significantly compromised when mutating either W123 or Y205 (Timonina, Kotova and Zoidl, 2020).

Glycosylation is thought to provide a steric hindrance to the docking of Panx1 channels on the adjacent cell membrane, thus preventing gap junction formation (Sosinsky et al.,

2011). Supporting evidence for this theory comes from ectopic Panx1 expression systems where junctional communication was detected in Hella cells (relatively rich in Gly0 Panx1), yet not in N2a or PC12 cells (rich in Gly2 and Gly1 Panx1) (Sahu, Sukumaran and Bera, 2014).

1.4.4.2. Impact on channel function

Aside from stability and subcellular localization, PTMs (such as phosphorylation, S-nitrosylation, and caspase cleavage) can play a role in regulating Panx1 channel gating properties. Excellent reviews have thoroughly covered this topic (Boyce *et al.*, 2014, 2018; Penuela, Simek and Thompson, 2014; Begandt *et al.*, 2017; Whyte-Fagundes and Zoidl, 2018).

The main focus of recent studies has been on the impact of phosphorylation on the Panx1 channel function. A number of serine (S), threonine (T), and tyrosine (Y) phosphorylation sites in the cytoplasmic loop and carboxyl-terminal tail of the Panx1 have been identified using in silico tools. However, there still is a lack of direct biochemical evidence to link specific amino acid/protein kinase pairs with channel function (D'hondt et al., 2013). For instance, Src family kinases (SFKs) were demonstrated to be critical intermediates of purinergic receptor-mediated Panx1 activation. Pharmacological disruption of ionotropic purinergic receptor 7 (P2X7R) interaction with Src inhibited downstream Panx1 currents and dye-uptake while P2X7R function itself remained unchanged. However, no specific phosphorylation site has yet been assigned to this effect (Iglesias et al., 2008). Subsequently, a study using in vitro and in vivo models of ischemic stroke showed under anoxic conditions, N-methyl-D-aspartate receptors (NMDRs) cause neuronal death

through the formation of a signaling complex comprising NMDRs, Src kinases, and Panx1 leading to Panx1 activation via Src phosphorylation (at Y308 within the c-terminus) (Weilinger et al., 2016). Similarly, another tyrosine residue (Y198; located within the intracellular loop of Panx1) was shown to be the target for Src phosphorylation downstream of TNF-α receptor signaling in primary human venous endothelial cells (Lohman et al., 2015). Taken together, these studies have established Src-mediated tyrosine phosphorylation as a pivotal regulator of Panx1 activation; however, the underlying Src phosphorylation site specificity driven by activation of different membrane receptors is not fully understood yet.

Nitric oxide (NO) may also influence protein function via S-nitrosylation. NO moieties reversibly interact with reactive cysteine residues, introducing conformational changes (Lohman et al., 2012). Modulation of Panx1 by S-nitrosylation has primarily been reported by Zang et al., where inhibition of neuronal NO synthase (nNOS) by reducing agents (like DTT and L-NAME) prevented Panx1 channels opening in hippocampal neurons during oxygen-glucose deprivation (Zhang et al., 2008). In the same line of evidence, Panx1 channels are closed by reducing agents (Bunse et al., 2009). Subsequently, C282 within the fourth transmembrane domain of the zebrafish Panx1a was shown to be a possible site for PTM since its mutation to tryptophan caused a robust reduction in the channel activity (Nora Prochnow et al., 2009). Furthermore, Lohman et al. found that mutation of C40 and C346 prevents Panx1 S-nitrosylation by S-nitrosoglutathione (GSNO, the NO donor) as well as the GSNO-mediated inhibition of Panx1 current and ATP release (Lohman et al., 2012). The above studies highlighted the implication of these cysteine

residues as the potential redox sensor in the Panx1; however, at present, the exact molecular mechanisms involved in the targeting of specific residues for NO-mediated modulation of Panx1 channel function in the context of physiological conditions is poorly understood.

Panx1 protein is also subjected to the proteolytic cleavage within the c-terminal domain, which critically impacts channel function. Truncation of human Panx1 by caspase-3 and -7 at the C-terminal position aa 376-379 leads to an irreversible opening of the channel. Consequently, ATP and UTP are released, resulting in the recruitment of macrophages and subsequent activation of the apoptotic pathway (Chekeni et al., 2010; Sandilos et al., 2012). More recently, Engelhardt and coworkers generated 14 truncated versions of rat Panx1 to address the question of a putative functional segmentation of the Panx1 C-terminus. The expression of truncated versions of Panx1 with lengths ranging from 370 to 393 aa had lethal effects both on X. laevis oocytes and Neuro2A cells (Engelhardt *et al.*, 2015). Notably, the caspase-3 and -7 cleavage site responsible for initiating nucleotides release during ongoing apoptosis (Chekeni et al., 2010) reside within this segment.

1.5. Functional properties of Panx1 channels

Panx1 function initiates with the activation of the channel; channel opening. Membrane depolarization has been shown as an experimentally convenient way to activate Panx1 channels. Though, the voltages required for channel activation are in the positive range and thus do not occur physiologically unless in excitatory cells for a brief period at the peak of action potential (Bruzzone et al., 2003; Bao, Locovei and Dahl, 2004; Dahl, 2015).

Nevertheless, several physiological stimuli such as mechanical stress (Bao, Locovei and Dahl, 2004), elevated extracellular potassium or intracellular calcium levels (Dahl and Locovei, 2006), and activation of purinergic receptors (Locovei, Wang and Dahl, 2006; Zhang et al., 2012) have been shown to activate the Panx1 channels, leading to efflux of ions and ATP from the cell (Boassa *et al.*, 2007; Ma *et al.*, 2012; Penuela, Gehi and Laird, 2013; Cheung, Chever and Rouach, 2014; Michalski, Johanna L Syrjanen, *et al.*, 2020; Ruan *et al.*, 2020). The extracellular ATP acts upon various receptors to exert its diverse effects in different physiological and pathophysiological conditions, which has been reviewed elsewhere (Dahl, 2015, 2018; Chiu et al., 2018). In the following section, the crosstalk between ATP receptors and Panx1 will be discussed.

1.6. ATP signaling pathway

Signaling via extracellular ATP is complex (***Figure 1.3***). The biological response to extracellular ATP could, in principle, be due to ATP or to one of its metabolic products, ADP, AMP, or adenosine, acting at P1- and P2- purinergic receptors (Surprenant and North, 2009; Burnstock et al., 2010). P1 receptors are four different G-protein-coupled receptors (A1, A2A, A2B, and A3 subtypes) that preferentially recognize adenosine. On the other hand, P2 receptors are activated by adenine and/ or uridine nucleotides and classified into two families: ionotropic P2X and G protein-coupled P2Y receptors (Zimmermann, 2006). P1 and P2 receptors signaling as primitive evolutionary systems are involved in neurotransmission and neuromodulation in the CNS and affect normal behavior, including memory, feeding, locomotion, and cognition (Burnstock et al., 2010; Gomes et al., 2011). More details on this system are given below.

1.6.1. P2X receptors

In the central nervous system, the P2 family is widely expressed in different cell types, including neurons, astrocytes, microglia, and oligodendrocytes (Burnstock and Knight, 2004; Velasquez and Eugenin, 2014). The homo- or heteromeric P2X receptors (seven subtypes, P2X1–7R) act as ligand-gated cation channels activated by the binding of extracellular ATP. When activated, they allow the influx of extracellular Na+ and Ca2+ and the efflux of cytoplasmic K+ ions (Burnstock et al., 2010; Khakh and North, 2012).

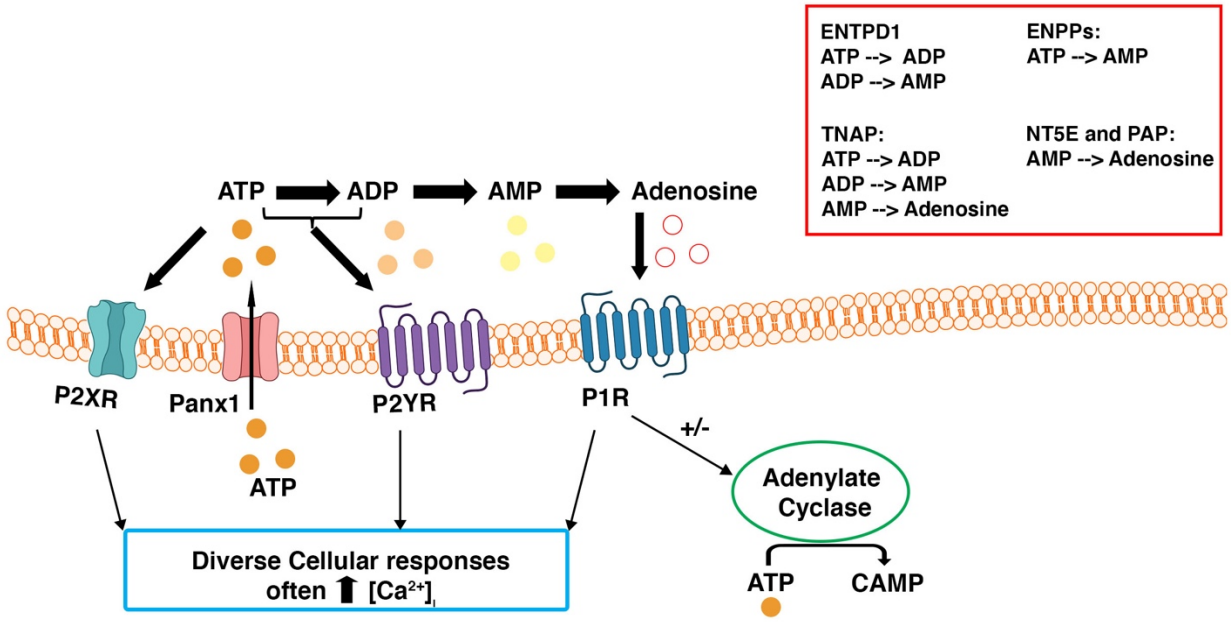

Figure 1.4. Purinergic signaling. ATP release through Pannexin 1 (Panx1) channels initiates a cascade of events. *ATP in the extracellular space can stimulate P2X or P2Y receptors. Ectoenzymes catalyze the stepwise hydrolysis of ATP to ADP, AMP, and adenosine, which are the ligands of certain receptors. P2 and P1 receptors frequently transduce signals that produce diverse effects (often via increasing the intracellular Ca^{2+} concentration). Representative ectoenzymes are shown in the red box on top. ENPP: Ectonucleotide pyrophosphatase/phosphodiesterase family, ENTPD1: Ectonucleoside triphosphate diphosphohydrolase-1, NT5E: ecto-5′-nucleotidase, PAP: peroxidase anti-peroxidase, TNAP: tissue-nonspecific alkaline phosphatase. The illustration was made using Photoshop software (https://www.adobe.com/ca/products/photoshop.html). (Created by N.S.).*

ATP required for activation of P2XRs is released from presynaptic neurons but may also be locally supplied by Panx1(Baroja-Mazo, Barberà-Cremades and Pelegrín, 2013; Dahl, 2015). Under normal physiological conditions, relatively low ATP amounts in the extracellular space are subject to rapid degradation by ecto-ATPases (Zimmermann, 1992; Plesner, 1995). Thus, activation of P2 receptors by ATP is best achieved if the release site is near the receptor. Another reason for the proximity of the release site and receptors is the low binding affinity of some P2 receptors for ATP. For instance, the physical association between Panx1 and P2X7R, activation of which requires up to millimolar concentrations of ATP (Surprenant et al., 1996), has been confirmed by several studies (Bao, Locovei and Dahl, 2004; Pelegrin and Surprenant, 2006; Locovei et al., 2007). Their direct interaction could also ensure that local increases in the intracellular Ca^{2+} are readily detected by Panx1 channels (Li, Tomić and Stojilkovic, 2011). Once activated, the P2X7R is permeable to various cations, leading to a rapid cellular depolarization and a Ca^{2+} dependent signaling cascade (Burnstock et al., 2010). Increased intracellular Ca^{2+} concentration activates Panx1, leading to more ATP release into the extracellular milieu (Pelegrin and Surprenant, 2006, 2009; Locovei et al., 2007; Iglesias et al., 2009; MacVicar and Thompson, 2010). This, in turn, re-activates P2X7R, thereby triggering a series of inflammatory responses and apoptotic cell death (Ma et al., 2009; Coddou et al., 2011; Khakh and North, 2012; Poornima et al., 2012). For example, in the retina, via the P2X7R, endogenous extracellular ATP triggers the death of cholinergic neurons during normal development, thereby controlling the total number, local density, and regular spacing of these neurons (Resta et al., 2005). Also, in age-

related macular degeneration (AMD) the most common cause of severe vision loss worldwide, a Panx1-dependent P2X7R activation has been linked to oxidative stress-induced retinal degeneration (Olivier et al., 2016).

1.6.2. P2Y receptors

P2Y receptors are a family of eight G-protein coupled receptors divided into P2Y1-like receptors (P2Y1, P2Y2, P2Y4, P2Y6, P2Y11) and P2Y12-like receptors (P2Y12, P2Y13, P2Y14) (Fischer and Krugel, 2007; Burnstock et al., 2010). Members of the first group signal through Gq pathways, the activation of which stimulates phospholipase C and subsequent release of Ca^{2+} from intracellular stores in response to inositol 1,4,5-trisphosphate (IP3) generation (Erb et al., 2006; Guzman and Gerevich, 2016). The P2Y11 receptor can also couple to Gs stimulating adenylate cyclase and increase generation of cyclic adenosine monophosphate (cAMP) levels (Nguyen et al., 2001). P2Y12–14 receptors couple to Gi, effectively inhibiting adenylate cyclase and decreasing cAMP production (Fischer and Krugel, 2007; Yegutkin, 2008; von Kugelgen and Harden, 2011; Guzman and Gerevich, 2016).

Activation of P2YRs by ATP plays roles in neurotransmission, neurogenesis, and glial cell communication (Guthrie et al., 1999; Burnstock and Knight, 2004; A. Weisman et al., 2012). It is also involved in pathophysiological processes, such as pain (Gerevich and Illes, 2004), ischemia (Kuboyama et al., 2011), and inflammation (Idzko, Ferrari and Eltzschig, 2014). Noteworthy, P2Y-dependent increase in intracellular calcium via IP3 has been reported as a direct mechanism to open Panx1 and propagate regenerative calcium waves in a variety of cells, including endothelial cells (Abbracchio et al., 2006; Dahl and

Locovei, 2006; Locovei, Wang and Dahl, 2006; Iglesias et al., 2009). Regenerative calcium waves allow for long-distance signaling by chemotactic ATP, for example, for attracting microglia to a site of neuronal injury (Chen et al., 2000; Honda et al., 2001; Schipke et al., 2002).

1.6.3. P1 receptors

The P1 receptor family includes four G-protein coupled receptors (A1, A2A, A2B, A3). Their activation by extracellular adenosine triggers adenylate-cyclase, thus modifying intracellular cAMP level. A1 and A3 are negatively coupled to adenylate cyclase, while A2A and A2B are positively coupled to it (Burnstock et al., 2010; Camici, Garcia-Gil and Tozzi, 2018; Antonioli et al., 2019).

In the CNS, A1Rs, which have a high affinity for adenosine (about 70 nM), are distributed both pre and post-synaptically. Presynaptically, they inhibit the release of excitatory and inhibitory neurotransmitters (like glutamate, dopamine, acetylcholine, and serotonin). In the postsynaptic membrane, A1Rs reduce neuronal excitability by increasing potassium's outflow, thereby exerting neuroprotective effects (Liu et al., 2019). A2ARs, which unlike A1Rs, promote excitatory neurotransmitter release, also have a high affinity for adenosine (150 nM). Interestingly, A2ARs can hetero-dimerize with A1Rs (Ciruela et al., 2006; Cristóvão-Ferreira et al., 2013) and dopamine D2 receptors (Fuxe et al., 2007). This enables a considerable potential for adaptive responses in the regulation of synaptic events (Fuxe, Agnati and Borroto-Escuela, 2014). A2BRs and A3Rs have a relatively lower binding affinity for adenosine (i.e., about 5100 and 6500 nM, respectively). These

receptors can be activated by adenosine, which reaches pathological concentrations present in the course of neuronal injury (Carman et al., 2011; Liu et al., 2019).

The adenosine signaling system promotes pre and post-synaptic modulatory effects on neurotransmission and plays roles in synaptic plasticity and neuroprotection (Gomes et al., 2011). However, the increase in the extracellular adenosine concentration from nanomolar to micromolar levels, which has been reported in many neuropathological conditions such as ischemia, inflammation, and epilepsy, can have detrimental effects on the course of illness (van Calker et al., 2019). Interestingly, the neuroprotective effect of A1R against epilepsy has been attributed to the activation of Panx1 channels. The ATP released through Panx1 channels breaks down to produce adenosine. The stimulation of P1Rs by adenosine inhibits neuronal excitability and, therefore, attenuates or even eliminates the symptoms of epilepsy (Kawamura, Ruskin and Masino, 2010).

1.7. Physiological relevance of Panx1 in the visual system

High expression of Panx1 in major sensory systems including the eye (Dvoriantchikova et al., 2006; Zoidl et al., 2008), inner ear (Tang et al., 2008; Wang et al., 2009), taste buds (Huang et al., 2007; Romanov et al., 2007) and the olfactory epithelium (Zhang, Chen and Zhang, 2012) has sparked interest in determining (patho)physiological relevance of Panx1-mediated ATP signaling in processing primary sensory information and cognitive behaviors (Prochnow et al., 2012; Cheung, Chever and Rouach, 2014). Since the visual system is of the focus of this research, the following section will address the findings relating to this system.

Initial studies on the retinae (***Figure 1.4***) of rodent models detected Panx1 expression in the ganglion cell layer (GCL), inner nuclear layer (INL), the outer nuclear layer (ONL), and to a lesser extent in the inner plexiform layer (IPL) (Ray et al., 2005; Dvoriantchikova et al., 2006). The mRNA and protein expressions were shown to peak transiently around birth and decline with age. Early in the development, Panx1 labeling was prominent in the GCL, amacrine cells, and horizontal cells (HCs). Whereas in the adult retinae, the staining mostly occurred in the GCL (Ray et al., 2005; Dvoriantchikova et al., 2006). Using single-cell RT-PCR, IHC, and ultrastructural analysis of mice retinae, Panx1 proteins were further localized on somata and dendrites of CB3a cells and in HCs dendrites with a less prominent expression in the cell body and axonal terminals (Kranz et al., 2013). It's worth mentioning that in the murine retina, there is only one type of HC that receives cone input at the dendrites and rod input at the axon terminals (Peichl and Gonzalez-Soriano, 1993). This contrasts with the zebrafish retina having two types of HC that either make synapse with cones or rods, with the Panx1a found at the HC-cone synaptic complexes in a band-like pattern (N. Prochnow et al., 2009). Panx1b, on the other hand, was later detected in the INL and GCL (Kurtenbach et al., 2013). The distinct localization of the two Panx1 proteins in the adult zebrafish retina raised a question about their possible distinct functions in the retina.

Physiological functions of Panx1 in the retina were primarily studied in Panx1$^{-/-}$ mice models (Kranz et al., 2013). In vivo and in vitro electroretinography (ERG) of the Panx1$^{-/-}$ mice revealed an increase in the a and b-waves amplitude under scotopic, but not photopic light conditions. The author suggested that the loss of Panx1 function interferes

with the dark-adapted retina activity without affecting signal transmission's temporal properties within the retina. Since the cone pathway under light conditions was not affected, the closure of Panx1 under conditions of prolonged light adaptation was speculated (Kranz et al., 2013), as observed for retinal gap junctions (Xin and Bloomfield, 1999). The a-wave is a measure of the light-induced reduction of the dark current following the photoreceptors' hyperpolarization. It is made up of an extracellular radial current from the photoreceptor synapse, which is negatively regulated by the feedback from HCs to photoreceptors (Hagins, Penn and Yoshikami, 1970; Penn and Hagins, 1972; Robson and Frishman, 2014). Since Panx1 channels contribute to this negative feedback mechanism, the enlargement of a-wave under the scotopic light conditions in the panx1^{-}

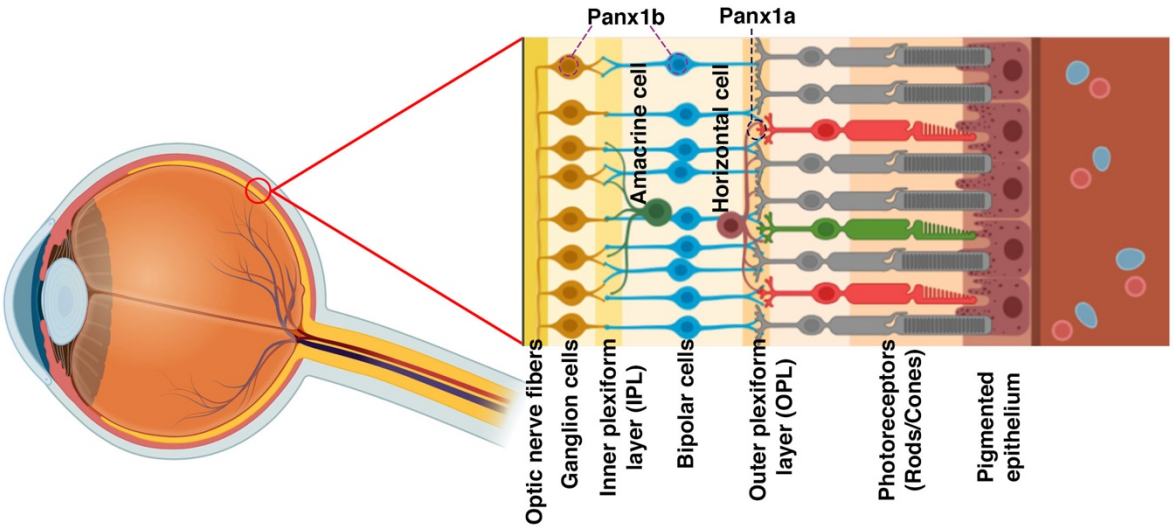

Figure 1.5. A drawing of a section through human eye with a schematic enlargement of the retina. *In all vertebrates, retinas are composed of three layers of nerve cell bodies and two layers of synapses. The outer nuclear layer (ONL) contains cell bodies of photoreceptors (i.e., the rods and cones), the inner nuclear layer (INL) contains cell bodies of the bipolar, horizontal and amacrine cells, and the ganglion cell layer contains cell bodies of ganglion cells. The connections between rod and cones, and vertically running bipolar cells and horizontal cells occur in the outer plexiform layer (OPL). The second synaptic layer is the inner plexiform layer (IPL), where the bipolar cells connect to ganglion cells. Light absorption by photoreceptors is translated into first a biochemical signal and then an electrical message. The electrical outputs are transmitted to the brain via ganglion cells axons that form the optic nerve fiber. In zebrafish, Panx1a proteins are located at the tips of HC-cone synaptic complexes (indicated with a dark blue circle), whereas Panx1b channels are found in the INL and GCS. Schematics were drawn using the biorender app (https://biorender.com). (Created by N.S.).*

$^{/-}$ mice was explained by the lack of Panx1 channels activity disrupting the negative feedback from HCs to photoreceptors. The ERG b-wave reflects light-induced currents of ON bipolar cells flowing towards the sink in the OPL (Stockton and Slaughter, 1989). It was proposed that Panx1 channels on the CB3a OFF bipolar cells provide a competing current to light-induced currents of the ON bipolar cells, leading to reduced radial current flow. Removal of this sink by loss of Panx1 in the knockout mice may lead to the enhancement of b-wave observed in the scotopic conditions (Kranz et al., 2013).

Soon after the primary proposal, a similar function as murine ortholog was assigned to the zebrafish Panx1a, being involved in the negative feedback from HCs to photoreceptors, thus enhancing contrast sensitivity (Vroman et al., 2014; Cenedese et al., 2017). Contrast sensitivity is recognized as an important diagnostic method for visual perceptual disorders. A decrease in contrast sensitivity may affect spatial awareness and reduce the ability to safely navigate the environment; for instance, walking down steps, driving at night, or reading instructions could become difficult. Decreasing contrast sensitivity is associated with ocular pathological conditions such as glaucoma (Arden and Jacobson, 1978; Ross, Bron and Clarke, 1984; Hawkins et al., 2003), age-related macular degeneration (ARMD) (Enger, Alexander and Fine, 1988; Stangos et al., 1995; Bellmann et al., 2003) and optic nerve degeneration (VÄRINEN, LAURINEN and ROVAMO, 1983; Wildberger, 1984; Volkers et al., 1987; Riordan-Eva, 2004), as well as neurodegenerative disorders like Alzheimer's disease (AD) (Livingstone and Hubel, 1987; Ward et al., 2018), multiple sclerosis (MS) (Balcer et al., 2003; Baier et al., 2005) and Parkinson disease (PD) (Regan and Neima, 1984; Weil et al., 2016). In this context, uncovering the

molecular mechanisms and signaling pathways through which Panx1 takes part in adjusting visual contrast level, which may raise new therapeutic potentials, seems necessary.

On the other hand, no physiological functions have yet been defined for Panx1b in vision. A novel electrophysiology study on adult mice's inner retina revealed that Off-type GCs possess the highest activity of Panx1 channels (Dvoriantchikova et al., 2018). Using pattern electroretinogram (PERG), which enables a direct measure of ganglion cell function, the author showed that Panx1 greatly contributes to the electrical output of the retina, consistently targeted ablation of Panx1 in the retinal GCs caused a significant reduction of PERG amplitude (Dvoriantchikova et al., 2018). Could the Panx1b channels, highly localized at the GCs layer, serve a similar function in shaping the final output of the retinal GCs needs further investigation.

1.8. Circadian clock system and its implications in the (patho)physiology of the visual system

Daily temporal patterns from cellular activities to animal behaviors are regulated by the endogenous circadian clock system (***Figure 1.5***). The central clock (i.e., the hypothalamic suprachiasmatic nucleus (SCN) in mammals and the pineal organ in lower vertebrates, including zebrafish) receives light information from the eye and relays it to other tissues in the body to synchronize biological processes with the 24h environmental light-dark cycle (Cahill, 2002; Pando and Sassone-Corsi, 2002; Cermakian and Boivin, 2009; Finger, Dibner and Kramer, 2020). Examples of physiological processes regulated by the clock include energy metabolism (Rutter, Reick and McKnight, 2002; Bass and

Takahashi, 2010; Panda, 2016), hormone production (Ota et al., 2012; Ikegami et al., 2019; Moustafa, 2020; Silva and Domínguez, 2020), daily rest/activity or sleep/wake cycle (Czeisler and Gooley, 2007; Mattis and Sehgal, 2016), and more complex behaviors such as cognition and memory formation (Schmidt et al., 2007; Gerstner and Yin, 2010; Foster and Kreitzman, 2014). On the other hand, disruptions of the circadian clock can lead to various pathologies ranging from diabetes (Sinturel et al., 2019; Oster, 2020) to psychological disorders like anxiety and depression (Milhiet et al., 2011; Lazzerini Ospri, Prusky and Hattar, 2017).

At the molecular level, circadian rhythms are generated by gene transcription-translation feedback loops (Buhr and Takahashi, 2013a). The core clock elements are six genes (*period* (*per*) 1 and 2, *cryptochrome* (*cry*) 1 and 2, *clock*, and *bmal1*) that constitute a self-sustained circadian clock that directly participates in the negative feedback loop mechanisms (Ruan et al., 2006). CLOCK and BMAL1 are basic helix-loop-helix (bHLH) PAS domain transcription factors that form a heterodimer complex that drives the expression of two *per* genes (*per1-2*) and two *cry* genes (*cry1-2*) by binding to circadian E-box enhancer elements in their promoters. Once transcribed and translated, the resulting PER and CRY proteins also form a heterodimer complex, which travels back into the nucleus to suppress their own transcription by inhibiting the CLOCK/BMAL1 action, shaping the basic negative feedback loop at the center of the molecular circadian clock (Buhr and Takahashi, 2013b). The CLOCK/BMAL1 complex also initiates a second feedback loop that acts in coordination with the loop described above. This involves the transactivation of two retinoic acid-related orphan nuclear receptors genes, *rev-erb*

α/β and *rorα/β* (Preitner et al., 2002; Guillaumond et al., 2005). The protein products of these genes subsequently compete for binding to retinoic acid-related orphan receptor response element (RORE) binding sites within the promoter of *bmal1*. While ROR proteins initiate *bmal1* transcription, REV-ERB proteins inhibit it, driving a daily rhythm of *bmal1* transcription (Preitner et al., 2002; Guillaumond et al., 2005; Buhr and Takahashi, 2013b; Partch, Green and Takahashi, 2014).

Besides the master clock in the brain, in most vertebrates species, the retinas can generate self-sustained circadian oscillations (Cahill and Besharse, 1995; Tosini and Menaker, 1996, 1998; Green and Besharse, 2004). Indeed, all six classes of retinal neurons (rods, cones, horizontal cells, bipolar cells, amacrine cells, and ganglion cells express most of the core clock genes. However, ex vivo studies demonstrated self-sustained rhythms are generated in the rods and cones on the one hand, and in the intrinsically photosensitive retinal ganglion cells (ipRGCs) on the other (Ruan et al., 2006; Tosini et al., 2008; McMahon, Iuvone and Tosini, 2014).

All three photoreceptor types contribute to the retinal pathways providing light information to the central master clock, therefore synchronizing (entraining) endogenous circadian clocks to the environmental light-dark cycle. However, the ipRGCs have been shown to be the principal anatomical site of non-image-forming vision (Göz et al., 2008; Güler et al., 2008; Hatori et al., 2008). The ipRGCs express melanopsin, a blue-sensitive opsin photopigment, allowing them to be directly photoreceptive (Hattar et al., 2002; Panda et al., 2005). Because of their intrinsic light response, ipRGCs can support photoentrainment

even in the absence of rods and cones (Berson, Dunn and Takao, 2002; Warren et al., 2003). The light absorption by melanopsin initiates an action potential that travels to the

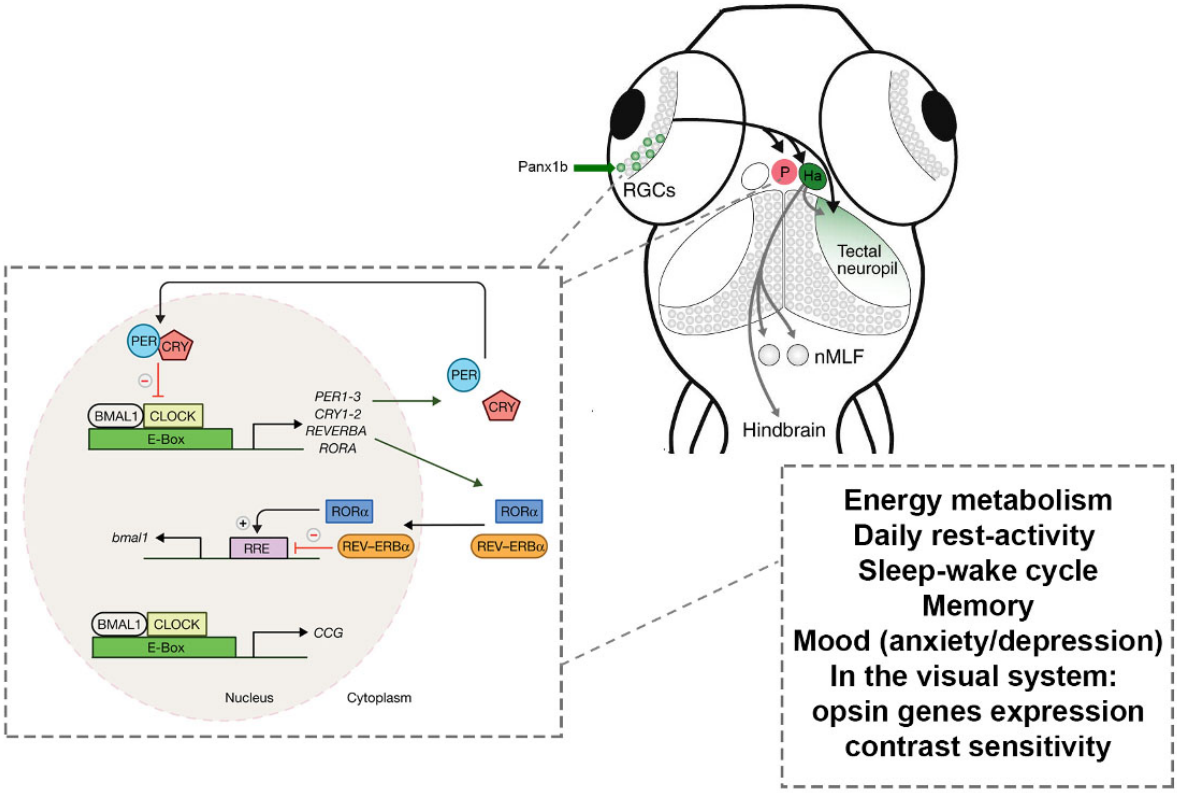

Figure 1.6. Schematic diagram of the vertebrate's circadian clock system*. External cues, such as light, food, and stress, entrain the central clocks in the brain (suprachiasmatic nucleus; SCN, in mammals, Pineal gland; P, in non-mammalian vertebrate) as well as peripheral clocks in other tissues. Light is detected by the rods and cones as well as intrinsically photosensitive retinal ganglion cells (ipRGCs), where Panx1b proteins are located. Light information is relayed to the brain via RGCs axons to synchronize an intracellular molecular clock mechanism, consisting of positive (BMAL1 and CLOCK) and negative (PER and CRY) elements. CLOCK and BMAL1 heterodimers drive the expression of per, cry, reverb, and ror genes by binding to the E-box enhancer elements in their promoters. Once transcribed and translated, the PER and CRY proteins inhibit the CLOCK/BMAL1 action, shaping a negative feedback loop. The second feedback loop is mediated by two other proteins, ROR and REV-ERB, where the expression of bmal1 is triggered or inhibited through competitive binding of ROR and REV-ERB proteins, respectively. These interconnected loops generate the circadian output, which is apparent in rhythms in biological pathways, examples of which are shown in the right panel. CCGs: clock-controlled genes; Ha: Habenula; nMLF: the nucleus of the medial longitudinal fasciculus. Neurons in the nMLF are the most rostral components of the reticulospinal (RS) track in larval zebrafish and possess dendrites that contact visual recipient regions as well as axonal projections that innervate circuits in the hindbrain and mediate visual-motor behaviors. (Created by N.S.)*

central clock in the brain via ipRGCs axons, which dominate the path from the retina to the SCN (Morin, Blanchard and Provencio, 2003; Sollars et al., 2003). The selective lesions of ipRGCs completely abolish the photoentrainment, confirming their significance for light entrainment (Göz et al., 2008; Güler et al., 2008; Hatori et al., 2008). The retinal clock system regulates many physiological functions within the retina, including opsin genes expression (Freedman et al., 1999), dopamine synthesis (Nir, Haque and Iuvone, 2000; Doyle et al., 2002); melatonin release (Cahill and Besharse, 1995; Tosini and Menaker, 1996, 1998), extracellular pH (Dmitriev and Mangel, 2001), neuronal transmission (McMahon, Iuvone and Tosini, 2014), and visual sensitivity as reflected in electroretinogram (ERG) b-wave amplitude (Storch et al., 2007; Cameron et al., 2008). Also, the retinal clock system influences cell growth and survival in the eye. For example, the vulnerability of photoreceptors to phototoxicity (Organisciak et al., 2000), the degree of refractive errors in primates models of myopia (Iuvone et al., 1991), and photoreceptors and ganglion cells viability during aging (Baba et al., 2009; Musiek et al., 2013) are modulated through clock system.

1.9. Zebrafish: a model organism for understanding the biology of the visual system

The zebrafish, a small tropical fresh-water fish, is quickly becoming a well-established experimental model in neuroscience research due to Its unique attributes (Best and Alderton, 2008; Panula et al., 2010; Sager, Bai and Burton, 2010). For example, rapid development, the ease of genetic manipulations, and the transparency of the zebrafish embryo and larva facilitate the functional analysis of genes in the nervous system's

development and pathologies. Also, zebrafish CNS shows all of the major divisions found in the mammalian brain with the same neurotransmitters (such as glutamate, GABA, dopamine, acetylcholine, serotonin, etc.) functioning within the nervous system and a large repertoire of behaviors. These features provide us with a rich arena to study the neural circuits underlying behavior (Guo, 2004; Best and Alderton, 2008; Panula et al., 2010). Among the readily accessible behaviors that can be approached by genetics are behaviors mediated by the visual system.

The visual system of zebrafish develops rapidly, which is likely a reflection of the need to actively search for food while avoiding predators in its natural environment. Like other vertebrates' retina, the zebrafish retina is arranged in a multilayered neuronal network composed of five retinal neuron classes-photoreceptor, horizontal cell, bipolar cell, amacrine cell, and ganglion cell (Easter and Nicola, 1996; Schmitt and Dowling, 1999). Visual stimulus is perceived by photoreceptors, transmitted through bipolar cells, and integrated by ganglion cells, whose axons form the optic nerve that is responsible for transducing the visual information from the retina to the optic tectum in the brain. Subsequently, corresponding behavioral responses will be initiated (Baden and Osorio, 2019). Zebrafish visual responses can be studied with a variety of approaches. For instance, electrophysiology recordings can provide insights into photopic and scotopic vision, while locomotor responses can be interrogated to measure visual acuity and color vision. Zebrafish display a range of instinctive locomotor activities following exposure to stimuli of different spatial and temporal frequencies, luminosity, contrast, and chromaticity (Bollmann, 2019). Tetrachromatic vision, which allows the zebrafish to

discriminate UV, blue, green, and red wavelengths, equates to the spectral properties of normal human eyesight (Allison et al., 2004). Noteworthy, advances in the optical methods and the availability of specific markers for the distinct retinal cell types have facilitated the monitoring of neuronal activity and connectivity in an intact and freely behaving translucent larval fish, which, at the moment, is not possible in mammals (Dunn et al., 2016). These attributes collectively make zebrafish an appealing experimental organism to study (patho)physiological processes in the human visual system.

1.10. Hypothesis and research objectives

Taken from other reported paralogs and the types of evolutionary models that help explain why duplicated gene pairs are retained, I hypothesized that *panx1a* and *panx1b,* showing very distinct retinal localization, have diversified their functions in regulating visual information processing and therefore visually driven behaviors.

The main focuses of my research were:

1) To identify potential downstream targets of *panx1* ohnologs and investigate molecular mechanisms whereby these two genes act;
2) To understand whether the distinct retinal localization of two *panx1* copies translates into differential influences on the processing of visual information, and therefore visually driven behaviors;
3) To determine how the impacts of the loss of both *panx1* genes functions on the visual performance of larval zebrafish differ from single-gene knockout conditions.

To address these aims, I generated *panx1a* and *panx1b* single, and *panx1a/panx1b* double-knockout lines. Data documenting in Chapter 3, which was published in *Scientific*

Reports (Safarian et al., 2020) titled 'Visuomotor deficiency in *panx1a* knockout zebrafish is linked to dopaminergic signaling', covers the *panx1a* angle of the study. Chapter 4 of this thesis presents the studies conducted on *panx1b* knockouts. It is part of a manuscript ready for submission titled 'Pannexin1b: an emergent candidate for delineating interactions between the circadian clock and visual system in the zebrafish'. Data documenting the third aim is presented in Chapter 5, which is part of a second manuscript titling: 'Cognition and the functional divergence of the zebrafish *panx1* genes'. The sub-aims in this chapter were to determine how the molecular signature, as well as visual phenotypes in the absence of both *panx1* ohnologs, might differ from single-gene knockout conditions.

Chapter 2. Material and methods

2.1. Fish husbandry and embryo collection

Adult zebrafish (Danio rerio) of strain Tupfel long fin (TL) were obtained for this study from the laboratory of Dr. Wen's lab (Zebrafish Centre for Advanced Drug Discovery, St. Michael's Hospital, Toronto, ON). The fish were maintained in the recirculation system (Aquaneering Inc., San Diego, CA) at 28°C with a photoperiod of 14 hours light and 10 hours dark. Embryos were obtained and reared in Egg water (Appendix A) according to the standard procedures(Brand, M. and Nüsslein-Vollhard, 2002). Experiments and procedures with animals were performed at York Universitie's zebrafish vivarium, according to the CACC guidelines of the Canadian Council for Animal Care (CCAC) after approval of the protocol by the Animal Care Committee (ACC) (GZ#2014-19 (R3). The

number of experiments, including zebrafish larvae, was kept to the necessary minimum. The York University Biosafety Committee (YUBC) approved all other experiments (Permit#04-11).

2.2. TALENs design

Potential TALENs target sites on *panx1a* (NM_200916.1) and *panx1b* (NM-_001100030.2) were identified using the Mojo Hand software (http://talendesign.org)(Neff et al., 2013). The following criteria were used for TALEN design: TALEN target sites were 15-17 bases long with an initial 5' T nucleotide to the TALE domain. The spacer length was restricted to 15-16 base pairs. Target sites with a unique restriction enzyme sequence located in the middle of the spacer sequence were selected to simplify screening for insertion-deletion (indel) mutations. The specificity of selected TALENs target sequences was determined using the BLAST interface build into the Mojo Hand software. The TALEN sequences for *panx1a* and *panx1b,* respectively, are 5′-GGAGCAGTACTTGAGGACCAAGCGCTACTCTAAAGCGGATCAGTAATCCT-3′ and 5'-CTCAGTGGTCTTGAATTGACTGAAGCTTGTTTTAAGTATCCTCTGGTAG-3' (spacer sequence underlined and the restriction site in red color). Sequence-specific TALEN constructs were assembled using Golden Gate cloning methods.

2.3. TALEN constructs

The TALEN constructs were synthesized in Dr. Stephen Ekker's lab (Mayo Clinic Cancer Center, Rochester, MN). Briefly, TALEN assemblies of the RVD-containing repeats were conducted using the Golden Gate approach (Cermak et al., 2011). Once assembled, the TALE repeats were cloned in the pT3TS-GoldyTALEN expression vector (Bedell et al.,

2012; Ma et al., 2013, 2016). TALEN expression vectors were linearized with the SacI restriction endonuclease (ThermoFisher Scientific, Canada) for 15 min at 37°C and used as templates for in vitro transcription. Capped cRNAs were synthesized from TALEN pairs mixed 1:1 using the mMESSAGE mMACHINE T3 Transcription kit (Life Technologies, Canada). The mixture of the two TALEN cRNAs was purified using the Oligotex mRNA Mini Kit (Qiagen Inc., Toronto, Canada). TALEN cRNAs were diluted in DNase/RNase-free water (Life Technologies) to the final concentration of 1 μg/µL and stored at –80 °C before microinjection.

2.4. TALEN activity screening

One-cell stage zebrafish embryos were injected with TALEN cRNAs pair at doses ranging from 30-100 pg/nl. The toxicity of the injected cRNAs was determined at 24 hours post fertilization (1dpf) by calculating the proportion of healthy, dead, and malformed embryos at each dose. The condition resulting in more than 50% post-injection survival was selected for further injections. Genomic DNA (gDNA) was extracted from groups of 10-20 injected embryos at four days post-fertilization (4dpf) To examine the TALEN mutagenesis efficiency. Briefly, the individual larva was incubated in 100mM NaOH at 95℃ for 15 min. After cooling to room temperature, the one-tenth volume of 1 M Tris (pH8.0) was added to the extracts to neutralize the NaOH (Meeker et al., 2007). Finally, 1 volume TE buffer pH8.0 was added, and gDNAs were stored at -20℃. A small indel mutation screen used PCR followed by AfeI (for *panx1a*) or HindIII (for *panx1b*) restriction enzyme (RE) digest. Indel mutations were confirmed by sequencing (Eurofins Genomics

LLC, KY, USA) of gel-purified PCR products cloned into the pJet1.2 cloning vector (Life Technologies.

2.5. Generation of panx1$^{-/-}$ zebrafish

Adult zebrafish (F0) were anesthetized in pH-buffered 0.2 mg/ml ethyl 3-aminobenzoate methanesulfonate solution (MS-222, Sigma-Aldrich). The caudal fin (2 mm of the end) was removed using dissecting scissors (WPI Inc., FL, USA) and placed into 1.5 ml collecting tubes. The fin gDNA was isolated and screened for indel mutations as described elsewhere (Bedell et al., 2012). Adult F0 zebrafish with a mutation in the related locus were out-crossed to normal TL zebrafish and, F1 offspring were analyzed by PCR and restriction digestion to verify germline transmission of mutations. Heterozygous (*panx1a*$^{+/-}$, *panx1b*$^{+/-}$) F1 mutants were in-crossed to establish homozygous F2 mutants (i.e., *panx1a*$^{-/-}$ and *panx1b*$^{-/-}$). To produce double knockout (DKO; *panx1a*$^{-/-}$/ *panx1b*$^{-/-}$) fish, two rounds of inbreeding were performed. First, F3 panx1a-/- fish were in-crossed with the *panx1b*$^{-/-}$ mutants. Next, the heterozygous F4 progenies (i.e., *panx1a* $^{+/-}$/ *panx1b*$^{+/-}$) were in-crossed, and the F5 fish bearing the homozygous mutations in both loci (i.e., *panx1a*$^{-/-}$/ *panx1b*$^{-/-}$) were selected (by gDNA screening) to produce DKO model. All experiments described here were performed with progenies of the F3 generation of *panx1a*$^{-/-}$ and *panx1b*$^{-/-}$ fish and progenies of F6 DKO fish.

2.6. RNA extraction and RT-qPCR

Total RNA was extracted from 6 dpf larvae using the RNeasy Plus Mini Kit (Qiagen). The iScript Reverse Transcription Supermix (Bio-Rad Laboratories, Mississauga, Canada) was used to reverse transcribe 1μg of total RNA. The cDNA equivalent of 15ng total RNA

was analyzed in triplicate by quantitative Real Time-PCR using the SsoAdvanced SybrGreen PCR mix (Bio-Rad). All experiments included a melt curve analysis of PCR amplicons generated in each reaction. Raw cycle threshold values (Ct-values) were exported from the CFX Manager Software (Bio-Rad, Canada), and the relative gene expression was calculated using the Relative Expression Software Tool (REST-2009)(Pfaffl, 2002). The statistical significance was tested by a PairWise Fixed Reallocation Randomisation Test © and plotted using standard error (SE) estimation. Gene information and primer sequences (Integrated DNA Technologies, Toronto, Canada) are listed in Table 2.1.

2.7. Transcriptome analysis

The RNA library preparation was performed following the NEB NEBNext Ultra II Directional RNA Library Preparation protocol (New England Biolabs Inc., Ipswich, MA, USA). RNA libraries were loaded on a Bioanalyzer 2100 DNA High Sensitivity chip (Agilent Technologies) to check for size, quantified by qPCR using the Kapa Library Quantification Illumina/ABI Prism Kit protocol (KAPA Biosystems, Wilmington, MA, USA). Pooled libraries were paired-end sequenced on a High Throughput Run Mode flow cell with the V4 sequencing chemistry on an Illumina HiSeq 2500 platform (Illumina, Inc., San Diego, CA) following Illumina's recommended protocol to generate paired-end reads of 126-bases in length. The post-sequencing processing to final read counts, normalization, and differential gene expression analysis used multiple software packages, including a two-condition differential expression analysis using the edgeR R-package, v.3.8.6 (http://www.bioconductor.org/packages/release/bioc/html/edgeR.html).

2.8. Development of an antibody against Panx1a

A gBlock gene fragment of 390 bp representing the carboxy-terminal 129 amino acids of Panx1a and flanking BamHI and EcoRI restriction endonuclease recognition sites was synthesized (Integrated DNA Technologies) and cloned into pGEX6P2 (GE Healthcare Life Science, USA) to generate a GST-Panx1a-CT fusion protein of 41.7 kDa. Davids Biotechnology GmbH (Regensburg, Germany) generated affinity-purified polyclonal rabbit anti-Panx1 antibodies, after the fusion protein was overexpressed in E. coli host BL21(DE3) and isolated from a denaturing SDS-PAGE gel.

2.9. Western blot and confocal microscopy

Neuroblastoma 2a (Neuro2a) cells were maintained using standard growth conditions (Ray et al., 2005; Bunse et al., 2011) and used for expression and localization studies. Neuro2a cells were transfected with 200ng plasmid DNA encoding C-terminally EYFP-tagged Panx1a fusion proteins, containing the full-length protein-coding region of Panx1a (amino acids (aa) 1-417; Gene ID: 393890), Panx1b (aa 1-422; Gene ID: 567417) or mPanx1 (aa 1-426; Gene ID: 55991). To compare the expression and localization of wild-type and the truncated Panx1a protein, the coding region corresponding to Panx1a aa 1-195 was cloned into the pEYFP-N1 expression vector (Clontech Laboratories Inc., Mountain View, CA, USA) as described (Ray et al., 2005; Nora Prochnow et al., 2009). The localization and western blot analysis were performed 48 hr after transfection. The anti-Panx1a antibody specificity was verified by western blot using Panx1a, Panx1b, or mPanx1 protein lysates. Whole-cell protein lysates (20µg) from transfected Neuro2a cells were separated by SDS-PAGE (10% polyacrylamide) and transferred to nitrocellulose

membrane (Bio-Rad) for immunodetection. Primary antibodies were rabbit anti-Panx1a (1:500 dilution, Davids Biotechnologie GmbH, Regensburg, Germany) and mouse anti-β-actin (1:1000 dilution, Sigma-Aldrich, Canada). The IRDye® 800cw or 680RD secondary antibodies (LI-COR Biosciences, St. Lincoln, NE, USA) were diluted 1:15,000. Signals were detected using an Odyssey CLx imaging system (LI-COR Biosciences). Confocal images of Neuro2a cells transiently transfected with wild-type and truncated Panx1a were collected and processed using the LSM 510 META software (Zeiss LSM700 system; Carl Zeiss MicroImaging, Oberkochen, Germany).

2.10. Immunohistochemistry (IHC) analysis

Adult zebrafish were euthanized in MS-222 solution (0.02% w/v, Sigma-Aldrich). Eyes were removed and fixed in 4% paraformaldehyde (PFA) in 1xPBS overnight at 4oC, followed by cryoprotection in 30% sucrose in 1xPBS. After embedding in Tissue-Tek O.C.T compound, 10 μm sections were cut on a cryotome (Thermofisher). Samples were washed three times for 5 min with 1xPBS containing 0.1% Tween-20 (PBST) at RT. Unspecific binding sites were blocked with freshly prepared 5% normal goat serum (NGS, Sigma-Aldrich) in PBST for 4hr at 4℃ (Lindsey et al., 2018). Following blocking, samples were incubated with primary antibody (1:100, affinity-purified rabbit anti-Panx1a antibody, code#ZOI-A2, Davids Biotechnologie GmbH; 1:500, anti-PSD-95, clone 7E3-1B8, Sigma-Aldrich) overnight at 4°C. Subsequent washes with PBST were for one hour at 4℃. Alexa 488 and Alexa 546 goat anti-rabbit/mouse secondary antibodies (1:3000 in 1% NGS PBST, Life Technologies) were applied for one hr at RT℃. After three washes with PBST followed by one wash with PBS, specimens were mounted on microscope slides using

ProLong Antifade with DAPI (Thermofisher). Confocal images were collected using LSM-ZEN2 software (Zeiss LSM700 system; Carl Zeiss MicroImaging, Oberkochen, Germany) with a Plan-Apochromat 63x/1.3 oil DIC M27 objective using the identical settings.

2.11. Whole-mount immunohistochemistry (WMIHC) analysis

Larvae at 3dpf were chosen over 6dpf larvae because of more efficient antibody penetration and low pigmentation. At this stage, all retina layers are fully developed (Malicki et al., 1996; Schmitt and Dowling, 1999). The larvae were euthanized in MS-222 solution (0.02% w/v, Sigma-Aldrich) and fixed in 4% paraformaldehyde (PFA) in 1xPBS overnight at 4℃. Samples were washed three times for 5 min with 1xPBS containing 0.1% Tween-20 (PBST) before a permeabilization step with pre-chilled acetone for 20 min at -20℃. Unspecific binding sites were blocked with freshly prepared 10% normal goat serum (NGS, Sigma-Aldrich) in PBST for 4hr at 4℃. Following blocking, samples were incubated with primary antibody (1:200, affinity-purified rabbit anti-TH antibody, Sigma-Aldrich cat# SAB2701683) for 2-3 days at 4°C. Subsequent washes with PBST were for 5 hours at 4℃. Alexa 488 goat anti-rabbit secondary antibody (1:500 in 1% NGS PBST, Life Technologies) was applied for 48 h at 4℃. Specimens were infiltrated with 75% glycerol in 1xPBS, mounted on microscope slides using 0.8% low melt point agarose (BioShop, Canada). Images were acquired using a Plan-Apochromat 20X/0.8 objective and were processed using Zeiss LSM-ZEN software and the Fiji program (Schindelin et al., 2012). The brightness and contrast of the images were adjusted using the Fiji program. Whole retinas were positioned laterally or flat, and Z-stack images were taken. The data were stored and used for off-line analysis. When indicated, z-stacks were deconvoluted using

the ImageJ plugins Iterative Deconvolve3D and Diffraction PSF3D (Dougherty, 2005). The cell bodies of the typical large tyrosine hydroxylase stained cells (Matsui and Sugie, 2017) were counted manually. Data were expressed as mean ± SD. Non-injected larvae or excluding the primary antibody served as controls.

2.12. Behavioral assays

All behavioral observations were performed on 5 or 6 dpf larvae of two genotypes, WT-TL and *panx1s*$^{-/-}$. Except for the habituation assays, all the experiments were performed between 12 to 4 pm, as larvae (6dpf) activity was previously reported to reach a stable level by early afternoon (MacPhail et al., 2009). A Zebrabox® behavior recording system (ViewPoint Life Technology, Lyon, France; http://www.viewpoint.fr) was used to record the tests. Only OMR assays were performed using a separate custom-built system. The detailed procedures are described below.

2.12.1. Freely swimming behavior assay

Larval swimming activity under constant Light-ON and Light-OFF conditions was tested using 24-well plates. Larvae were adapted to the environment for 3 hrs before recording. For tracking in light, larvae were adapted to ambient light (30% of final output intensity), whereas for tracking in the dark, larvae were acclimatized to darkness (0% of final output intensity). The locomotor behavior was tracked for 60 min. Three thresholds were defined for the speed of movements: slow (<2 mm/sec), medium (2-20 mm/sec), and fast (>20 mm/sec). The mean traveled distance (mm) and velocity (mm/sec) in two swim speeds (medium and fast) was used for statistical analysis.

2.12.2. The visual motor response (VMR) assay

We implemented the VMR assay based on the same configurations established elsewhere (Emran, Rihel and Dowling, 2008). Typically, the activities of 48 larvae were recorded simultaneously. The larvae were placed into the Zebrabox system to adapt to the darkness for 3.5 h. After 3 hours of dark adaptation, the video recording started to obtain the baseline activity data. Then, the actual test started, which consisted of three trials of alternating light onset (Light-ON) and light offset (Light-OFF) periods, with each period lasted for 30 minutes (for a total of 180 min). The Light-ON stimulus was set to 100%, and the Light-OFF stimulus was set at 0% of the final output intensity.

The Quantization® mode of the Zebralab software was used to collect the behavioral data. In this mode, two thresholds need to be adjusted in order to detect larvae movement. First, a detection threshold value should be set to define active pixels. In this study, the detection sensitivity was set at 6. It implies if changes in the grey level in successive frames were more than 6, the larva was considered moving. Next, a burst cut-off value was set to distinguish between small and large movement episodes. The burst threshold of 20 was used in this study. When the number of active pixels between frames was larger than 20, it was counted as a large (burst) movement. Any changes less than 20, was regarded as the small (medium; mid) movement. The activity data were collected per second. We noticed the sum of mid and burst activity duration, a parameter that is defined as “Total Activity Duration (TAD)”, provides valuable information for a better understanding of Panx1a deficiency effects on locomotion. We conducted triplicates of the VMR assay and calculated the TAD value for each larva at every second of the

experiment. To specifically examine the larval behavior upon abrupt light change, we analyzed the mean activity of the animals from 1 min before the light change to 1 min after the light change.

2.12.3. Optomotor response (OMR)

The optomotor response is an innate visual behavior of all animals and humans to follow their surroundings' motion to stabilize location or course (Naumann et al., 2016; Kist and Portugues, 2019; Bahl and Engert, 2020). OMR experiments were performed using custom-built apparatus (***Supplementary Fig. 2.1)***. Briefly, stimuli were presented from below using an ASUS P3B 800-Lumen LED portable projector (https://www.asus.com/ca-en/Projectors/P3B/). The fish movements were recorded using a USB 3.1 high-speed camera (XIMEA GmbH, Germany) equipped with a 35mm C Series Fixed Focal Length Lens (Edmund Optics Inc., USA). An 830 nm long-pass filter (Edmund Optics Inc., USA) was used to block infrared illumination coming from a source at the bottom of the test environment. The videos were recorded using XIMEA Windows Software Package (https://www.ximea.com/support/wiki/apis/XIMEA_Windows_Software_Package). The visual stimuli were generated using the "Moving Grating" program, an online stimulus generator freely available at http://michaelbach.de/stim/.

The Visual stimulus consisted of sequences of binary (i.e., "black and white" or "gray and white") bars. The stimuli were generated with three spatial frequencies (64,128 and 256 pixels/cycles). Each spatial frequency was tested at two different speed rates (72 and 144 pixels/sec), and two contrast levels (i.e., 10 and 100% of the final contrast output on the

program, resulting in “gray and white” or “black and white” bars, respectively). Stimuli were presented to larvae (n=10) for 90 sec, twice in each left or right direction.

Larvae (6 dpf) were transferred to a 3 cm Petri dish (Thermo Scientific) and allowed to acclimatize for 5 min before video recording. To quantify the population response to optomotor stimuli, the Petri dish was subdivided into three zones: for each grating motion direction, the last section of the area was denoted as the “target zone.” The proportion of the larvae in the “target zone” at the end of each trial was counted in relation to the total number of fish and called the percentage of positive response (PPR). The difference in the PPR of the fish after a rightward or a leftward presentation of a stimulus is a measure of the strength of the optomotor response.

2.12.4. Color preference test

Color preference test was performed in a cross maze (***Supplementary Fig. 2.2***). The custom-made maze was built using 5mm transparent acrylic sheets. The maze consisted of 4 double-walled arms and remained uncovered on top. The interior dimension of each arm was 15 (W) × 35 (L) × 10 (H) mm. The space between the two walls of each wall was filled with different color sleeves to provide different color cues (B; blue, G; green, R; red, Y; yellow, N; no color). In each test, a total number of up to 20 larvae (6 dpf) was used. Dark-adapted (for 2 hours) larvae were video tracked first for 5 min in the dark to map the random distribution of larvae among the arms, then for 30 min in light condition (set at 30% final intensity output) in the zebrabox system (ViewPoint Life Technology, Lyon, France; http://www.viewpoint.fr). The test’s output videos were analyzed manually for the

larvae count in each arm at the end of the experiments. To eliminate any spatial bias, color sleeves were moved to opposite arms after each experiment.

2.12.5. Visual habituation

Dark flash-induced scape responses were elicited and measured as described previously (Wolman et al., 2011; Randlett et al., 2019). We developed a paradigm that consists of four training blocks of 60 dark flashes (1 sec) at 59 sec interstimulus intervals, with blocks separated by 1 hour resting period. Larvae were maintained in the dark when not training or testing. Memory retention (MR) was tested in a "Post-test" block 24 hours after training. The Dark flash responses were identified as movement events with a burst of hyperactivity greater than the threshold (i.e., 15 in the Zebrabox quantization mode). The larvae that did not perform a response for a given stimulus were excluded from the analysis at that stimulus.

The space training-induced habituation was calculated by measuring the reduction of mean responsiveness for the 60 flashes in training Trial 4, relative to that in Trial 1, using Formula 2.1.

$$Percent\ Habituation\ (PH) = \left(\frac{Trial\ 1 - Trail4}{\text{Trial 1}}\right) \times\ 100$$

Formula 2.1.

To quantify larval memory retention, the averaged response at each dark flash in the Post-test block was divided by the mean responses in Trial 4. These distributions were plotted using a bar plot.

The differences in dark flash responsiveness in trained and untrained larvae were calculated using the mean response across groups population at each dark flash for Trial 1 and Post-test Trial. The calculated mean vector trained larvae was divided by the untrained mean vector, and the result was plotted using a bar graph. The statistical analysis is done in R and explained below.

2.13. Pharmacology

All drugs were purchased from Sigma-Aldrich (Mississauga, Canada), catalogue numbers: R-(–)-apomorphine hydrochloride hemihydrate (cat#A4393); R-(+)-SCH-23390 hydrochloride (cat#D054); haloperidol (cat#H1512), Probenecid (cat#P8761), Adenosine (cat#), Ethyl3-aminobenzoate methanesulfonate (MS-222; A5040). Except for haloperidol, all compounds were dissolved in E3 buffer. Haloperidol stock solution was made in dimethyl sulfoxide (DMSO), and DMSO served as vehicle control where appropriate. The final concentration of DMSO was always <0.5% v/v, which has shown no effects on zebrafish larvae locomotion (Christou et al., 2020).

The dose-response curves for each compound were first generated. Larvae in a 48-well plate were exposed to a range of drug concentrations and allowed to incubate for 10 minutes before recording. The activity was video recorded for 90 min in constant dark (0% final light output) or light (30% final light output) conditions. Each compound was tested at six concentrations (0.1, 1, 5, 10, 20, 50 μM), eight wells per concentration, and in triplicate. The concentrations selected for the VMR assays represent doses that illustrate the trends discussed in the text.

2.14. Inferential statistics

Unless otherwise stated, all statistical analyses were performed in R software version 3.4.0 (http://www.r-project.org), and results are represented as the mean ± standard error of the mean (SEM) of 3 repeated experiments. A p-value<0.05 was considered statistically significant. The average values for protein assays, cell count, electrophysiology data, traveled distance, velocity, color vision, and OMR were compared between two groups using Student's t-test (with equal variance) or Welch's t-test (without equal variance) as indicated. Details of procedures and software packages used for the VMR and Habituation analyses are described below.

2.14.1. Analysis of VMR data

VMR data represent seven variables: the counts and the duration of time larvae spend performing each of the three predefined swimming parameters (i.e., freeze, scoot, and burst) plus the total activity duration (TAD). In order to unambiguously evaluate the nature of behavioral responses to visual stimuli, the multiple components were disentangled by a principal component analysis (PCA) using the "FactoMineR" and "Factoextra" packages. First, the PCA scores were Varimax rotated according to the standard PCA approach (Cattell, 1978). The orthogonal configuration of varimax rotation guarantees the different components are uncorrelated; thus, each represents an independent behavioral pattern. The resulting values termed "eigenvalues" signify the amount of variance explained by each of the components. To visualize and compare the size of the eigenvalues we used Scree plots. Only the first two components were retained for further interpretation since their eigenvalues were greater than 1 and they accounted for more

than 90% of total variance in the data. Next, the variables contribution percentage to each of the two retained components were computed and plotted. The most informative variable, "TAD", was compared between groups using nonparametric rank-based exact multiple contrast testing and simultaneous confidence intervals (MCTP/ SCI) (nparcomp package; http://www.R-project.org). Mean TAD values of the entire test period were plotted to show control and mutant larvae activity patterns. The activity data from 1 min before (-60 sec) to 1 min after (+60 sec) light changes were plotted separately to visualize the locomotor activity differences of the two genotypes upon after abrupt light switches. To visualize the effects of different drugs treatments on "TAD" of larvae upon light switches, we used line charts. The baseline activity (from 1 min before light switches) were used to compare the amount of change occurring in any of the two mentioned activity features during the first 1 second after light switches.

2.14.2. Analysis of habituation data

The multiple regression model was used to assess the statistical significance of the difference between groups' PH and MR mean vectors. Two R packages, i.e., "tidyverse" and "car," were used for the analysis. The normality and homogeneity of the data variance were checked by the "Shapiro-Wilk Test" and "Levene's Test," respectively. The "lm" and the model statistical "summary" functions were used to fit a regression model. Then, the "TukeyHSD" function was used to detect the significant differences (significant: p-value<0.05).

2.15. Supplementary Figures

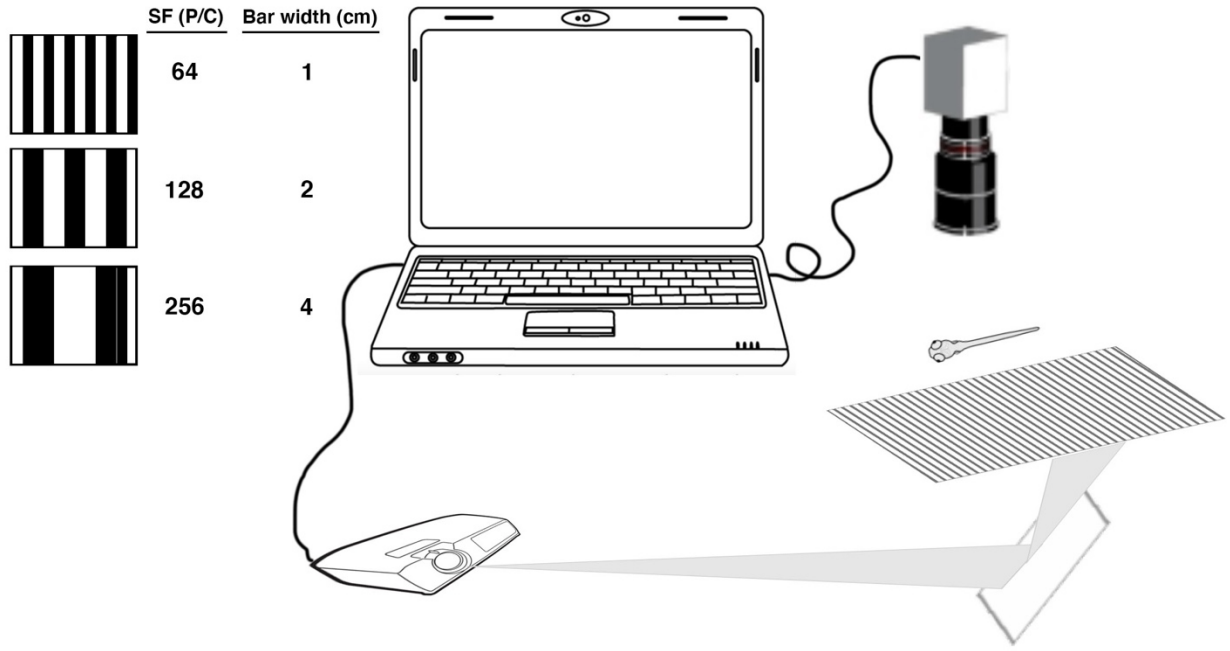

Supplementary Figure 2.1. Optomotor response (OMR) test apparatus. *The visual stimuli were generated using "Moving Grating" software, freely available on http://michaelbach.de/stim/, and presented to the fish from below. The fish movements were recorded by an XIMEA USB 3.1 high-speed camera. The tree spatial frequencies (SF) used in this experiment were 64, 128, and 256 (pixels/cycle). The bar width of each SF is shown in centimeter (cm). (Created by N.S.).*

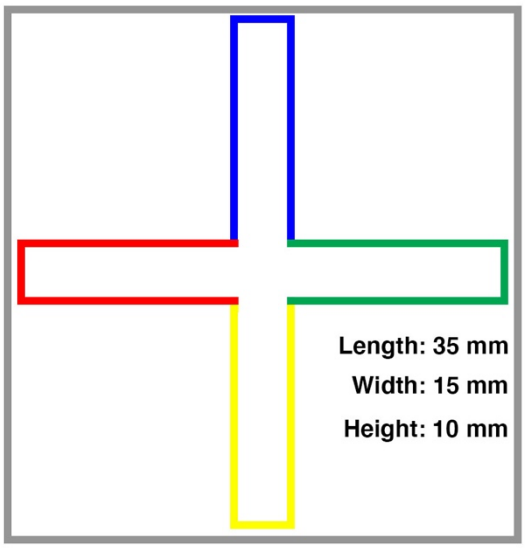

Supplementary Figure 2.2. Color maze. *The custom-made maze was built using 5mm transparent acrylic sheets. The maze consisted of 4 double-walled arms and remained uncovered on top. The interior dimension of each arm was 15 (W) × 35 (L) × 10 (H) mm. The space between the two walls of each wall was filled with different color sleeves to provide different color cues (B; blue, G; green, R; red, Y; yellow, N; no color; designed by N.S.).*

2.16. Supplementary Tables

Supplementary Table 2.1. Summary of genes and primers.

Gene	*Gene-ID*	*Function*	*Forward Primer (5‘ – 3‘)*	*Reverse Primer (5‘ – 3‘)*	*Application*
opn1lw2	NM_001002443	G-protein coupled receptor	CCAACAGCAATAACACAAGGG	GCGACAACCACAAAGAACATC	RT-qPCR
opn1mw1	NM_131253	G-protein coupled receptor	GGCTGTGTAATGGAGGGATTC	ATGGTTTGCGGAGAATTTGAAG	RT-qPCR
opn1mw2	NM_182891	G-protein coupled receptor	GCTTTCGCTGGAACAATTATGG	ACAAGAGACCAAAGAGCAACC	RT-qPCR
opn1sw1	NM_131319	G-protein coupled receptor	TCATTTTCTCCTACTCACAGCTC	CACAAAAGAGCCAACCATCAC	RT-qPCR
opn1sw2	NM_131192	G-protein coupled receptor	GGTTCCTTTCAGCACCATTG	AGAAGCCGAACACCATTACC	RT-qPCR
opn4.1	NM_178289	G-protein coupled receptor	GTGATTGGAAATGCACTGGTG	CTGTGTAAACTGGCTGCAAAG	RT-qPCR
rho	NM_131084	G-protein coupled receptor	AGTCCTGCCCAGACATCTAG	GTACTGTGGGTATTCGTATGGG	RT-qPCR
gnat1	NM_131868	heterotrimeric G-protein	CGTCAAGTTTGTGTTCGATGC	GAGGAAACGAGCTACAAGGAG	RT-qPCR
gnat2	NM_131869	heterotrimeric G-protein	CAAACCTGACTACCTTCCCAC	TCTTCCTCTCGGACCTCTG	RT-qPCR
pde6c	NM_200871	cGMP 3',5'- cyclic phosphodiesterase	CATATTTGCCACAGTCATCGC	AGAGCCTTGTGAAACTGACG	RT-qPCR
pde6ha	NM_001305554	cGMP 3',5'- cyclic phosphodiesterase	AAGTTCAAGCAGAGGACCAC	TCCATGTCTCCAAACGCTTC	RT-qPCR
guca1c	NM_194393	guanylate cyclase activator	TTTCGTGGAGTACATCGCTG	GGTCTCCATTTCATCTCTGTCG	RT-qPCR

gucy2d	NM_131866	guanylate cyclase	AGAAGGAAACTGAATGACGAGAG	CCCAGTCACCCTCAAATACAG	RT-qPCR
gna11b	NM_001007773	heterotrimeric G-protein	TTTGTGGATCTGAACCCTGAC	AAGCGGATGTTCTCTGTGTC	RT-qPCR
grk7b	NM_001033090	non-receptor serine/threonine protein kinase	ACGAGAAGGAGATCAAGAAACG	ACTGACGGAAACATGCTCTC	RT-qPCR
p2rx1	NM_198982	P2X purinoreceptor	CCCAGTTTGATGTAGTCAGGAG	AAACTGAACCCGTATCGCTC	RT-qPCR
p2rx5	NM_194413	P2X purinoreceptor	AGTAAATGGAAAGGCTGGGAG	CTCTCGGTAAAAGGAGCTCTTG	RT-qPCR
p2rx7	NM_198984	P2X purinoreceptor	CCTTACAGGAGCAACTGTGC	AAAGCGTTCTCCAGGACAGA	RT-qPCR
adora1b	NM_001128584	adenosine receptor subunit	GGAACAATTTACACAGCCTGC	ACGAGCATGAAAAGCAGAGG	RT-qPCR
cacna1da	NM_203484	voltage-dependent l-type calcium channel subunit	GGATGAGAAGGATAATGCCGAG	GGGTTTGTGTTGCTGAAGATG	RT-qPCR
kcnc1a	NM_001128725	potassium voltage-gated channel subfamily c	TGTAAGTCTGCCATGAACTCG	TTCACTTTGGGATCTGCTCTG	RT-qPCR
kcnc1b	NM_001195197	potassium voltage-gated channel subfamily c	CTGTCCTCACATCGACCAAG	CATAACCCTTCCTGACTCTTCC	RT-qPCR
kcna2b	NM_001362628	potassium voltage-gated channel subfamily a	CATTGGAGGCAAAATCGTGG	TGTTCCTCTCCCTCTGTCTC	RT-qPCR
kcnh4a	NM_001322433	potassium voltage-gated channel, subfamily h	CACAACCTCACCTACAACCTC	GTCTCCTGCCTAAATCCTGC	RT-qPCR
trpv4	NM_001042730	transient receptor potential cation channel subfamily v	GAGATCCCAACTTCCCCATG	TTCTGCTTCTGGTCGTTCTG	RT-qPCR
trpm6	NM_001251831	transient receptor potential cation channel subfamily m	TGTCGTGCTAAGTATGTGCG	GAAGTTATCTGTCCCTCCGTG	RT-qPCR

drd1a	XM_017359120	G-protein coupled receptor	CTCATCTCCTTCATCCCAGTG	ATATGTTCGGTTGAGGCTGG	RT-qPCR
drd1b	NM_001135976	G-protein coupled receptor	ACGCTGTCCATCCTTATCTC	TGTCCGATTAAGGCTGGAG	RT-qPCR
drd2a	NM_183068	G-protein coupled receptor	ATCGGGATGGGTGCATTTC	TGGTACTCCGGAAAAGACG	RT-qPCR
drd2b	NM_197936	G-protein coupled receptor	ACCTCCAAGTCCCAATCATG	GTTCGGGTTTTGCCATTAGG	RT-qPCR
drd2c	AY333792	G-protein coupled receptor	ACCTCCAAGTCCCAATCATG	GTTCGGGTTTTGCCATTAGG	RT-qPCR
drd3	NM_183067	G-protein coupled receptor	ATCAGTATCGACAGGTATACAGC	CCAAACAGTAGAGGGCAGG	RT-qPCR
drd4a	NM_001012616	G-protein coupled receptor	CTTACCGCTGTTTGTGTATGC	ATGAACCTGTCTATGCTGATGG	RT-qPCR
drd4b	NM_001012618	G-protein coupled receptor	TTACCCCTGTTTGTCTATGCTG	GGCTATAAACCTGTCCACACTG	RT-qPCR
drd5a	XM_003199767	G-protein coupled receptor	ACCAACTCTTCGCTCAACC	TCGTTGCTGATGTTGACCG	RT-qPCR
th	NM_001001829	monooxygenase	TTGTGTCCGAGAGCTTTGAG	AAGCATTCTGGATCTTGGAGG	RT-qPCR
ddc	NM_213342	decarboxylase	CCGCAAGCATGTAGGACTG	GCTGTTGATCCTCTTCAGCAG	RT-qPCR
slc6a3 (DAT)	NM_131755	transporter	GAATCGACAGTGCTATGGGAG	CAGATGAGCGAGATGAGGAAG	RT-qPCR
slc18a2 (VMAT2)	NM_001256225	transporter	AGCTCCTTTTCTTATCCTGGC	TGCAATGAGGATGTATGGGTC	RT-qPCR
comta	NM_001030157	methyltransferase	TGACCACTATTGCAGACACAG	GATGCGAACAGTAGAGTATCCG	RT-qPCR

mao	NM_212827	oxidase	CGGCTTTGTGGTTTCTTTGG	GCTTCACTCGATCACCCAG	RT-qPCR
panx1a	NM_200916	pannexin	TGGATACAAACAGCTCTGTGATAG	ATCCTTTAGAGTAGCGCTTGG	RT-qPCR
panx1b	NM_001100030	pannexin	AAGTATAAAGGCGTGCGGCTGG	TGATCTGAGTACCCACGGAGAC	RT-qPCR
panx2	NM_001256641	pannexin	TCGACTGAGAGGACAAACCC	TCGCCACCAACTTCACAACTC	RT-qPCR
panx3	XM_001919826	pannexin	CATACAACCGCTCTGTCCGT	GCTTGCGTTTGGCTCTCTC	RT-qPCR
panx1a	NM_200916	pannexin	AGCTCTGTGATAGACCTCACTGAGAGC	GATGTAGCTCAGGAGCTGAAAGATGC	genotyping
actb1	NM_131031	actin, cytoplasmic	TGAGCAGGAGATGGGAACC	CAACGGAAACGCTCATTGC	Normalization
actb2	NM_181601	actin, cytoplasmic	GCCCCTAGCACAATGAAGATC	GACTCATCGTACTCCTGCTTG	Normalization
tuba1b	NM_194388	tubulin, cytoplasmic	GAGCGTCCTACTTACACCAAC	AGGGAAGTGGATACGAGGATAG	Normalization
b2m	L05383	major histocompatibility complex antigen	GCCTTCACCCCAGAGAAAGG	GCGGTTGGGATTTACATGTTG	Normalization
tbp	NM_200096	tata box- binding protein-like protein	CGGTGGATCCTGCGAATTA	TGACAGGTTATGAAGCAAAACAACA	Normalization

eef1a1l1	NM_131263	eukaryotic translation elongation factor 1 alpha 1, like 1	GTACTTCTCAGGCTGACTGTG	ACGATCAGCTGTTTCACTCC	Normalization
per1a	NM_001030183.1	Period circadian clock 1a	GGAAAAGGCTCAGCCACAGA	TGAACTTCCGCTCAAAAGAC	RT-qPCR
per1b	NM_212439.2	Period circadian clock 1b	GAGGGAGACAGTCAAACAGAAG	AGAAGGGCTGTGAGAGTTTG	RT-qPCR
per2	NM_182857.2	Period circadian clock 2	CGTGCCCATTACAGTGAAGAG	ATGTTGACAGACCTGACTGC	RT-qPCR
per3	NM_131584.1	Period circadian clock 3	CAAGTACAAGCAAACAGCGAG	ACTACCACAAAAGAGTCCGTG	RT-qPCR
arntl1a/bmal1a	NM_131577.1	aryl hydrocarbon receptor nuclear translocator-like 1a	TCAGATTGTTCCTGGTATTCCTG	GCGTGGCAGTGATGTTTAAAG	RT-qPCR
arntl1b/bma11b	NM_178300	aryl hydrocarbon receptor nuclear translocator-like 1b	GAGTTCATGTCTCCCAGTTCC	GTCCTTGTCTGTGTCCATACTG	RT-qPCR
arntl2/Bmal2	NM_131578.2	aryl hydrocarbon receptor nuclear translocator-like 2	ATGAACTCAAGCACCTCGTC	CTCTGTCCAATTAACTCCGTCC	RT-qPCR
nr1d1	NM_205729.2	nuclear receptor subfamily 1, group d, member 1	AGCGACCTCCAAACAGTAAC	GGGTCTGAGTAAGGATGCATG	RT-qPCR
clocka	NM_130957.2	clock circadian regulator a	CATCTCTTGTGTCTCAGCCTC	GTCTCTGGATGTTTGCCTCA	RT-qPCR
clockb	NM_178295.2	clock circadian regulator b	GGTGGATCATGGAGAAGTGT	ATATACAGGCGGTTTCTTGGG	RT-qPCR

clock2/npas2	NM_178299.1	Neuronal PAS domain protein 2	AACATCCTGAACTTCCTGCC	GTTTCCCCTCGCTATATGACAG	RT-qPCR
cipca	NM_001327903.1	CLOCK-interacting pacemaker a	TTGTCCTCAAGCAGCCGAAC	GTACTGTCACCGCTGGGTAA	RT-qPCR
cry1a	NM_001077297.2	cryptochrome circadian regulator 1a	CTCCACGACAATCCTTCACTC	CGTCCAAGTCTTCCAAACAC	RT-qPCR
cry1b	NM_131790.4	cryptochrome circadian regulator 1b	GGTTGGACAAGCTCACAAAC	TTCCTTGGTTAGATGCCGTC	RT-qPCR
cry2	NM_131786.2	cryptochrome circadian regulator 2	CTGTCATGTCGCGTGTTTTAC	CAAAGTTAGGGTTATTGGTGCC	RT-qPCR
cry3b	NM_131792.2	cryptochrome circadian regulator 3b	CAGCAAATGTAAACCGTGGAG	CCTGACCCTATAAGACGATGC	RT-qPCR
cry5	NM_131788.1	cryptochrome circadian regulator 5	CATGACTCAGTTACGACAGGAG	TCAGCGACCAATCAGAATCC	RT-qPCR

Chapter 3. Visual-motor deficiency in panx1a$^{-/-}$ larval zebrafish is linked to the dopaminergic system

Nickie Safarian[1,3], Paige Whyte-Fagundes[1,3], Christiane Zoidl[1], Jorg Grigull[2], Georg Zoidl[1,3*]

Affiliations:

[1]Department of Biology, York University; Toronto, Ontario, Canada

[2]Department of Mathematics and Statistics, York University; Toronto, Ontario, Canada

[3]Center of Vision Research, York University; Toronto, Ontario, M3J1P3; Canada

Acknowledgments

The authors would like to thank Drs. Stephen C. Ekker and Karl J. Clark (Mayo Clinic, Rochester, MN, USA) for generating the TALEN constructs. We would like to thank members of the Center for Applied Genomics (SickKids, Toronto, Canada) for the RNA-seq service. Special thanks to Janet Fleites-Medina for animal husbandry. This work was funded by a Natural Sciences and Engineering Research Council (NSERC) – Discovery Grant (GZ) and a Brain Canada Platform grant (GZ).

Author contributions

Designed the study and wrote the manuscript (N.S. and G.Z); executed experiments (N.S., P.W.F., C.Z.); analyzed data (N.S., P.W.F., J.G.).

Declarations: The authors declare no conflict of interest

3.1. Targeted ablation of panx1a

The *panx1a* mutant allele was generated by TALEN-mediated mutagenesis targeting the single AfeI restriction endonuclease recognition site in the fourth exon of *panx1a* (***Fig. 3.1.a***). Three doses of 30, 60, and 100 pg/TALEN cRNA pair were injected into 1-cell stage embryos of the TL strain. 61% and 38.6% of all F0 embryos developed typically after injection of 30pg/nl and 60pg/nl cRNA, whereas 90% of the embryos developed malformations or died within 24hrs after injection of 100pg/nl (***Fig. 3.1.b***). A concentration of 30pg/nl cRNA was used in follow-up gene-targeting experiments. The restriction fragment length polymorphism test (RFLP) of ten randomly selected embryos revealed a mutagenesis efficiency of ≈ 50%, as evidenced by a partial loss of the restriction enzyme recognition site at the TALENs cut sites (***Fig. 3.1.c***). DNA sequence analysis of multiple microinjected embryos confirmed the efficient introduction of short, 4 to 7 long nucleotide deletions in the *panx1a* exon 4 (***Fig. 3.1.d***). A founder fish carrying a four bp deletion (*panx1a*$^{\Delta 4}$) was selected for further experimentation. The four base pair deletion caused a frameshift at amino acid 195, resulting in a premature stop codon leading to truncated 201-amino-acid protein, lacking most of the 416 amino acid long Panx1a sequence, including two transmembrane regions and the entire carboxyterminal domain (***Fig. 3.1.e***). After transfection into mouse Neuroblastoma 2a (Neuro2a) cells, the subcellular localization of the truncated *panx1a*$^{\Delta 4}$*-EGFP* protein had a diffuse cytoplasmic signal suggesting that the mutant protein was unable to traffic efficiently to the cell membrane (***Fig. 3.1.f***) and unlikely to form functional channels (***Fig. 3.1.f***, left panel). The full-length

panx1a^{wt}*-EGFP* protein was detectable in the plasma membrane (***Fig. 3.1.f***, right panel) in line with previous reports.

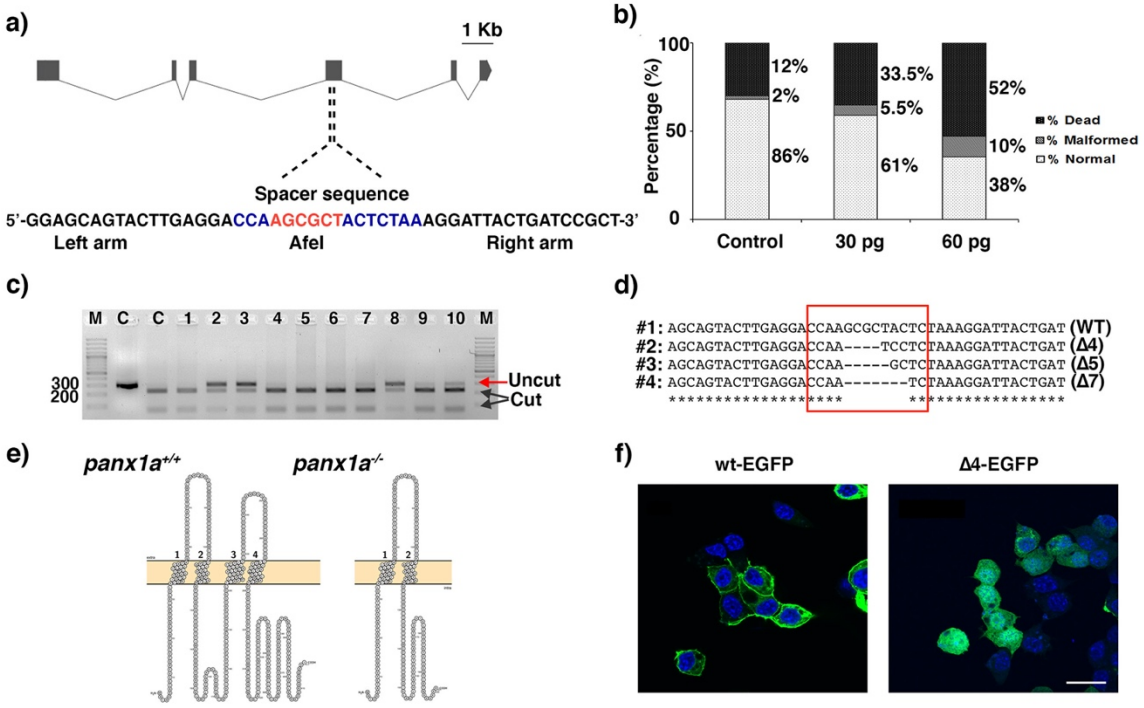

Figure 3.1. Generating panx1a$^{-/-}$ fish using TALENs. *a) The zebrafish panx1a gene structure with six coding exons. The left and right TALENs sequence with the spacer sequence and AfeI restriction site in blue and red is highlighted. b) Larval survival rates (in %) one day after (1dpf) microinjection. A dose of 30pg TALENs pair resulted in more than 50% survival rate and was selected for the experiments generating the panx1a$^{-/-}$ fish line. c) The RFLP-assay shows the loss of the AfeI recognition sequence (indicated by uncut) in four out of ten F0 larvae tested. d) A sequencing alignment is demonstrating small deletions causing frameshift mutations found in three different F0 larvae. e) The predicted sequence features of the mutated panx1a were visualized using the Protter open-source tool (wlab.ethz.ch/protter). A 4 bp deletion in Panx1a exon 4 resulted in a frameshift causing a premature stop codon at amino acid 195. f) Localization of the truncated panx1a protein – Confocal images of transiently transfected proteins panx1a^{wt}-EGFP (left panel) and panx1a$^{\Delta 4}$-EGFP (right panel) in Neuro2a cells. Nuclei were stained with DAPI. Scale bar: 10µm.*

3.2. Characterization of panx1a$^{-/-}$ larvae

The larval survival rate was monitored at 1 and 6 dpf. While at 1dpf a significant reduction in the survival of *panx1a*$^{-/-}$ embryos was detected compared to TL controls (values in %: TL 80; *panx1a*$^{-/-}$ 59.8; TL vs. *panx1a*$^{-/-}$ p = 0.0048), the survival rate improved by day 6 (values in %: TL 83; *panx1a*$^{-/-}$ 86.67; TL vs. *panx1a*$^{-/-}$ p = 0.671; ***Fig.3.2.a***).

A comparison of *panx1*$^{-/-}$ and TL control larvae (F4 generation, 6dpf) revealed no gross anatomical defects (***Fig. 3.2.b***). The body length of 6dpf larvae was measured as an indication of growth which showed a significant reduction in *panx1a*$^{-/-}$ larvae head-to-tail size compared to TL controls (TL control = 3.83±0.27 mm; *panx1a*$^{-/-}$ =3.63±0.31 mm; TL vs. *panx1a*$^{-/-}$ $p < 0.0001$; n=60; ***Fig. 3.2.c***).

Juvenile fish were visually indistinguishable from age-matched TL siblings. Adult *panx1a*$^{-/-}$ zebrafish were viable and fertile like the parental TL strain or heterozygous fish, suggesting that developmental differences were restricted to early developmental stages.

The *panx1a* mRNA level was significantly reduced in 6dpf *panx1a*$^{-/-}$ larvae indicating small deletion-mediated RNA decay (***Fig. 3.2.d***). Compensatory regulation of three other pannexin genes similar to previous reports using Panx1$^{-/-}$ mouse models were excluded. Panx1b mRNA was expressed at equal levels in both TL controls and *panx1a*$^{-/-}$ *larvae*. A low level of *panx3* mRNA expression was detected, but not *panx2* mRNA.

IHC experiments confirmed the reduction of Panx1a expression in the retina of adult zebrafish. No gross anatomical alteration of the retina was noticeable, with immunoreactivity found in TL controls' outer retina, which was reduced in age-matched knock-out retina (***Fig. 3.2.e***). Occasional residual immunoreactivity was found. This was

attributed to cross-reactivity of the affinity-purified antibody with the Panx1b protein, sharing 66% amino acid identity with Panx1a in the carboxyterminal domain.

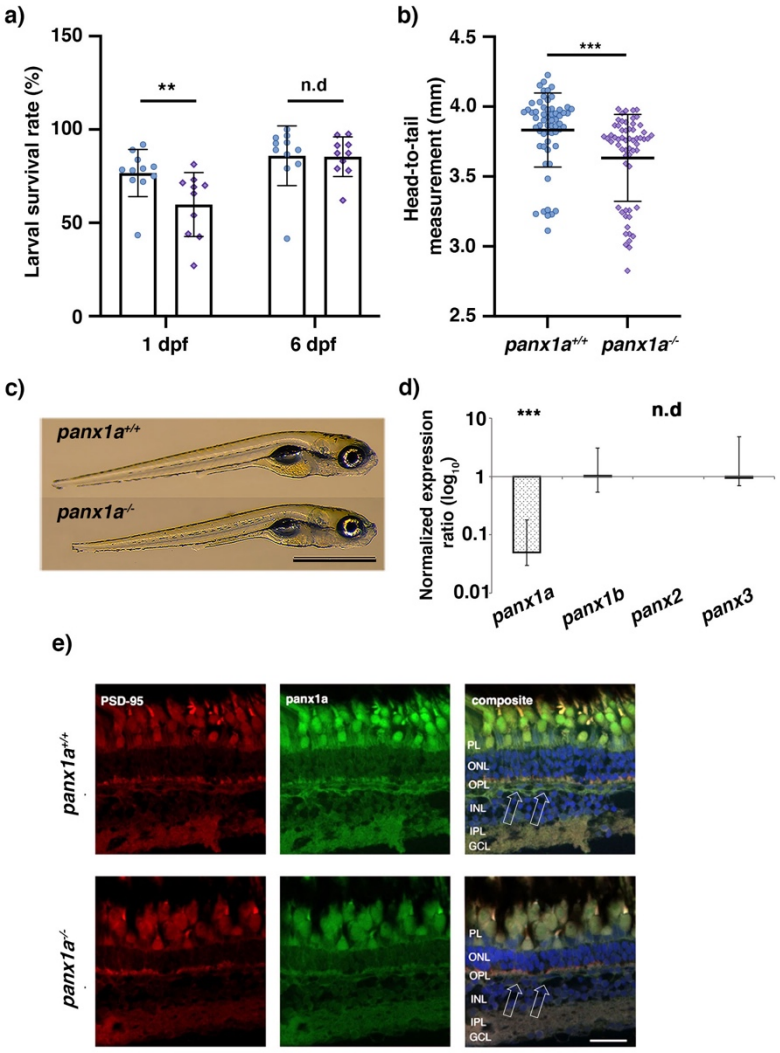

Figure 3.2. Phenotypic characterization of panx1a$^{-/-}$ larvae. *a) Age-matched TL control and panx1a$^{-/-}$ larvae (6dpf) showing regular morphology. b) RT-qPCR analysis of pannexin expression in 6dpf larva. c) Reduction of panx1a expression in the adult panx1a$^{-/-}$ zebrafish. The expression of panx1a was determined using an affinity-purified rabbit anti-panx1a antibody directed against the carboxy-terminal 129 amino acids of the Panx1a protein. Detection of the PSD-95 protein in cone terminals served as an internal control. Cell nuclei were stained with DAPI. Please note Panx1a immunoreactive cells in the cytoplasm and extensions of cells located in the horizontal cell layer of panx1$^{+/+}$ fish. This immunoreactivity is significantly reduced in knockout fish. Residual staining appears to be overlapping with DAPI stained nuclei. Abbreviations: PL, photoreceptor layer; ONL, outer nuclear layer; OPL, outer plexiform layer; INL, inner nuclear layer; IPL, inner plexiform layer; GCL, ganglion cell layer. Scale bar 100μm. n.d., Not detected. Significance: p-value<0.05.*

3.3. Transcriptome profiling of 6dpf panx1a$^{-/-}$ larvae

The transcriptomes of *panx1a*$^{-/-}$ and TL control larvae were compared at 6dpf (NCBI Gene Expression Omnibus (GEO) database; data deposit GSE147068). A total of 12302 RNAs was found in each of the six samples (TL control, n=3; *panx1a*$^{-/-}$, n=3) sequenced. In *panx1a*$^{-/-}$ larva, 1902 RNAs were downregulated, and 933 RNAs upregulated when the cutoff for the false discovery rate (FDR) was set to 0.05, and the significance of regulation was defined as p-value<0.0001. Gene-specific expression information retrieved from the Zebrafish Information Network (ZFIN) database allowed categorizing the representation of regulated genes to those previously described as expressed in the central nervous system (CNS) or visual system. Three hundred seventy-seven upregulated genes and 646 downregulated genes matched genes expressed in the central nervous system (***Fig. 3.3.a***, left panel). Furthermore, 317 upregulated genes and 473 downregulated genes matched genes expressed in the visual system (***Fig. 3.3.a***, right panel).

The AmiGO2 analysis (http://amigo.geneontology.org/amigo/landing) revealed enriched Gene Ontology (GO) terms and pathways (***Supplementary Tables 3.1 and 3.2***). The most significant enriched Reactome processes (cut-off: p-value<0.001; fold change of expression>2.5) (***Fig. 3.3.b***) represented the phototransduction cascade, as well as the processing of mRNAs (***Fig. 3.3.b***. left plot, upregulated genes). Processes such as development and cell signaling through membrane receptors represented downregulated genes (***Fig. 3.3.b***, right plot).

RNAseq data (cutoff: p-value<0.0001; FDR 0.05) were also validated by RNA-qPCR (cutoff: p-value<0.05). This experiment confirmed that targeting *panx1a* upregulated

mRNAs specific for phototransduction and the visual system's development (***Fig. 3.3.c***, ***Supplementary Table 3.3***). Selected purinergic receptors and genes representing voltage-gated ion channel families were confirmed as downregulated in *panx1a*$^{-/-}$ larva (***Fig. 3.3.c***, ***Supplementary Table 3.3***). We concluded that the genetic ablation of *panx1a* in the zebrafish caused a molecular phenotype in which both the visual system and central nervous system were affected in 6 dpf old larvae.

3.4. Loss of panx1a impairs locomotion in the dark

Visually guided behavior was investigated after transcriptome analysis suggested changes to visual functions. At 6dpf, both genotypes, *panx1a*$^{+/+}$ and *panx1a*$^{-/-}$, swam longer distances and more rapidly during the Light-ON phase than during the Light-OFF phase when baseline swimming activity of unrestrained larvae was tested. In light, both genotypes showed no significant difference in the average distance traveled ($t = 1.86$, $df = 133.52$, p-value = 0.06531; n=60) and average velocity ($t = 1.03$, $df = 133.74$, p-value= 0.3065; n=60) (***Fig. 3.4.a***). A representative example illustrates the preference of larvae for swimming close to the wells' circumferences, with spontaneous crossings of the central zone. During the dark phase, *panx1a*$^{-/-}$ larvae were less active and showed intermittent episodes of swimming bouts with slow and medium speeds. *Panx1a*$^{-/-}$ larvae swam significantly less ($t = -3.08$, $df = 135.9$, p-value= 0.002529; n=70) and with lower velocity ($t = -2.79$, $df = 131.73$, p-value= 0.006056; n=70) compared to TL-controls (***Fig. 3.4.b***). Furthermore, *panx1a*$^{-/-}$ larvae avoided crossing the central zone of the well in the dark.

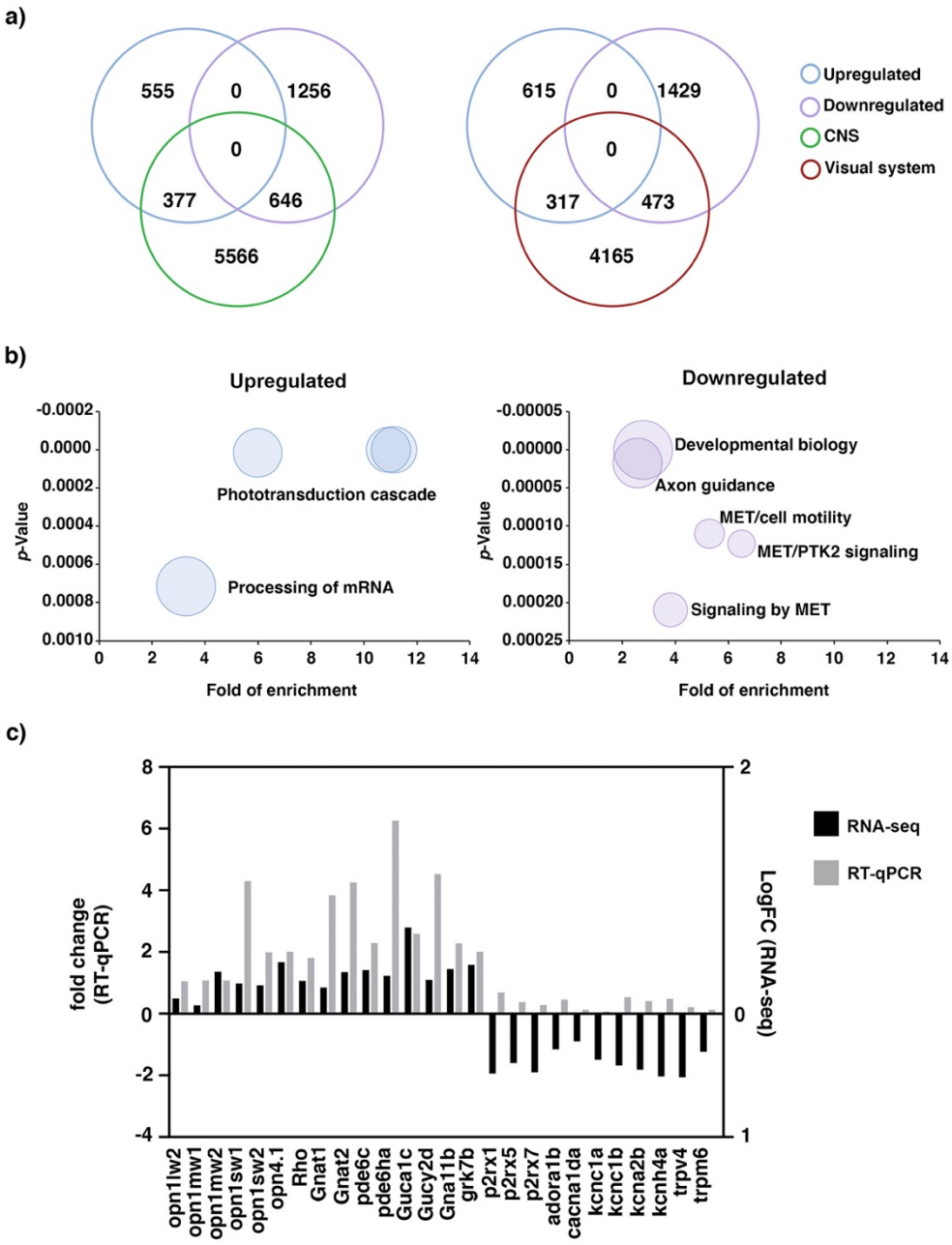

Figure 3.3. RNA-seq analysis of 6dpf panx1a$^{-/-}$ larvae. *a) Comparison of deregulated genes against two categories: central nervous system (CNS) and the visual system. b) GO annotation of RNA-seq data: the upregulated genes were enriched in the phototransduction cascade and mRNA processing pathways. The downregulated genes were annotated for developmental processes and signaling pathways. c) Validation of RNA-seq data by RT-qPCR.*

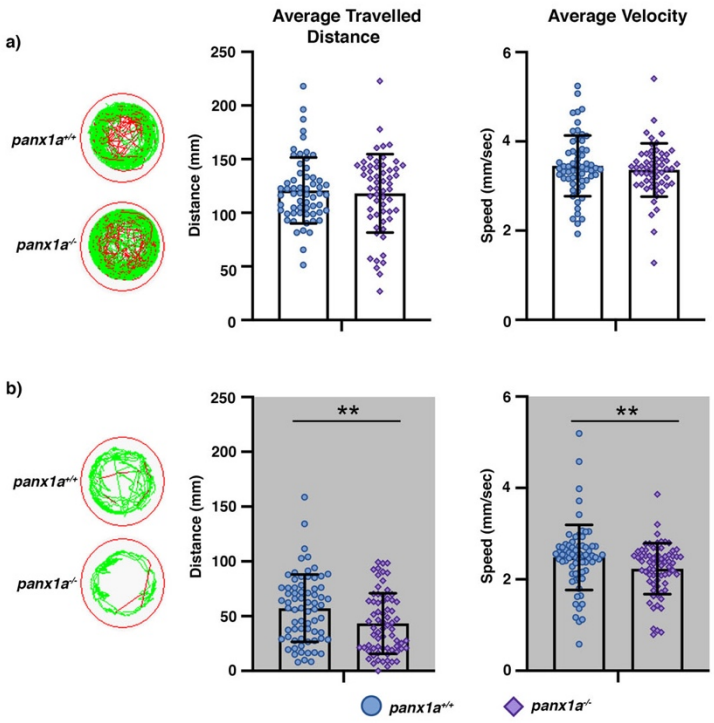

Figure 3.4. Locomotor activity in Light-Dark conditions. *Locomotion was video tracked for 60 min in a) Light-ON and b) Light-OFF conditions. The wells on the left show examples of panx1a$^{-/-}$ and panx1a$^{+/+}$ locomotion patterns. Medium (<20 mm/sec) or high-speed movements (>20 mm/sec) are visualized with green and red colors. Graphs demonstrate the averaged traveled distance (in mm) and the average velocity (mm/sec) of n = 60 larvae for each genotype. Significance: p-value<0.05.*

3.5. Visual-motor response (VMR) in panx1a$^{-/-}$ larvae

The visual-motor response (VMR) assay measured the responsiveness of zebrafish larvae to light changes. The orthogonal transformation of the multidimensional VMR data by principal component analysis (PCA) was used to identify the most relevant of seven behavioral parameters. PC1 and PC2 captured more than 76% and 21% of the data variance (***Fig. 3.5.a***). Two-dimensional PCA plotting confirmed that both genotypes were separated into two distinct clusters (***Fig. 3.5.b***). The variable correlation plot allowed concluding that the total activity duration (TAD; in red) had the most significant

contribution to the variability in PC1 (***Fig. 3.5.c***). Thus, TAD was chosen to determine the differences between genotypes in VMR assays.

TL control and *panx1a*$^{-/-}$ larvae showed distinct VMR, as demonstrated by the corresponding average TAD plots in an experimental paradigm of 3 cycles of alternating Light-ON and Light-OFF periods (***Fig. 3.5.d***; top panel). In all cycles, the larval activity was consistently reduced in the absence of *panx1a* (***Fig. 3.5.d***). In the 1 min period before the Light-ON stimulus (-60-0 s), *panx1a*$^{-/-}$ larvae showed a significantly lower activity level than TL controls (p-value= 0.015). At Light-ON (0-1 sec), both TL controls and mutant larvae augmented their activity immediately; only the peak response to the light stimulus was trending lower in *panx1a*$^{-/-}$ larvae compared to TL controls (p-value= 0.382). During the subsequent light period, both mutants and TL controls gradually returned to the baseline activity level (in 1-60 sec, p-value= 0.876; ***Fig. 3.5.e***).

Notably, at Light-OFF, the mutants responded differently to control TL larvae. For the 1 min period before Light-OFF stimulus (-60-0 s), *panx1a*$^{-/-}$ larvae had lower baseline activity (p-value= 0.036). Following the abrupt loss of illumination (0-1 s), TL control larvae initially increased their locomotor activity, then remained more active for 10$\pm$2 minutes. After that, the magnitude and duration of swim bouts gradually returned to baseline activity level. In contrast, *panx1a*$^{-/-}$ larvae demonstrated a significant reduction (p-value= 0.001) of dark stimulus-response and continued to show a reduced activity during the dark period. This observation was supported by the corresponding TAD plots (***Fig. 3.5.f***), in which the activity of mutants after the light change was noticeably lower when compared to TL controls (p-value= 0.0249). These results indicated that the *panx1a*

mutant fish readily detected the Light-ON stimulus but responded weakly to the Light-OFF condition. Therefore, *panx1a* functions appear important for detecting light decrement and the corresponding behavioral response in larval zebrafish.

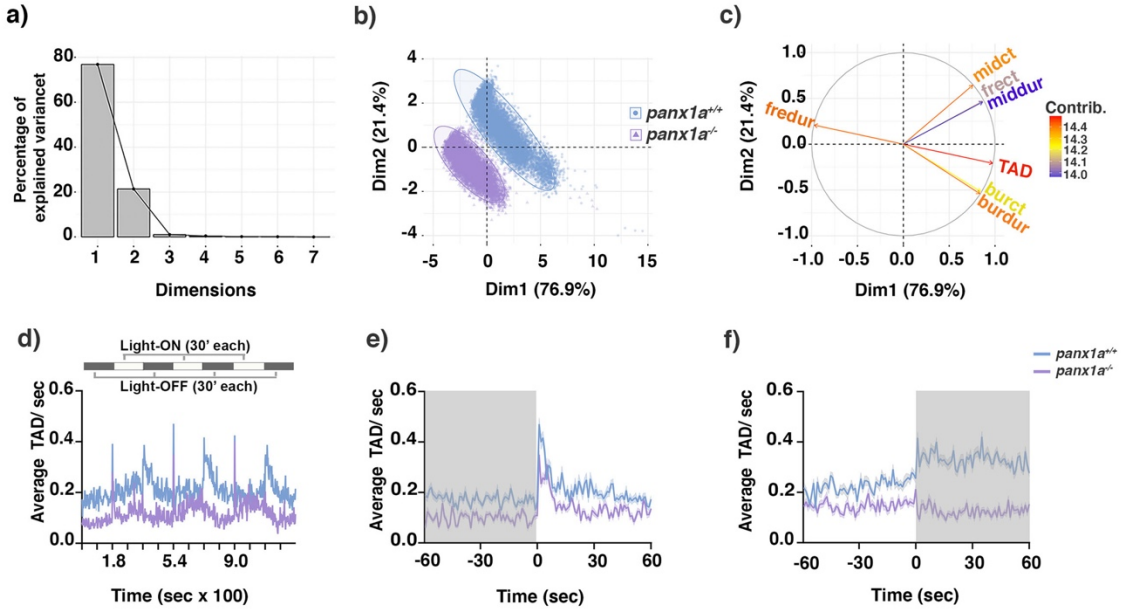

Figure 3.5. Visual-motor response (VMR) changes in panx1a-/- larvae. *a) Principal component analysis (PCA) transforming of the VMR multidimensional data. The scree plot shows that Dimensions 1 and 2 capture more than 76% and 21% of the data variance. b) Mapping individual samples on a two-dimensional space revealed that the two genotype groups were separated into two distinct clusters. c) The variable correlation plot represented the coordinates of the seven variables (i.e., freeze counts(frect) and duration (fredur), medium activity counts (midct) and duration (middur), hyperactivity counts (burct) and duration (burdur), and the total activity duration (TAD)) in the first two dimensions. The variables were colored from blue to red as their contribution to PCs increases. Total activity duration (TAD; in color red) showed the highest contribution to the variability in Dimension 1 and was chosen to visualize differences between genotypes. d) The outline of the experimental paradigm is shown on top. The line graph shows the average TAD of panx1a$^{-/-}$ and panx1a$^{+/+}$ larvae from a representative test with n=24 larvae for each genotype. The activity was defined as the fraction of frames per second that a larva spent swimming (see methods for the detailed information). e, f) The results for average Light-ON and Light-OFF VMR are shown from 1 min before the light switch to 1 min after the light switch. The color ribbons surrounding the average activity line graph correspond to 1 S.E.M. The values are the average of the second trial from four independent tests with n=96 larvae for each genotype. The Light-ON and Light-OFF periods are indicated by white and black bars at the top of the panels. Significance: p-value<0.05.*

3.6. Alterations of the dopamine (DA) signaling pathway in panx1a mutants

Based on the RNA-seq data that revealed D2-type dopamine receptors were among deregulated genes in *panx1a*$^{-/-}$ larvae and observation of their locomotion deficit in the dark, changes to dopaminergic signaling was hypothesized. This idea was tested first by RT-qPCR. Among transcripts of dopaminergic genes located in the presynaptic compartment, a significant up-regulation of the tyrosine hydroxylase gene, which catalyzes the rate-limiting step in DA synthesis, was detected when cut-off criteria for the expression ratio was >1.5, and the p-value <0.05. Other prominent regulated transcripts were slc6a3/dat, a sodium-dependent dopamine transporter, and slc18a2/vmat2, an ATP-dependent vesicular monoamine transporter involved in the dopamine neurotransmitter release cycle (***Fig. 3.6.a***; ***Supplementary Table 3.4***)

Dopamine receptor genes significantly upregulated in *panx1*$^{-/-}$ larvae represented both D1/D2 subfamilies (***Fig. 3.6.a***; ***Supplementary Table 3.4***). A three-fold upregulation of the tyrosine hydroxylase protein in *panx1*$^{-/-}$ larvae (***Fig. 3.6.b***; n=4; p-value < 0.01), along with a significantly higher TH-positive cell count in the retina of *panx1a*$^{-/-}$ larvae (***Fig. 3.6.c***; n=6; p-value = 0.034) complemented the qRT-PCR result.

Apomorphine (Apo), a non-specific dopamine receptors agonist, was used to investigate the overall role of augmented dopamine signaling in *panx1a*$^{-/-}$ and control larvae. Dose-response assays confirmed the known U-shape relationship between Apo concentrations and larval activity in the light and dark (***Supplementary Fig. 3.1.a*** and ***3.1.b***). A concentration of 50 μM Apo, representing the most substantial effect, was selected. The

larval activity during the second trial was analyzed (i.e., 90-120 min) when the maximal effect of Apo was reached.

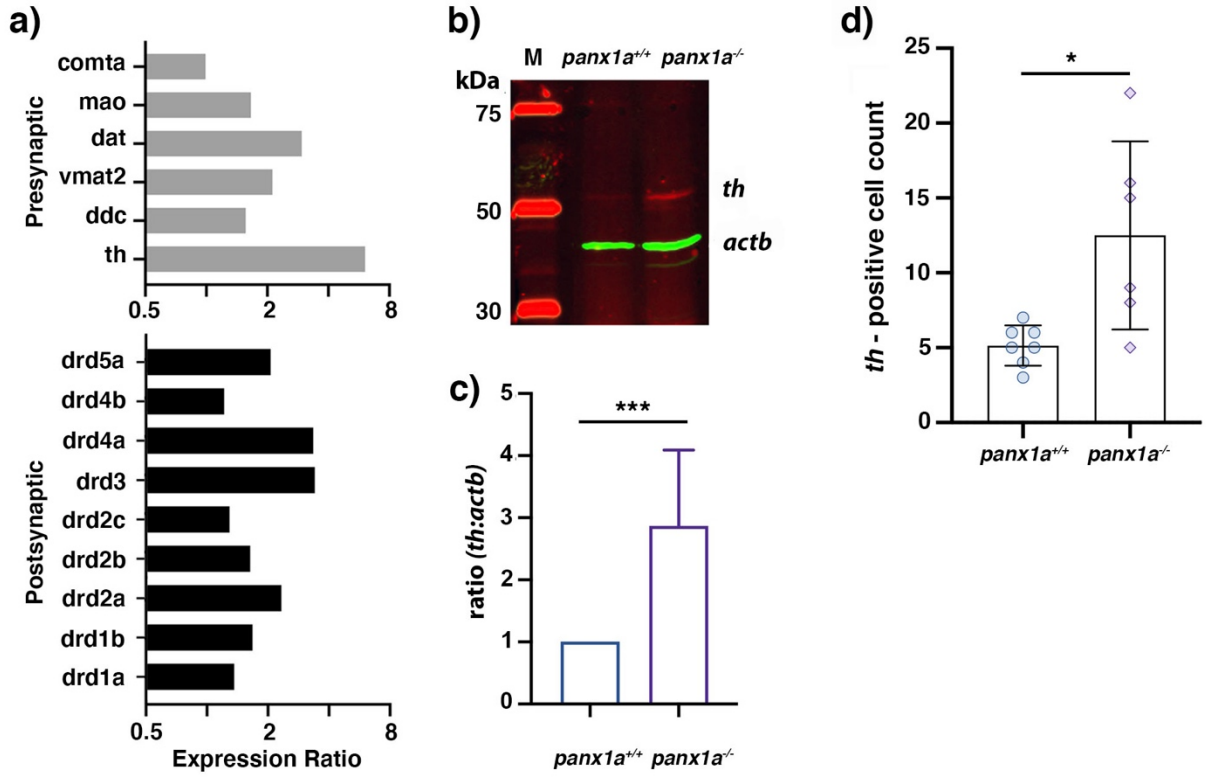

Figure 3.6. Expression modulation in the dopaminergic pathway. *a) RT-qPCR quantification of expression changes. Genes are arranged by typical localization in a dopaminergic synapse. b) Western blot analysis of protein lysates from whole 6dpf larvae showing tyrosine hydroxylase (TH) immunoreactivity and the beta-actin control (ACTB). c) The quantification of TH:ACTB ratio for n=4 independent experiments. d) The count of TH-positive cells in the retinal tissue of TL control and mutant larvae (3 dpf). Mean± SD of n=6 larvae for each genotype is presented. Significance: p-value<0.05.*

Figure 3.7.a exemplifies larvae of both genotypes, which appeared to be hyperactive in the dark period preceding the Light-ON (i.e., -60 to 0 sec). Though, the increment of activity was significant only in mutants. Also, Apo treatment affected the Light-ON peak response (0 to 1 sec period) similarly in both groups. It significantly raised the magnitude of the Light-ON peak response, so no further difference was detected between groups (All the p-values are given in ***Table 3.1***).

When the larval activity was analyzed during the second Light-OFF trail, differing patterns of effects were observed in the two groups. In the light period preceding dark (i.e., -60 to 0 sec), Apo (50 μM) markedly decreased activity in TL controls but did not significantly alter that in *panx1a*$^{-/-}$ larvae (***Fig. 3.7.b***). At the light offset (0 to 1 sec), similar behaviors occurred. Apo abolished the larval peak response to the sudden darkness in TL controls to the point that it resembled a mutant response. No significant difference was observed in the *panx1a*$^{-/-}$ larvae Light-OFF peak response (***Fig. 3.7.b***; All the p-values are given in Table 3.1).

The mean activity data suggested that changes in the lighting conditions affected the levels of activity of larvae given 50 μM Apo (***Fig. 3.7.a*** and ***3.7.b***). While Apo treatment enhanced larval reaction to the sudden illumination (Light-ON) regardless of their genotypes, it suppressed larval response to the sudden darkness (Light-OFF) only in *panx1a*$^{+/+}$. Stimulation of D1/D2 dopaminergic signaling with Apo induced in *panx1a*$^{+/+}$ larvae a *panx1a*$^{-/-}$ like Light-OFF response suggesting a new causal relationship between *panx1a* function, augmentation of dopaminergic signaling, and the described behavioral phenotype.

To accomplish dopamine signaling characteristics in *panx1a*$^{-/-}$ larvae, we investigated which class of dopamine receptor mediates the Light-OFF response. Therefore, we tested the effects of D1- as well as D2-like dopamine receptor antagonists on the Light-OFF component of VMR. In the presence of the D2-antagonist Haloperidol (20 μM) the dopamine-induced Light-OFF response deficiency was robustly rescued in mutants (p-value$<$0.001; n=64), but no significant changes were observed in TL controls (p-

value=0.27; n=64; ***Fig. 3.7.c***). The D1-antagonist SCH23390 (20 μM), resulted in a significant attenuation of the Light-OFF response in TL control larvae (n=34, p-value=0.004), but no effect was exerted on mutants' peak response (n=34; p-value=0.76; ***Fig. 3.8.d***). These results suggest participation of D2-class receptors in dopamine-induced Light-OFF response deficiency observed in *panx1a*$^{-/-}$ zebrafish larvae. All the p-values are given in ***Table 3.2***.

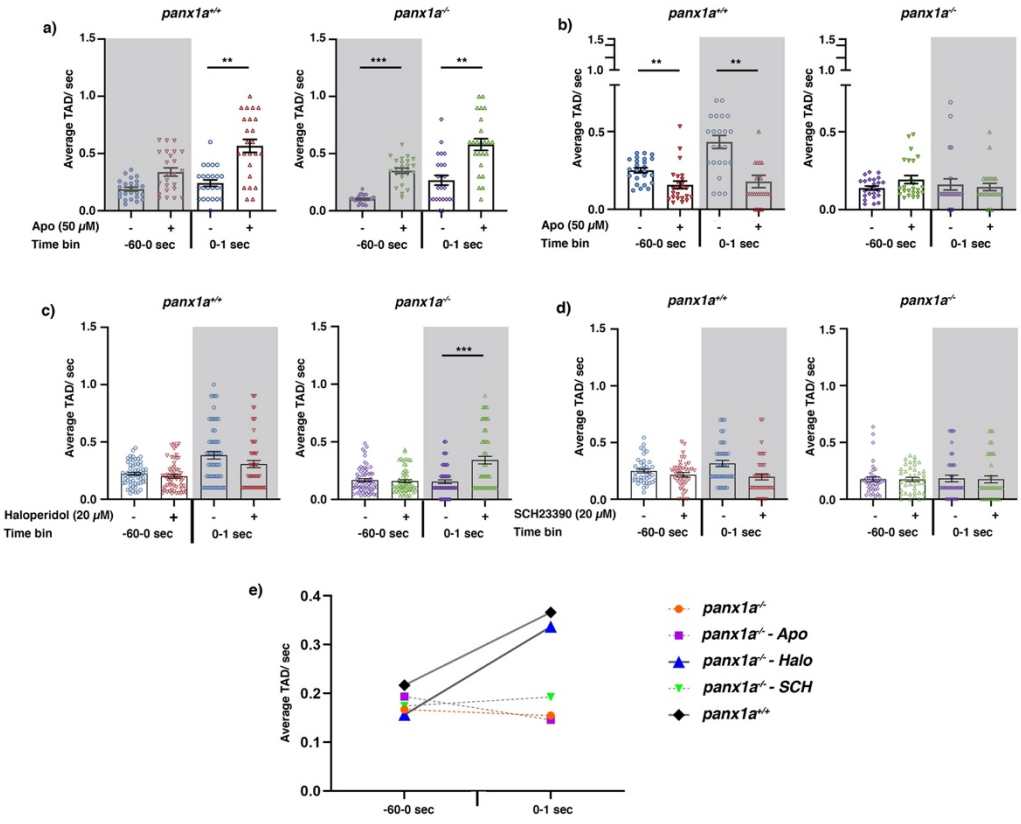

Figure 3.7. Dopaminergic signaling modulates larval visuomotor activity. *The average a) Light-ON and b-d) Light-OFF VMR from 1 min before the light switch to 1 sec after the light switch is graphed as mean±SEM for panx1a*$^{+/+}$ *controls (left panels) and panx1a*$^{-/-}$ *(right panels). a) Apomorphine (a D1/D2-receptor agonist; 50 μM) significantly increases the Light-ON peak response in both genotypes (n=68). b) The suppression of the Light-OFF response observed in control larvae was lost in mutants after Apo treatment (n=68). c) Haloperidol (a D2-receptor antagonist; 20 μM) significantly increases the Light-OFF peak response in mutants (n=64); however, it does not affect the peak response in TL control larvae (n=60). d) Treatment with SCH23390 (a D1-receptor antagonist; 20 μM) slightly attenuates the Light-OFF response in TL controls (n=40) but exerts no significant changes on the phenotype in panx1a*$^{-/-}$ *animals (n=40). e) Changes in the average TAD at the Light-OFF are cross-compared between mutants under different treatments and TL control larvae with no treatment. The line graph illustrates how effectively haloperidol rescues the Light-OFF phenotype in panx1a*$^{-/-}$ *larvae. Significance: p-value<0.05.*

Table 3.1. The multivariate comparisons of VMR between Apo-treated and untreated larvae.

	Type of treatment	Control	Treatment (Apomorphine; 50 μM)		
Typ of stimulus	Genotype / Time bin	+/+ : -/-	+/+	-/-	+/+ : -/-
Light-ON	Before (-60-0 S)	$3.43e^{-07}$	$5.52e^{-01}$	$5.17e^{-08}$	$9.012e^{-01}$
	At (0-1 S)	$6.15e^{-01}$	$7.86e^{-02}$	$3.14e^{-06}$	$4.81e^{-01}$
Light-OFF	Before (-60-0 S)	$4.91e^{-08}$	$2.18e^{-03}$	$5.74e^{-04}$	$9.16e^{-03}$
	At (0-1 S)	$3.408e^{-03}$	$4.86e^{-03}$	$7.87e^{-01}$	$9.74e^{-01}$

Table 3.2. The multivariate comparisons of VMR(Light-OFF) between Haopperidol-treated and untreated larvae.

Type of treatment		Control	Treated		
Antagonists	Genotype / Time bin	+/+ : -/-	+/+	-/-	+/+ : -/-
Haloperidol (20 μM)	Before (-60-0 S)	0.017	0.428	0.942	0.318
	At (0-1 S)	2.73e-06	2.71e-01	1.12e-04	8.25e-01
SCH23390 (20 μM)	Before (-60-0 S)	0.051	0.59	0.98	0.40
	At (0-1 S)	0.018	0.004	0.76	0.99

3.7. Adenosine receptors lie at the interface between Panx1a channels and D2-type dopamine receptors

The interactions between adenosine and dopamine signaling pathways in the CNS are a well-known phenomenon. Specifically, the antagonistic interaction between A2A and D2-type receptors (i.e., postsynaptic inhibition of D2-type receptors by A2AR) has implications in both pathophysiology and treatment of basal ganglia disorders (Ferré et al., 1992; Fuxe et al., 2007, 2010; Collins et al., 2010). Adenosine in the extracellular space is generated through the enzymatic conversion of ATP molecules, mainly released from cells via Panx1 channels. Here, we hypothesized that in the absence of Panx1

function, adenosine's extracellular level might decline, leading to the removal of adenosine receptor-mediated inhibition of D2-type receptors, thus causing excessive dopaminergic signaling. To further examine this hypothesis, we conducted a VMR assay on larvae treated with adenosine, an agonist of adenosine receptors. As shown in Fig. 3.8, adenosine treatment (0.1 μM) was able to rescue Light-OFF deficiency in *panx1a*$^{-/-}$ larvae (p-value =0.0007; n = 60). However, no significant difference in the Light-OFF peak response of TL controls was observed (p-value =0.99; n = 60). Interestingly, adenosine (0.1 μM) treatment also improved mutants' response to the light onset (p-value =0.004; n = 60); thus, their Light-ON peak response became similar to that in TL controls. Though, no apparent effects were observed on this response in TL controls (p-value =0.76; n = 60). All the p-values are given in ***Table 3.3***.

Table 3.3. The multivariate comparisons of VMR between Ado-treated and untreated larvae.

	Type of treatment	***Control***	***Treatment (Adenosine; 0.1 μM)***		
Typ of stimulus	***Genotype*** / ***Time bin***	***+/+ : -/-***	***+/+***	***-/-***	***+/+ : -/-***
Light-ON	***Before (-60-0 S)***	0.018	$1.04e^{-10}$	$6.93e^{-12}$	$3.02e^{-07}$
	At (0-1 S)	0.011	0.762	0.0046	0.760
Light-OFF	***Before (-60-0 S)***	0.99	$3.33e^{-16}$	$2.67e^{-14}$	0.99
	At (0-1 S)	0.025	0.99	0.0007	0.042

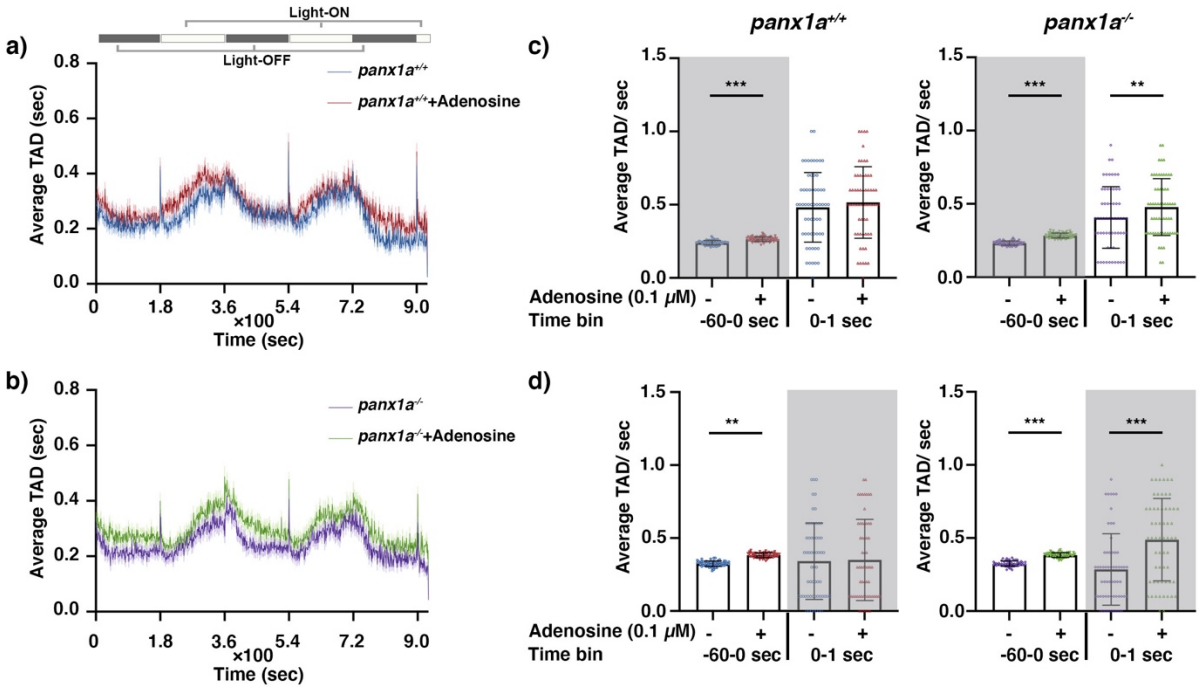

Figure 3.8. Adenosine treatment improves visual motor performance of mutants. *The average TAD values for a) panx1a+/+ and b) panx1a-/- over the entire test period indicate that adenosine (0.1 μM) treatment enhanced larval activity during both light and dark periods. The Light-ON and Light-OFF periods are indicated by white and black bars at the top of the panels. Except for the last Light-ON (5 min), all trials are 30 min in length. c) Light-ON and d) Light-OFF VMR from 1 min before the light switch to 1 sec after the light switch is graphed as mean±SEM for panx1a+/+ controls (left panels) and panx1a-/- (right panels). Adenosine (0.1 μM) significantly increased the c) Light-ON and d) Light-OFF peak responses only in mutants (n=60). Though, no significant alterations were observed in the Light-ON or the Light-OFF peak responses of TL controls (n=60). Significance: p-value<0.05.*

3.8. Supplementary Figures

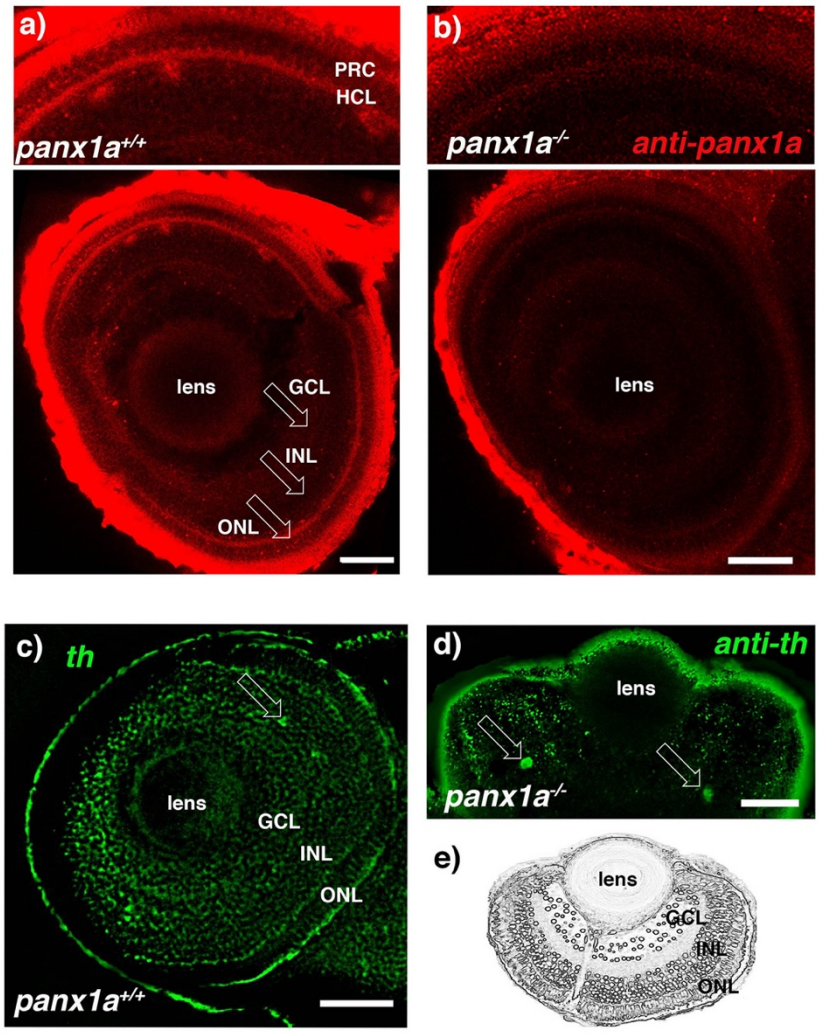

Supplementary Figure 3.1. Whole-mount immunohistochemistry. *a) panx1a$^{+/+}$ and b) panx1a$^{-/-}$ larva. Panx1a immunoreactivity was identified in the region associated with horizontal cells (HCL) adjacent to the photoreceptor cell layer (PCL). Arrows indicate the position of the lens, ganglion cell layer (GCL), inner nuclear layer (INL), and outer nuclear layer (ONL). Reduced Panx1a immunoreactivity was found in the outer retinal layer of 3dpf panx1a$^{-/-}$ larva only when the image's brightness was enhanced. The significant fluorescence observed in the eyes of the age-matched larva was attributed to cross-reactivity of the antibody, most likely with collagen fibers produced by endothelial cells in the sclera-choroid region. Note that images are collapsed from three 0.64-µm-thick optical sections. Scale bar: 25µm c) Tyrosine hydroxylase-immunoreactivity (th) was detectable in the inner nuclear layer of an age-matched eye of a panx1a$^{+/+}$ larva. The arrow indicates the body of a th-immunoreactive cell. Scale bar = 30µm d) Cross-section of a panx1a$^{-/-}$ eye. Arrows point at the position of th-positive cell bodies located in the inner nuclear layer. Scale bar = 20µm. In both c-d) th-immunoreactivity was speckled across multiple layers similar to those described for th-positive cells in higher vertebrates(Debertin et al., 2015). Note that the images in c-d represent 0.83-µm-thick single optical sections after deconvolution. e) Graphic representation of a cross-section through the zebrafish retina showing the position of different retinal layers.*

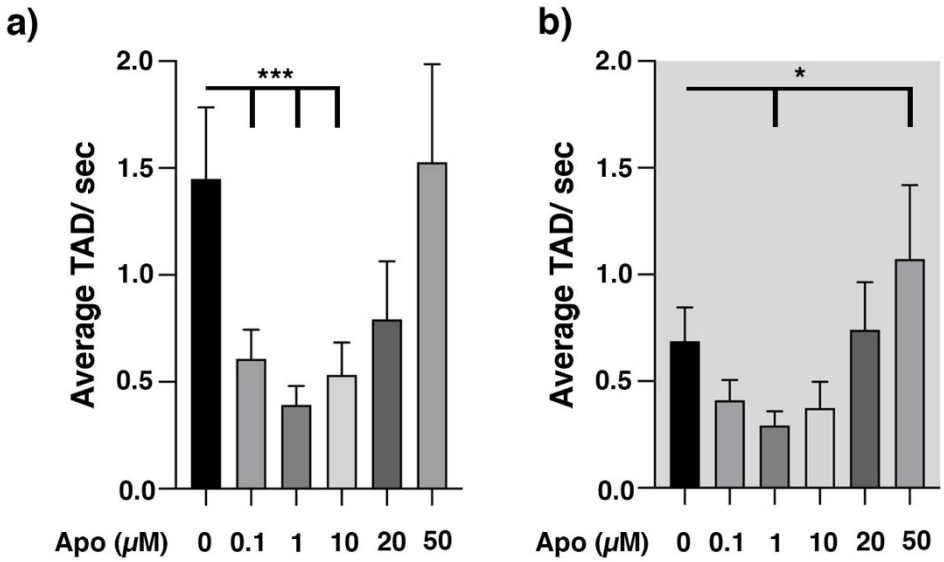

Supplementary Figure 3.2. Apomorphine Dose-Response Test. *Apomorphine administration had dose-dependent effects on locomotion in Light-ON (a) and Light-OFF conditions (b). a) Doses in the 0.1μM to 10 μM range significantly decreased larval activity in light (p-value<0.001). Doses in the 20μM and 50 μM range did not significantly alter locomotion. b) In the dark, significant changes in activity levels were detected after treatment with a low dose (1 μM; p-value=0.02) and a high dose (50 μM; p-value=0.043). TAD data are presented as mean activity ± SEM, n = 24/dose. Significance: p < 0.05.*

3.9. Supplementary Tables

Supplementary Table 3.1. GO annotation for upregulated genes.

Reactome pathways	Danio rerio (REF) #	upload #	Fold Enrichment	p-value
Unclassified	16859	475	0.86	0
The phototransduction cascade	44	16	11.13	0.000000054
Inactivation, recovery and regulation of the phototransduction cascade	42	15	10.93	0.000000273
Visual phototransduction	92	18	5.99	0.0000166
Processing of Capped Intron-Containing Pre-mRNA	242	26	3.29	0.000716
mRNA Splicing	194	22	3.47	0.0024
Activation of the phototransduction cascade	14	7	15.31	0.00371
mRNA Splicing - Major Pathway	185	20	3.31	0.0135
Gene expression (Transcription)	803	51	1.94	0.0232
G alpha (i) signalling events	341	28	2.51	0.0412

Supplementary Table 3.2. GO annotation for downregulated genes.

Reactome pathways	Danio rerio (REF)	upload #	Fold Enrichment	p-value
Unclassified	16859	902	0.8	0
Developmental Biology	395	73	2.78	7.25E-10
Metabolism	1825	205	1.69	4.95E-09
Axon guidance	303	52	2.58	0.0000174
Neutrophil degranulation	497	71	2.15	0.000048
MET promotes cell motility	54	19	5.29	0.00011
MET activates PTK2 signaling	37	16	6.5	0.000123
Signaling by MET	98	25	3.83	0.00021
Hemostasis	500	69	2.07	0.000229
Signal Transduction	2196	212	1.45	0.000332
Signaling by Receptor Tyrosine Kinases	449	62	2.07	0.001
Innate Immune System	879	100	1.71	0.00165
Formation of the cornified envelope	39	14	5.39	0.00469
Keratinization	39	14	5.39	0.00469
Neuronal System	434	58	2.01	0.00472
Immune System	1420	143	1.51	0.0051
Membrane Trafficking	518	64	1.86	0.0182

Vesicle-mediated transport	541	65	1.81	0.0291
CRMPs in Sema3A signaling	19	9	7.12	0.0499

Supplementary Table 3.3. Comparison of transcriptional changes of selected transcripts by RNA-seq and RT-qPCR.

Gene	***RNA-seq Log2 expression***	***p-value***	***FDR***	***RT-qPCR Expression (REST)***	***S.E. (REST)****	***P-value (REST)****	***Result***
opn1lw2	0.496	0.073	0.417	1.052	0.508 - 2.153	0.799	
opn1mw1	0.276	0.104	0.572	1.075	0.302 - 2.463	0.836	
opn1mw2	1.366	0.103	0.000	1.074	0.601 - 1.935	0.671	
opn1sw1	0.976	2.105	0.016	4.301	1.903 - 12.773	0	UP
opn1sw2	0.918	0.995	0.025	1.993	0.722 - 4.186	0.001	UP
opn4.1	1.672	1.006	6.23E-05	2.009	1.216 - 3.579	0.001	UP
rho	1.066	0.861	0.010	1.816	0.674 - 3.811	0.008	UP
gnat1	0.850	1.940	0.012	3.837	2.058 - 8.380	0	UP
gnat2	1.353	2.090	0.002	4.257	2.313 - 8.121	0	UP
pde6c	1.418	1.196	0.001	2.291	1.236 - 5.034	0	UP
pde6ha	1.225	2.646	0.007	6.26	3.374 - 11.990	0	UP
guca1c	2.791	1.375	1.54E-06	2.593	1.017 - 5.043	0	UP
gucy2d	1.094	2.179	0.018	4.529	2.527 - 8.475	0	UP
gna11b	1.447	1.189	6.69E-05	2.28	1.180 - 4.497	0	UP
grk7b	1.587	1.006	6.96E-05	2.009	1.216 - 3.579	0.001	UP
p2rx1	-1.941	1.6E-04	0.007	0.682	0.382 - 1.122	0.019	DOWN
p2rx5	-1.602	0.9E-04	0.008	0.379	0.098 - 1.251	0.009	DOWN
p2rx7	-1.899	1.51E-10	3.86E-08	0.278	0.031 - 1.179	0.019	DOWN
adora1b	-1.256	0.9E-04	0.023	0.454	0.201 - 0.994	0.001	DOWN
cacna1da	-0.898	0.9E-04	0.008	0.124	0.040 - 0.281	0	DOWN
kcnc1a	-1.497	8.72E-08	7.55E-06	0.073	0.015 - 0.323	0	DOWN
kcnc1b	-1.680	2.29E-07	1.58E-05	0.537	0.252 - 1.047	0.005	DOWN
kcna2b	-1.815	2.48E-06	1.0E-4	0.413	0.205 - 0.783	0.001	DOWN

kcnh4a	-2.035	4.01E-06	1.0E-4	0.483	0.212 - 1.177	0.006	DOWN
trpv4	-2.065	0.001147	0.009	0.216	0.060 - 0.659	0	DOWN
trpm6	-1.237	0.00043	0.005	0.124	0.040 - 0.281	0	DOWN

*Values were calculated using the Relative Expression Software Tool (REST) (Pfaffl, 2002).

Supplementary Table 3.4. RT-qPCR results for transcripts associated with the dopaminergic pathway.

Gene	***RT-qPCR Expression (REST)***	***S.E. (REST)***	***P-value (REST)***	***Result***
drd1a	1.364	0.812 - 2.237	0.045	UP
drd1b	1.676	0.696 - 3.555	0.027	
drd2a	2.328	1.294 - 3.938	0.000	UP
drd2b	1.635	0.677 - 3.535	0.028	UP
drd2c	1.294	0.796 - 2.110	0.096	UP
drd3	3.397	1.359 - 9.037	0.001	UP
drd4a	3.336	1.519 - 7.193	0.000	
drd4b	1.216	0.765 - 1.990	0.190	UP
drd5a	2.060	0.815 - 4.818	0.003	UP
th	6.082	2.919 - 13.157	0.000	UP
ddc	1.566	0.732 - 3.248	0.060	UP
mao	1.660	0.805 - 3.589	0.026	
comta	0.991	0.493 - 1.948	0.970	
slc6a3	2.958	1.122 - 6.871	0.001	UP
slc18a2	2.119	1.209 - 4.015	0.000	UP

Chapter 4. Pannexin1b, an emergent candidate for delineating interactions between the circadian clock and visual system in the zebrafish

4.1. Targeted ablation of panx1b

Using TALEN genome editing, the 4th exon of *panx1b* was targeted for disruption (***Fig. 4.1.a***). Twenty-five picograms (pg) of TALEN cRNA pair targeting *panx1b* gene was microinjected into one-cell staged embryos. The RFLP test of 17 randomly selected embryos revealed a mutagenesis efficiency of ~ 88%, as evidenced by a partial loss of the restriction enzyme recognition sequence at the TALENs cut site (***Fig. 4.1.b***). DNA sequence analysis of multiple microinjected embryos confirmed the efficient introduction of deletion mutations of varying lengths in the *panx1b* exon 4 (***Fig. 4.1.c***). A positive founder transmitting an 11-nt frameshifting deletion (*panx1b*$^{\Delta 11}$) was used to establish the knockout line and further experimentation. The eleven base pair deletion caused frameshifts at amino acid 196, resulting in premature stop codon leading to the expression of a truncated 179-amino-acid protein (instead of the 422-residue wild-type Panx1b), lacking two transmembrane regions and the entire carboxyterminal domain (***Fig. 4.1.d***). After transfection into mouse Neuroblastoma 2a (Neuro2a) cells, the subcellular localization of the truncated *panx1b*$^{\Delta 11}$-EGFP proteins was assessed. *Panx1b*$^{\Delta 11}$-EGFP had a scattered cytoplasmic signal suggesting that the mutant protein could not traffic efficiently to the cell membrane (***Fig. 4.1.e***, left panel). *Panx1b*^{wt}-EGFP protein was detectable in the prenuclear region and the plasma membrane (***Fig. 4.1.e***, right panel) in line with previous reports (Boassa et al., 2007; N. Prochnow et al., 2009).

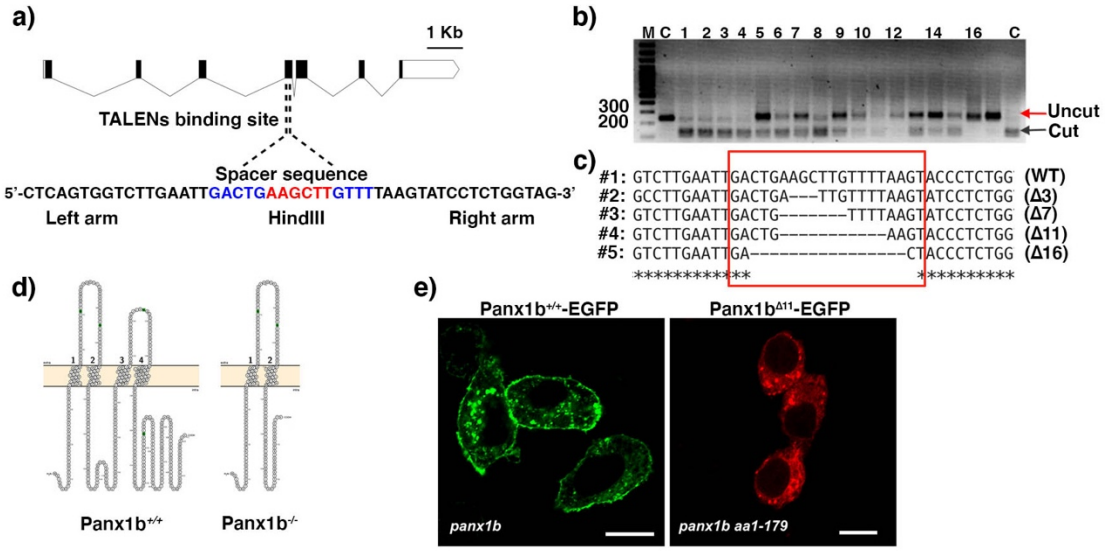

Figure 4.1. Generating panx1b$^{-/-}$ fish using TALENs. *a) The zebrafish panx1b gene structure with seven coding exons. The left and right TALENs sequence with the spacer sequence and HindIII restriction site in blue and red is highlighted. b) The RFLP-assay shows the loss of the HindIII recognition sequence (indicated by uncut) in fourteen out of sixteen F0 larvae tested. c) A sequencing alignment demonstrates small (3 to 16 bp) deletions causing frameshift mutations found in four different F0 larvae. d) The predicted sequence features of the mutated panx1b were visualized using the Protter open-source tool (wlab.ethz.ch/protter). An 11 bp deletion in Panx1b exon 4 resulted in a frameshift causing a premature stop codon at amino acid 196. e) Localization of the truncated panx1b protein – Confocal images of transiently transfected proteins panx1b$^{+/+}$-EGFP (left panel) and panx1b$^{\Delta 11}$-EGFP (right panel) in Neuro2a cells. Nuclei were stained with DAPI. Scale bar: 10 µm.*

4.2. Characterization of panx1b$^{-/-}$ larvae

Panx1b$^{-/-}$ survival rate was significantly lower than TL controls at 1 dpf (values in %: TL 80; *panx1b$^{-/-}$* 62.19; TL vs. *panx1b$^{-/-}$* p = 0.0062). However, their survival rate improved by day 6 (values in %: TL 83; *panx1b$^{-/-}$* 88.56; TL vs. *panx1a$^{-/-}$* p = 0.538; ***Fig. 4.2.a***).

Gross anatomical screening focused on 3 and 6 dpf larvae. At 3dpf (after hatching), *panx1b$^{-/-}$* mutants showed a spectrum of phenotypes from normal to malformed. Swimming bladder edema, ventricular hypertrophy, an irregularly shaped yolk sac, and spinal curvature were observed in approximately 11±4% of mutants (***Supplementary***

Fig. 4.1). These are most likely deriving from the microinjection process itself or as a consequence of other, unrelated developmental irregularities. The larvae representing malformations could not survive beyond 5-7 dpf and were excluded from the experiments. The physical malformations observed in *panx1b*$^{-/-}$ larvae were distinct from *panx1a*$^{-/-}$ or DKO groups. ***Fig. 4.2.b*** represents normal-looking *panx1b*$^{-/-}$ and TL control larvae (F4 generation) at 6dpf. The head-to-tail size of 6dpf *panx1b*$^{-/-}$ larvae was significantly bigger than TL controls (TL control = 3.83±0.27 mm; *panx1b*$^{-/-}$ =4.00±0.17 mm; TL vs. *panx1b*$^{-/-}$ $p < 0.0001$; TL, n=60; *panx1b*$^{-/-}$, n=44; ***Fig. 4.2.c***).

About 6.6% of *panx1b*$^{-/-}$ mutants showed mandibular malformations accompanied by markedly smaller body size and an indistinct sexual maturity at the juvenile stage. These features highlight a potential role for Panx1b in the development of the musculoskeletal system. The malformed fish could not survive beyond three months and were sacrificed according to the ACC animal care protocol as soon as the phenotype was confirmed. The majority of adult *panx1b*$^{-/-}$ zebrafish (93.4%) were viable and fertile like the parental TL strain or heterozygous fish.

No significant reduction in the *panx1b* mRNA level was detected in 6dpf *panx1b*$^{-/-}$ larvae indicating that the deletion did not lead to RNA decay. Compensatory regulation of the other pannexin genes similar to previous reports using Panx1$^{-/-}$ mouse was experimentally excluded (data not shown).

A quantitative prove of loss-of protein expression by western blot analysis was impossible after several attempts to generate high-affinity polyclonal or monoclonal antibodies directed against both GST-Panx1b fusion proteins or peptides failed.

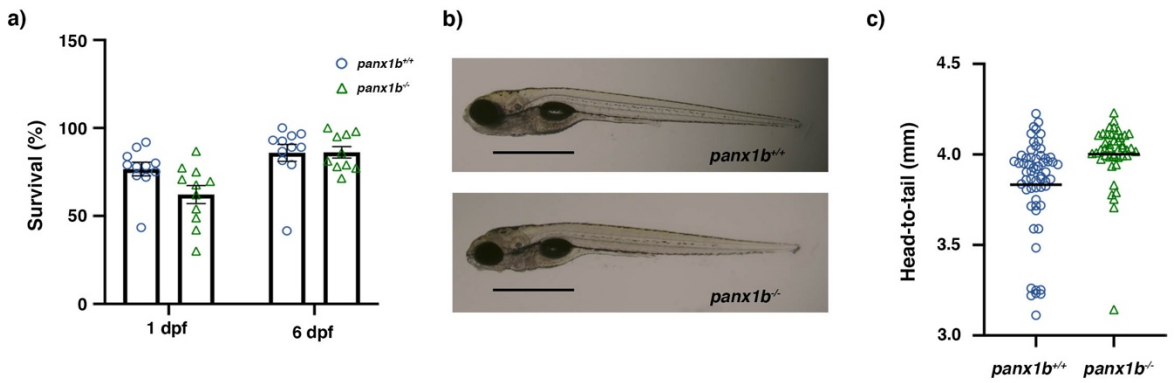

Figure 4.2. Phenotypic characterization of panx1b$^{-/-}$ larvae. *a) Survival rate at the first 24 hours post-fertilization (hpf) showed a significant reduction in mutants than TL controls. b) Age-matched TL control and panx1b$^{-/-}$ larvae (6dpf) showing regular morphology. Scale bar = 100μm c) The head-to-tail size measurement revealed panx1b$^{-/-}$ are longer than control TLs. d) RT-qPCR analysis of pannexin expression in 6dpf larva. Significance: p-value<0.05; nd: Not detected.*

4.3. Transcriptome profiling of 6dpf panx1b$^{-/-}$ larvae

The transcriptomes of *panx1b$^{-/-}$* and TL larvae were compared at 6 dpf (NCBI Gene Expression Omnibus (GEO) database; at the time of the Ph.D. submission *panx1b$^{-/-}$* data are scheduled for deposition at the GSE).

A total of 58,616 RNAs was found in each of the six samples (TL control, n=3; *panx1b$^{-/-}$,* n=3) sequenced. In *panx1b$^{-/-}$* larva, 1213 RNAs were downregulated, and 764 RNAs upregulated when the cut-off for the false discovery rate (FDR) was set to 0.05, and the significance of regulation was defined as p-value<0.001. Gene-specific expression information retrieved from the Zebrafish Information Network (ZFIN) database allowed categorizing the representation of regulated genes to those previously described as expressed in the central nervous system (CNS) and visual system. Sixty-two upregulated genes and 92 downregulated genes matched genes expressed in the central nervous system (***Fig. 4.3.a***, left panel). Furthermore, 43 upregulated genes and 77 downregulated genes matched genes expressed in the visual system (***Fig. 4.3.a***, right panel).

The AmiGO2 analysis (http://amigo.geneontology.org/amigo/landing) revealed enriched Gene Ontology (GO) terms and pathways (***Supplementary Tables 4.1*** and ***4.2***). The most significantly enriched biological processes (cut-off: FDR<0.05, p-value <0.001) represented the regulation of primary and macromolecules metabolic processes (***Fig. 4.3.b***, left panel). Downregulated genes represented several biological processes, including the circadian regulation of gene expression, RNA processing, and G-protein coupled receptors signaling pathways (***Fig. 4.3.b***, right plot).

The downregulation of circadian clock genes observed in the RNAseq data (cut-off: p-value<0.001; FDR 0.05) were also validated by RNA-qPCR (cut-off: p-value<0.05). Selected transcription factors driving the rhythmic 24-h expression patterns of core clock components were confirmed as downregulated in *panx1b*$^{-/-}$ larvae (***Fig. 4.3.c***, ***Table 4.1***). The disruption of the circadian clock pathway in the absence of *panx1b* highlights a novel mechanism through which *panx1b* might affect a diverse array of physiological functions such as sleep-wakefulness cycle, locomotor activity, metabolic processes, and immunity in 6 dpf old larvae.

Table 4.1. RT-qPCR results for transcripts associated with the circadian clock pathway.

Gene	*RT-qPCR Expression (REST)*	*SEM (REST)*	*p-value (REST)*	*Result*
bmal1a	-2.277	0.050	0.005	Down
bmal1b	-1.609	0.053	0.019	Down
bmal2	1.273	0.135	0.246	
cipca	-1.988	0.060	0.055	
clock2	-1.568	0.063	0.017	Down
cry1a	-1.749	0.109	0.004	Down
cry1b	-2.43	0.086	0.002	Down
cry2	-1.569	0.073	0.058	
cry3b	-2.42	0.052	0.11	
cry5	-9.002	0.033	0.0012	Down
nr1d1	-1.142	0.065	0.279	
per1a	-1.142	0.062	0.451	
per1b	-1.732	0.159	0.245	
per2	-1.503	0.082	0.154	
per3	-1.422	0.184	0.289	

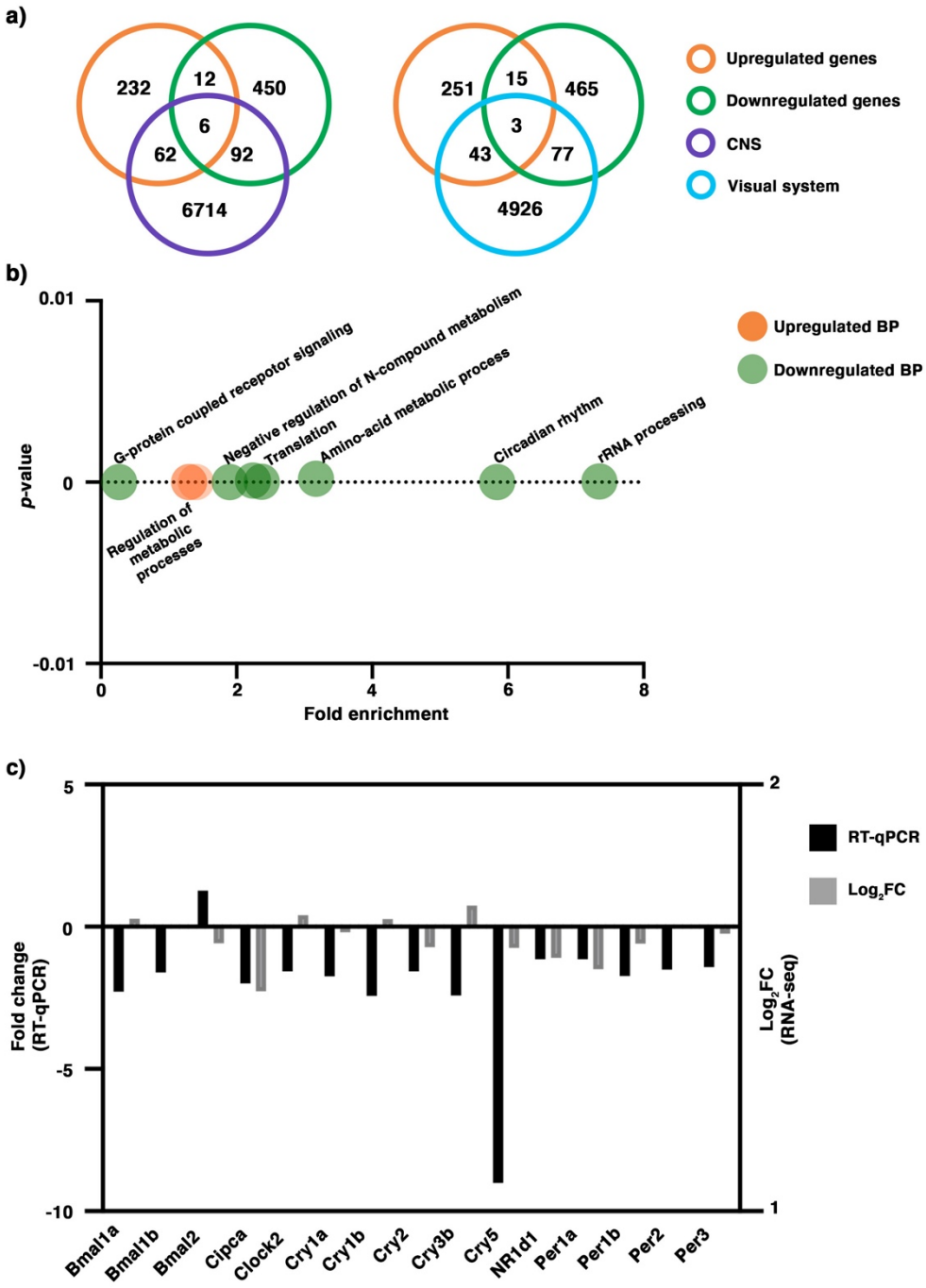

Figure 4.3. RNA-seq analysis of 6dpf panx1b$^{-/-}$ larvae. *a) Comparison of deregulated genes against two categories: central nervous system (CNS) and the visual system. b) GO annotation of RNA-seq data in terms of biological process (BP): the upregulated genes were enriched in the regulation of metabolic processes, whereas the downregulated genes were annotated for RNA processing, circadian rhythms, amino-acid metabolic process, translation, negative regulation of nitrogen (N) compounds metabolism, and G-protein coupled receptor signaling. c) Validation of RNA-seq data by RT-qPCR. Significant downregulation of cry1, cry5, bmal1a, bmal1b, clock2 genes in panx1b$^{-/-}$ 6 dpf larvae were confirmed.*

4.4. Loss of panx1b affects larval visually guided locomotor activities

Physiological, molecular, and behavioral studies have revealed that several functional aspects of the visual system, for example, visual sensitivity, display robust circadian rhythmicity in zebrafish (Cahill, 2002; Fleisch and Neuhauss, 2006). Since the transcriptome data analysis provided evidence that lack of Panx1b cause changes in both the visual and the circadian clock systems, the consequential changes in the visually-mediated locomotor activities were studied. The next sections present the results of four types of visually guided locomotion-based tests, e.g., 1) locomotion in a stimulus-free environment, 2) visual-motor response (VMR), 3) optomotor response (OMR), and 4) color discrimination.

4.4.1. General locomotor activity

Baseline locomotor performance of the *panx1b* mutant and TL control larvae were compared under constant light (Light-ON) or dark (Light-OFF) conditions. Under the Light-ON condition, both *panx1b*$^{+/+}$ and *panx1b*$^{-/-}$ swam longer distances and more rapidly than the Light-OFF condition. In Light-ON (***Fig. 4.4.a***), both genotypes displayed similar locomotor activity. The average of distance traveled ($t = 0.28628$, $df = 52.295$, p-value = 0.7758; n=30) and velocity ($t = 0.68582$, $df = 50.325$, p-value = 0.496; n=30) were comparable between these two groups. Both groups similarly showed a preference for swimming more in the outer zone relative to the central area (***Fig. 4.4.a***; well illustration). During the Light-OFF phase, *panx1b*$^{-/-}$ larvae were hyperactive. They swam significantly longer distances ($t = 2.189$, $df = 45.194$, p-value = 0.0338; n=30) although with similar velocity ($t = -1.6098$, $df = 46.751$, p-value = 0.1142; n=30) as TL-controls (***Fig. 4.4.b***). No

significant differences was observed in thigmotaxic behavior between two genotypes during Light-OFF period, both groups stayed closer to the walls and avoided crossing the open space in the central zone (***Fig. 4.4.b***; well illustration).

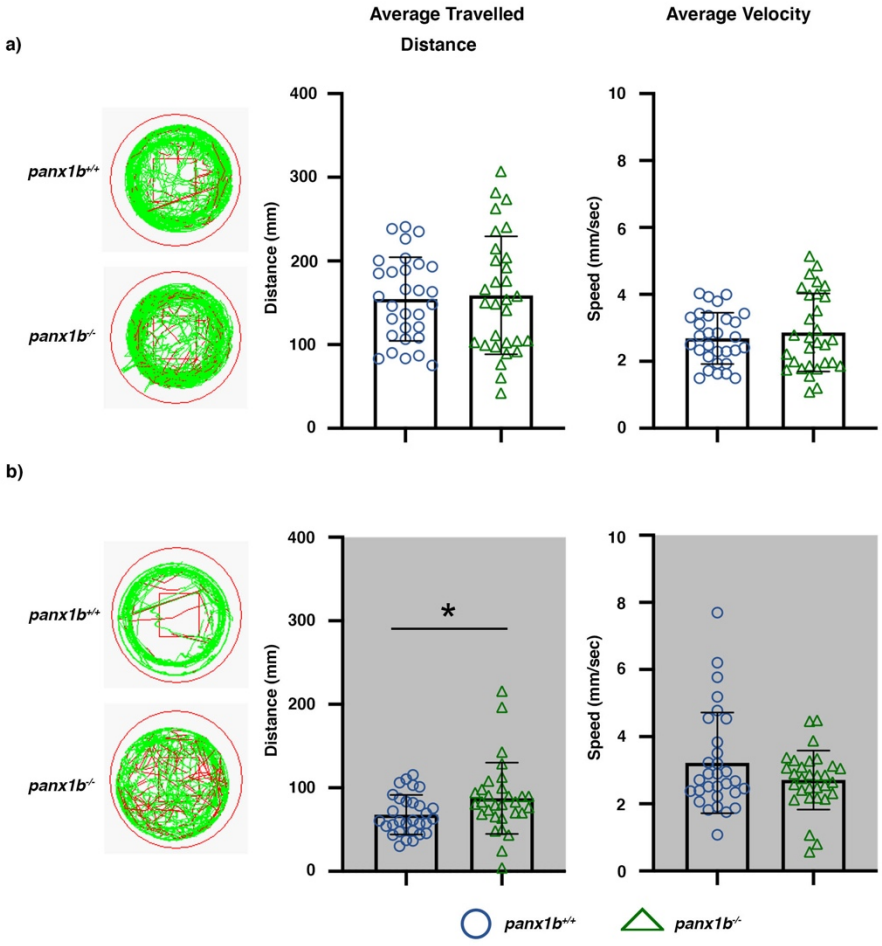

Figure 4.4. Locomotor activity in Light-Dark conditions. *Locomotion was video tracked for 60 min in a) Light-ON and b) Light-OFF conditions. The wells on the left show examples of panx1b$^{-/-}$ and panx1b$^{+/+}$ locomotion patterns. Medium (<20 mm/sec) or high-speed movements (>20 mm/sec) are visualized with green and red colors. Graphs demonstrate the averaged traveled distance (in mm) and the average velocity (mm/sec) of n = 60 larvae for each genotype. Significance: p-value<0.05.*

4.4.2. Visual-motor response (VMR)

The observation of the different locomotor activity of mutants in a dark environment advocated for testing visual-motor response (VMR). The VMR requires an intact retina

and can reveal how well *panx1b*$^{-/-}$ larvae can detect light changes. As described earlier, the PCA was used to identify the most informative variable for describing differences between groups. PC1 and PC2 captured more than 65.5% and 29.5% of the data variance (***Fig. 4.5.a***). Among seven measured variables (i.e., count and duration of freeze, bouts, and bursts of activity, plus total activity duration), the total activity duration (TAD; in red) had the most significant contribution to the observed variability in PC1 (***Fig.4.5.b***) and was chosen to determine the VMR differences between genotypes.

As indicated by the mean larval activity during 3 cycles of light onset (Light-ON) and light-offset (Light-OFF), the larval VMR differs from TL control when the *panx1b* gene is ablated (***Fig. 4.5.c***). While the mutants' motor activity during the Light-ON phases was markedly lower than TLs, they had comparable activity levels during the dark periods. To determine the VMR differences between groups, a pairwise non-parametric t.test (nparcomp package; R) was performed on the larval activity data during these two time periods: -60–0 sec (i.e., before light change), 0-1 sec(i.e., at the light change stimulus) and 1–60 sec (i.e., after light change).

For the 1 min period before the Light-ON stimulus (-60-0 sec), there was a statistical difference in the activity between TL & *panx1b*$^{-/-}$ (p-value=0.001), in which the activity level of *panx1b*$^{-/-}$ before the light change was greater than that of TL. At the dark-light transition (Light-ON; 0-1 sec), synchronous increase in locomotor activity was observed in both TL and *panx1b*$^{-/-}$ groups (p-value= 0.083), which was followed by a rapid activity decline to the baseline level during the subsequent light period (in 1-60 sec, p-value<0.699; ***Fig. 4.5.d***).

At the light-dark transition, a synchronous and abrupt increase in motor activity was observed in TL control larvae, corresponding to the O-bend response. Following this trend, larval motor activity remained elevated for several minutes and then slowly declined within 10 – 15 minutes, until activity fell below the baseline level in light ***(Fig. 4.5.e***). Interestingly, *panx1b*$^{-/-}$ larvae responded to the dark differently compared to control TLs. For the 1 min period before the Light-OFF stimulus (-60-0 sec), *panx1b*$^{-/-}$ larvae activity was markedly lower than TLs (p-value<0.0001). Notably, the peak response to the abrupt loss of illumination was absent in mutants (0-1 sec; p-value<0.0001). Rather than sharply increasing their motor activity, mutants responded to the Light-OFF by freezing for several seconds. Then, they gradually increased their activity to the comparable levels as TL during the subsequent dark period. For the 1 min period after the Light-OFF, no significant difference between TL and mutant's activity was observed (1-60 sec; p-value=0.06), which is corroborated by the corresponding activity plot (***Fig. 4.5.e***). These data show that *panx1b*$^{-/-}$ larvae can detect and respond to light. However, their peak response to a dark pulse is abolished, which suggests *panx1b* plays important functions in detecting light decrement and eliciting the corresponding behavioral response in larval zebrafish.

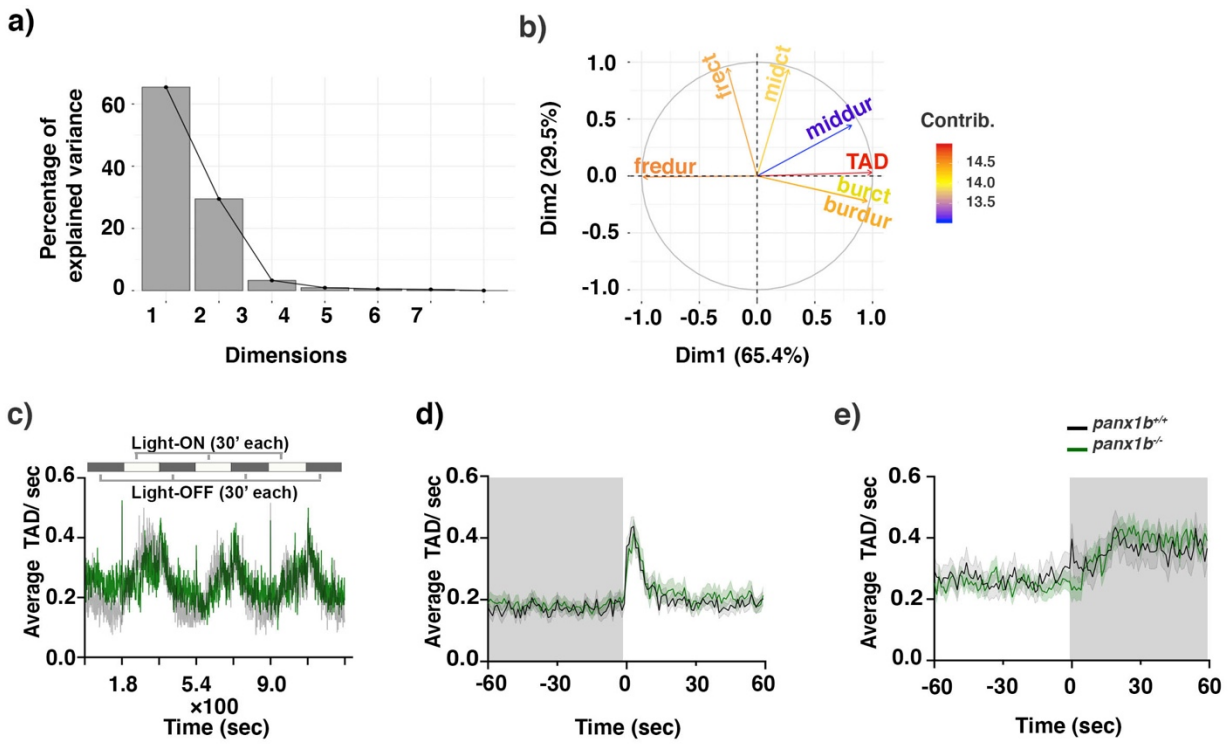

Figure 4.5. Visual-motor motor response (VMR) changes in panx1b$^{-/-}$ larvae. *a) Principal component analysis (PCA) transforming the VMR multidimensional data. The scree plot shows that Dimensions 1 and 2 capture more than 65.4% and 29.5% of the data variance. b) The variable correlation plot represented the coordinates of the variables in the first two dimensions. The variables were colored from blue to red as their contribution to PCs increases. Total activity duration (TAD; in color red) showed the highest contribution to the variability in Dimension 1 and was chosen to visualize differences between genotypes. c) The outline of the experimental paradigm is shown on top. The line graph shows the average TAD of panx1b$^{-/-}$ and panx1b$^{+/+}$ larvae from a representative test with n=24 larvae for each genotype. The activity was defined as the fraction of frames per second that a larva spent swimming (see methods for the detailed information). d, e) The results for average Light-ON and Light-OFF VMR are shown from 1 min before the light switch to 1 min after the light switch. The color ribbons surrounding the average activity line graph correspond to 1 S.E.M. The values are the average of the second trial from four independent tests with n=48 larvae for each genotype. The Light-ON and Light-OFF periods are indicated by white and black bars at the top of the panels. Significance: p-value<0.05.*

4.4.3. Optomotor response (OMR)

A quantitative OMR assay was used to further assess details of visually evoked behavior. The OMR is an innate behavior of zebrafish, found in many animals, enabling them to follow visual motion in the surrounding environment to stabilize their location or course of movement (Neuhauss et al., 1999; Orger et al., 2000). To determine the optimal stimulus parameters for distinguishing mutants from TL control larvae, moving gratings of three

(64, 128, and 256 pixels/cycle) spatial frequencies (SF) at two velocities of 72 and 144 deg/s and two contrast levels of 10 and 100 percent were used. ***Fig. 4.6*** shows the percentage of positive response (PPR) of 40 larvae after 90 s of grating motion toward each direction (right and left). For all combinations of tested SFs, velocities, and contrasts, the percentage of *panx1b*$^{-/-}$ larvae responding to the stimulus was lower than that in the TL control group, especially when the direction of moving stripes was set towards left.

At low contrast level (10%; left panels), *panx1b*$^{-/-}$ larvae became markedly distinct from TL controls when tested with left-ward moving stripes at a spatial frequency of 256 (pixels/cycle) and speed of 144 (pixels/s). The PPR of TL and *panx1b*$^{-/-}$ larvae were 85.83$\pm$16.41% and 24.44$\pm$21.43%, respectively (p-value=0.0012; n=40). For the low-spatial frequencies (i.e., 64 and 128 pixels/cycle), both genotypes swam most often in the direction of the moving stimulus when tested with a velocity of 72 or 144 (deg/s), and no significant differences were observed within or between groups. However, when spatial frequencies were increased from 128 to 256 pixels/cycle, the PPR average was augmented at high velocities in TL controls. This data is in line with the previous reports on the larval zebrafish visual acuity peaking at the spatial frequency of 256 (pixels/cycle) at a speed of 144 (deg/s) (Stiebel-Kalish et al., 2012). Similarly, a slight increase in the larval response was observed in the mutant group only when tested with the rightward moving grating. *Panx1b*$^{-/-}$ larvae showed a significant impairment for following the leftward moving stripes of the same combination of SF and velocity. These data suggest that the visual acuity of *panx1b*$^{-/-}$ larvae is compromised in low contrast conditions, which is in line with the aforementioned VMR results in the dark environment as mentioned earlier.

Furthermore, the peak response deficiency, observed at SF of 256 pixels/cycle and speed of 144 pixels/s, for the leftward direction provides evidence of cognitive impairment in *panx1b*$^{-/-}$ larvae. Thus, Panx1b appears to play a role in encoding and/ perception of the motion direction signals.

On the other hand, at high contrast level (100%), none of the tested combinations of SFs and velocities at 100% contrast elicited a statistically significant difference between mutants' and TLs' OMR (***Fig. 4.6***, right panels). Further, pairwise comparisons for each spatial frequency revealed no statistically significant differences within groups for either velocity. These results indicate that a high contrast condition when the environment is bright, and the edges of objects are sharp can improve *panx1b*$^{-/-}$ larvae's visual performance. All the p-values are given in ***Table 4.2***.

Table 4.2. The multivariate comparisons of OMR between TL control and panx1b$^{-/-}$ larvae.

Contrast levels		***Low (10%)***			***High (100%)***		
Speed (pixels/sec)	***Direction***	***Spatial Frequencies (pixels/cycles)***					
		64	***128***	***256***	***64***	***128***	***256***
72	***Leftward***	0.061	0.51	0.16	0.23	0.22	0.22
	Rightward	0.52	0.77	0.44	0.89	0.8	0.33
144	***Leftward***	0.22	0.13	0.0012	0.63	0.26	0.66
	Rightward	0.97	0.97	0.97	0.65	0.99	0.77

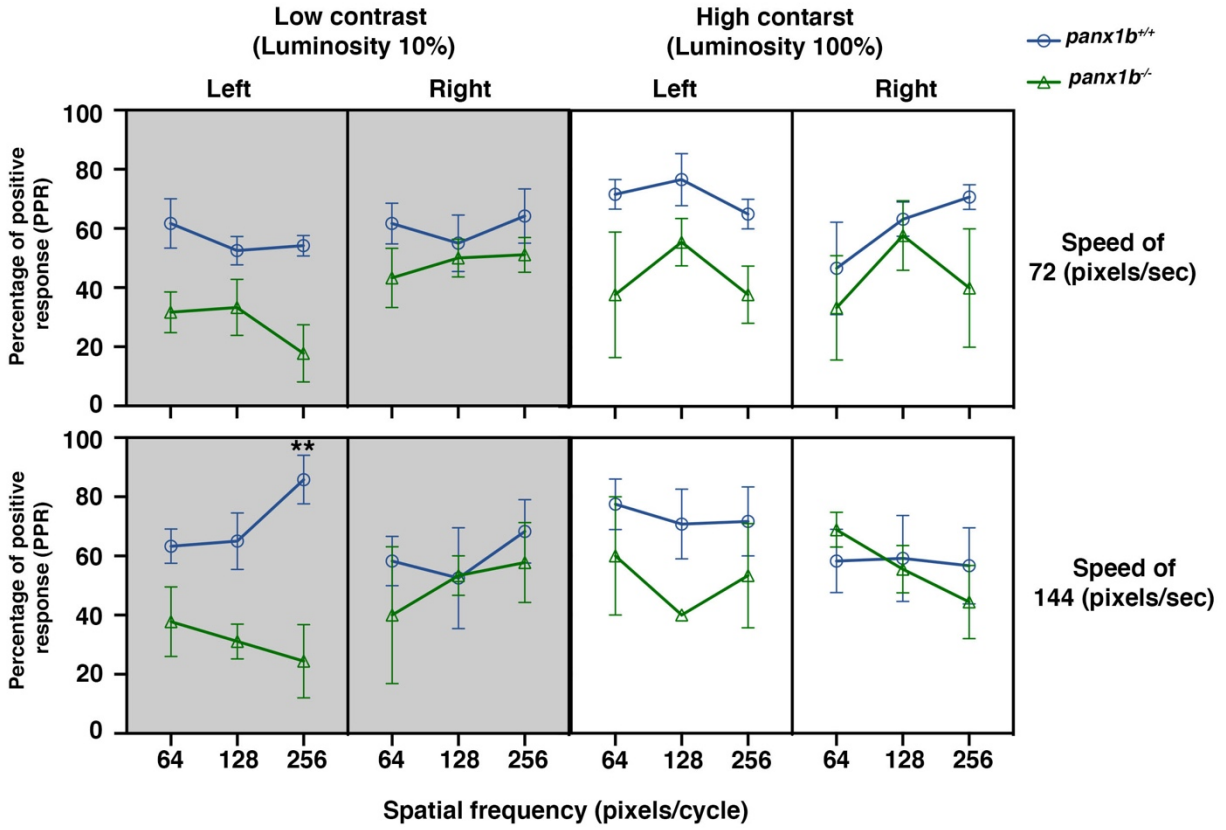

Figure 4.6. Optomotor response (OMR) declines in the absence of panx1b functions. *Three spatial frequencies (SF) at two different speed rates and two luminosity levels were used to assess larval zebrafish's visual acuity. The percentage of positive response (PPR) explains the average number of larvae that responded to a particular setting. The PPR values for each setting are the average of four tests ±SEM. In all tested settings, panx1b$^{-/-}$ were able to elicit an appropriate response, as observed in TL controls. However, their visual acuity was lower than controls when the direction of motion was towards the left. The difference between genotypes' PPR for the left-ward motion became very significant at SF=256, speed of 144, and low contrast setting (n=40). Significance: p-value<0.05.*

4.4.4. Color discrimination

To test RGBY color preference of larvae, a cross maze with four arms, each showing one color, was used (check ***Supplementary Fig. 2.1***). Previous studies reported an innate preference for blue/ short-wavelength light in both adult (Colwill et al., 2005; Risner et al., 2006; Bault, Peterson and Freeman, 2015; Oliveira et al., 2015; Peeters, Moeskops and Veenvliet, 2016) and larval (Park et al., 2016; Peeters, Moeskops and Veenvliet, 2016) fish. Similarly, here we report both TL control and *panx1b*$^{-/-}$ 6dpf larvae show a higher

tendency to blue color than three other colors used in the test (***Fig. 4.7.a and b***). Although the percentage of mutant larvae gathered in the blue zone was significantly lower than normal TLs (TL 71.47% , n=80; *panx1b*$^{-/-}$ 52.9%, n=92; p-value = 0.0024), yet *panx1b*$^{-/-}$ larvae demonstrated the zebrafish natural high preference for blue light. In the second place after blue, *panx1b*$^{-/-}$ larvae preferred red color/ higher wavelengths, whereas TL controls gathered in the yellow zone. There was a significant difference between genotypes for preferring red light (TL 9.85% , n=80; *panx1b*$^{-/-}$ 21.8%, n=92; p-value = 0.027). No preference or biases were found between groups for yellow and green light, both colors were equally preferred (Green: TL 7.7%, *panx1b*$^{-/-}$ 5.05%, p-value = 0.508; Yellow: TL 11.3%; *panx1b*$^{-/-}$ 9.53%, p-value = 0.901; TL n=80, *panx1b*$^{-/-}$ n=92).

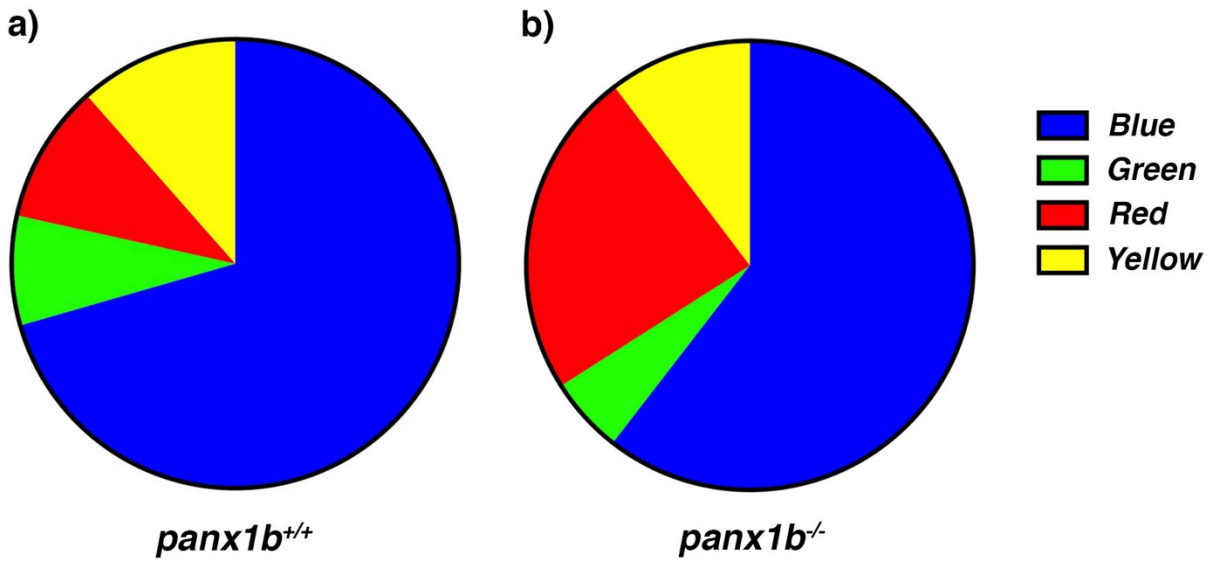

Figure 4.7. The color preference ranking pattern slightly differs in panx1b null larvae compared to TL controls. *a) TL: B>>Y>R>G; b) panx1b-/-: B>>R>Y>G. while the innate blue preference trait is preserved in mutants, their tendency towards red light was significantly higher than that observed in controls. No preference or biases were found between groups for the yellow and green light; both colors were equally preferred.*

4.5. Habituation to visual stimuli

To dissect the learning capacity and memory phenotype of *panx1b* mutants, we subjected larvae to repetitive visual stimulation and then tested for responsiveness to the trained stimulus. When exposed to an abrupt loss of illumination (dark flash), larval zebrafish elicit a unique turning maneuver called the "O-bend" (Burgess HA, Granato M, 2007, Wolamn 2014). This dark flash response is known to be habituatable, as evidenced by a gradual decline in responsiveness to repeated stimuli (Wolman *et al.*, 2011, 2014; Randlett *et al.*, 2019).

The test consisted of 4 training blocks of 60 dark flashes (DF; 1 sec) delivered at 59-sec interstimulus intervals (ISI), with training blocks separated by 60 minutes of rest (***Fig. 4.8.a***). The average DF responses magnitudes over the entire trials are shown in ***Fig. 4.8.b***. The average DF response of *panx1b*$^{-/-}$ larvae in the first training trial was markedly lower than TL controls (Trial 1: TL vs. *panx1b*$^{-/-}$, p-value<0.0001, n=96), confirming the previous VMR data suggesting a diminished Light-OFF response in mutants. During the second trial, increased response levels compared to the naïve levels (those observed in the first trial) was observed for both normal controls and mutant larvae, indicating larval sensitivity to the stimuli (Trial 2: TL vs. *panx1b*$^{-/-}$, p-value<0.02, n=96). After that, the mutant's response trend was completely distinct from that of TL controls. While a gradual decrement was detected in TL controls' response levels, *panx1b*$^{-/-}$ larvae remained hyperactive during the third and fourth trials (TL vs. *panx1b*$^{-/-}$: Trial 3, p-value<0.048; Trial 4, p-value<0.0002; n=96). This result indicated while the space-training induced

habituation in TL control larvae, consistent with the previous observations (Wolman et al., 2011; Randlett et al., 2019), it over-sensitized *panx1b* mutants.

To better quantify the larval learning, we measured the percentage of DF response habituation using formula 2.1 and compared it between genotypes (***Fig. 4.8.c***). Notably, larvae null for *panx1b* exhibited very poor learning capacity relative to the TL controls (TL =14.5%; *panx1b*$^{-/-}$= -66.6%; p-value=0.0043, n=96), suggesting that lack of functional Panx1b interferes with the learning process in the larval zebrafish.

Learning is the building block of memory formation, and the duration of learned behaviors provides a metric for it (Hyman, Shores and North, 2005; Levine et al., 2006; Isenberg et al., 2013). Here, we tested larvae's ability to recall the learned behavior in the 'Post-test' trial, 17 hours after training. The 17-hours time period simply represents the next morning after the training day. We avoided testing larval memory function during the night time immediately following the training program to reduce the interference of observed misalignments of the circadian clock system in the mutants' behavior. As shown in ***Fig. 4.8.b***, the average DF response in the 'Post-test' trial was greatly lower than that in the last training trial (i.e., the fourth trial) for both genotypes (Trial 'Post-test' vs. Trial 4: TL, *p*-value<0.0001; *panx1b*$^{-/-}$ *p*-value<0.0001; n=96). Dividing the 'Post-test' trial responses by the responses in the fourth trial (***Fig. 4.8.d***) provided a practically simplified measure of the memory retention (values less than 1) and also of the response recovery rates (values greater than 1). The normal TLs were able to retain their memory well, which is consistent with the previous reports on long-term habituation in wild-type larval zebrafish (Wolman et al., 2013; Randlett et al., 2020). However, the great response reduction in

panx1b mutants could not be associated with memory retention since they did not show any sign of training-induced learning. To further verify if the observed DF response reductions were due to the learning and memory retention, we compared the DF response levels of the trained with untrained larvae (***Fig. 4.8.e***). Contrary to the trained group, the responses of untrained TL larvae did not show any significant changes between trial one and 'Post-test' (p-value<0.21, n=48). In contrast, the response reduction was substantial in untrained mutants (p-value<0.02, n=48), similar to the trained mutants. These results confirmed that the observed response reductions in TL controls were based on training experience and that the habituation paradigm presented here induces memory that lasted for up to 17 hours. Though, in the larvae null for *panx1b,* the observed decline in responses reflected the involvement of other mechanisms, such as clock system deregulations, affecting the learning process and memory formation in mutants.

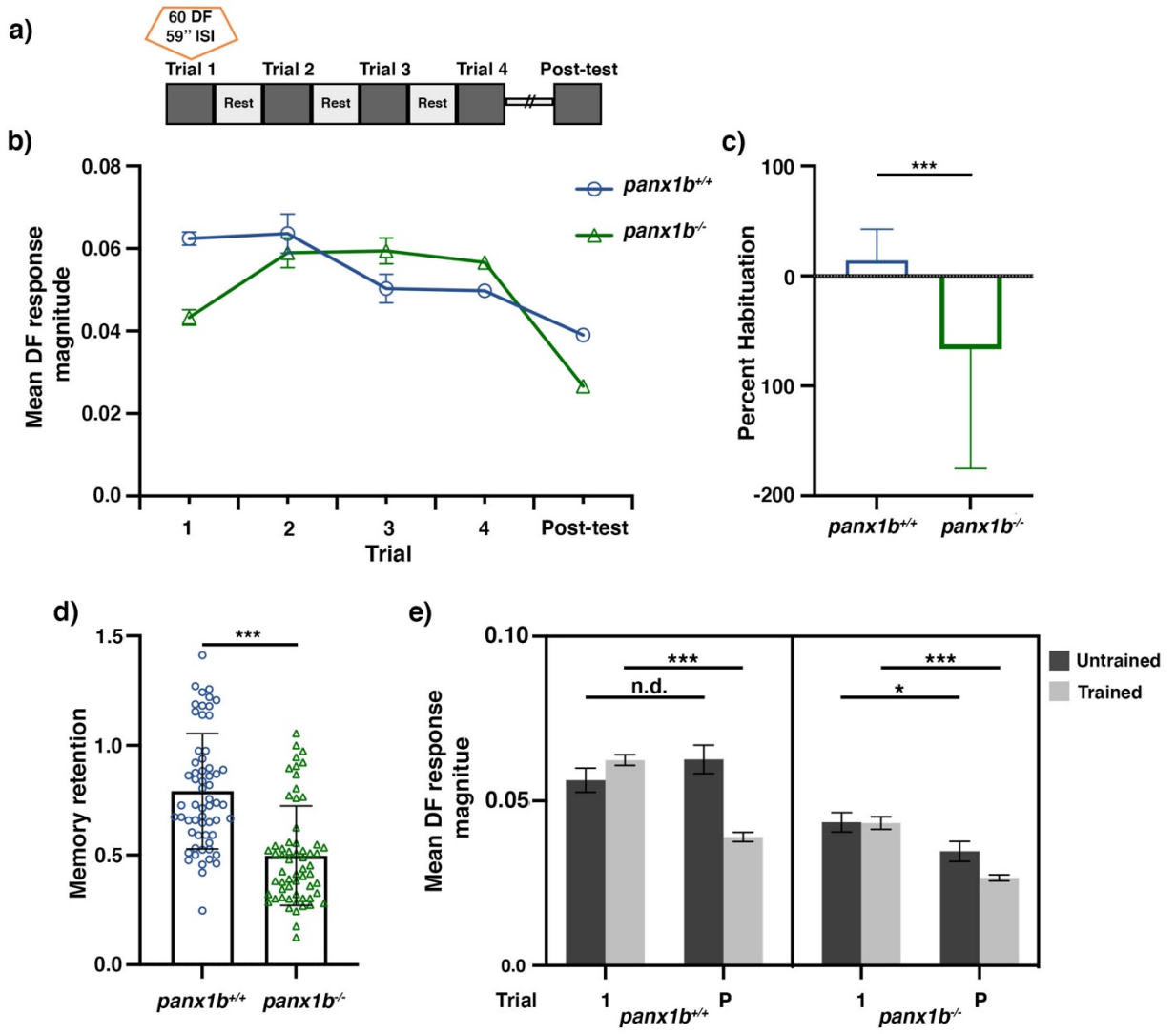

Figure 4.8. Loss of panx1b interferes with normal learning process and memory formation. *a) A space training regimen consisting of 4 blocks of 60 dark flashes (DF; 1 sec) delivered at 59-sec interstimulus intervals (ISI), with blocks separated by 60 minutes of rest. b) The average DF response magnitude across TL control larvae population progressively decreased throughout the 4 blocks of training. In contrast, panx1b$^{-/-}$ larvae responses to the stimuli remained elevated over 4 trials, indicating sensitization, not habituation occurrence. Larval response at the 'Post-test' trial (17 hours after training) reflects Memory formation. c) Comparing the percent habituation between groups demonstrates a significant non-associative learning deficit in panx1b$^{-/-}$ larvae. d) Memory formation was tested 17 hours after training (at the 'Post-test' trial; 7 dpf) and computed as the mean values across larvae for the 'Post-test' trial, divided by those in trial 4 (the last training trial). Values less than 1 indicate memory retention, whereas values greater than 1 reflect a recovery of the response. The memory retention was significantly higher in TL controls compared to mutants. e) To verify if reduced responsiveness is due to the training or the experimental time, we compared the larval responses of trained and untrained groups in trial 1 and 'Post-test' trial. Bar plot shows that the average DF responses in trial 1 (when larvae are 6 dpf) are similar between untrained and trained groups of each genotype. The larval response in the 'Post-test' trial shows a significant decline for the trained TLs, accounting for memory recall of a trained behavior. However, the significant response decrement was independent of the training in mutants, suggesting other mechanisms are involved in the panx1b mutants' loss of response. Error bars denote SEM in b and e and SD in c and d. Significance: p-value<0.05. Post-test' (P).*

4.6. Supplementary Figures

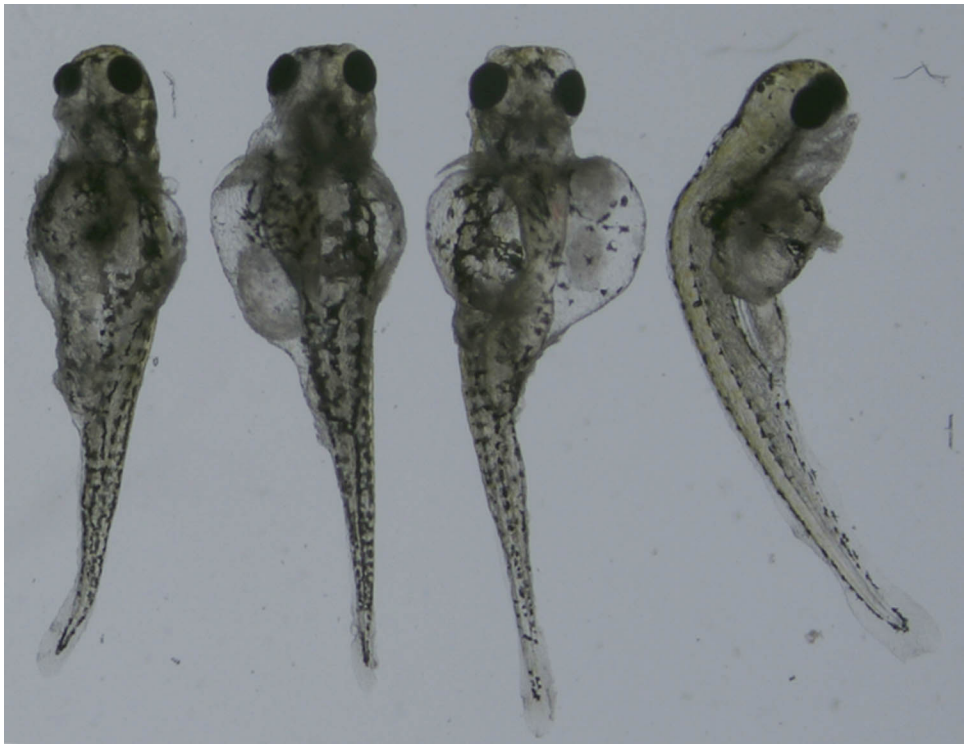

Supplementary Figure 4.1. Anatomical malformations observed in panx1b$^{-/-}$ larvae. *Swimming bladder edema, ventricular hypertrophy, an irregularly-shaped yolk sac, and spinal curvature were observed in approximately 11±4% of panx1b$^{-/-}$ 3 dpf larvae. The larvae representing malformations could not survive beyond 5-7 dpf.*

4.7. Supplementary Tables

Supplementary Table 4.1. GO annotation for upregulated genes.

Biological Process	*Danio rerio (REF) #*	*upload #*	*Fold Enrichment*	*p-value*
Regulation of primary metabolic process (GO:0080090)	4132	170	1.4	0.0000062
Regulation of nitrogen compound metabolic process (GO:0051171)	4076	167	1.39	0.000009
Regulation of macromolecule metabolic process (GO:0060255)	4368	178	1.39	0.00000623

Supplementary Table 4.2. GO annotation for downregulated genes.

Biological Process	*Danio rerio (REF) #*	*Upload #*	*Fold Enrichment*	*p-value*
cleavage involved in rRNA processing (GO:0000469)	26	8	7.35	0.0000474
circadian regulation of gene expression (GO:0032922)	45	11	5.84	0.0000119
cellular modified amino acid metabolic process (GO:0006575)	113	15	3.17	0.000199
mRNA processing (GO:0006397)	332	33	2.37	0.0000185
translation (GO:0006412)	320	30	2.24	0.0000975
negative regulation of nitrogen compound metabolic process (GO:0051172)	756	60	1.9	0.00000729
G protein-coupled receptor signaling pathway (GO:0007186)	1134	13	0.27	0.00000000543

Chapter 5. Zebrafish lacking both panx1a and panx1b genes retain normal phenotypes both morphologically and behaviorally

As documented in previous chapters, Panx1a and Panx1b share a similar physiological function: shaping the retinal OFF-pathway's final output. However, molecular mechanisms underlying each of the two gene copies' functions are completely different. It was intriguing to explore if any interactions exist between these two proteins and how that would affect the degree of severity of visual dysfunctions. In this chapter, anatomical, molecular, and behavioral characteristics of the larval zebrafish carrying mutations in both *panx1* genes (*panx1a*$^{-/-}$/ *panx1b*$^{-/-}$) are presented.

5.1. Panx1 double knockout (DKO; panx1a$^{-/-}$*/ panx1b*$^{-/-}$*) zebrafish maintain normal anatomy*

Studies using Panx1 knockout mice have reported physiological alterations to the retinal function (Kranz et al., 2013; Dvoriantchikova et al., 2018). Despite the strategically distinct localization of the two Panx1 copies in the zebrafish retina, they both contribute to the retinal OFF pathway's output, as reported in the previous chapters. However, the underlying molecular mechanisms through which the two Panx1 channels function are different. To further analyze the functional implications of *panx1a* and *panx1b* interactions in the zebrafish visual behaviours, a double knockout (DKO; *panx1a*$^{-/-}$/*panx1b*$^{-/-}$) zebrafish model was generated.

The *panx1a* and *panx1b* double knockout (DKO) zebrafish model on TL background was generated from the single *panx1a*$^{\Delta 4}$ and *panx1b*$^{\Delta 11}$ zebrafish. In brief, *panx1a*$^{\Delta 4}$ and

panx1b$^{\Delta 11}$ single knockouts were crossed twice. In the first round, heterozygous double mutants were produced. Then heterozygotes were intercrossed to generate homozygous DKO fish. Survival rate of DKO larvae didn't differ from that for TL controls at neither 1 dpf (values in %: TL 80.01; DKO 78.34; TL vs. DKO *p*-value= 0.76) nor 6 dpf (values in %: TL 82.94; DKO 88.56; TL vs. DKO *p*-value= 0.508; ***Fig. 5.1a***). Morphometric analysis revealed no gross abnormal anatomy in DKO larvae during the development. ***Fig. 5.1b*** represent an example of a 6 dpf DKO and normal TL larvae, which showed no difference in their body length measures compared to TL controls (TL controls= 3.83±0.27 mm; DKO =3.80±0.12 mm; TL vs. DKO *p*-value < 0.51; TL, n=60; DKO, n=44; ***Fig. 5.1.c***). The adult DKO zebrafish were viable and fertile like the normal parental TLs.

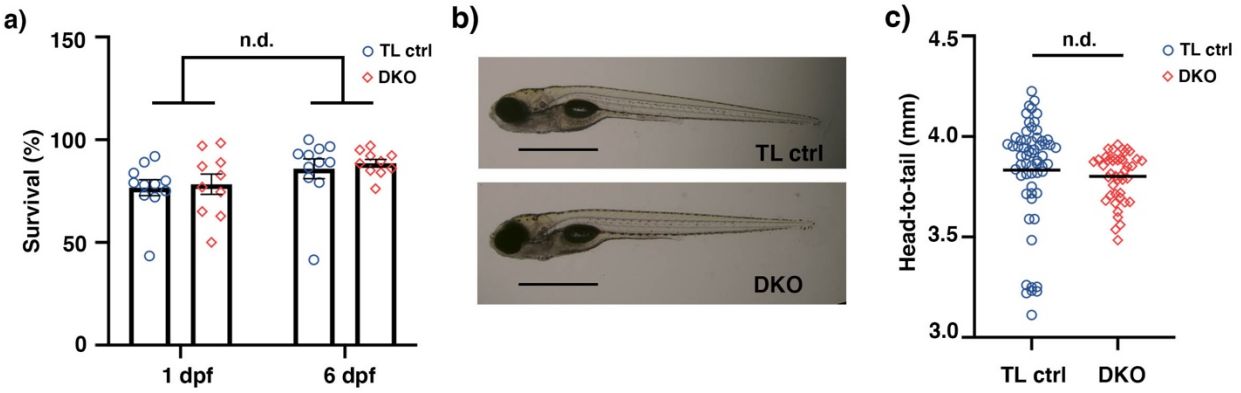

Figure 5.1. Phenotypic characterization of DKO larvae. *a) Survival rate at 1 and 6 dpf did not significantly reduce in mutants compared to TL controls. b) Age-matched TL control and DKO larvae (6dpf) showing regular morphology. Scale bar = 100μm c) The head-to-tail size measurement revealed no differences between DKO and control TLs. Significance: p-value<0.05; n.d.: No difference. Ctrl: control.*

5.2. Transcriptome profiling of 6 dpf DKO larvae

The transcriptomic analysis of DKO and TL larvae at 6 dpf (NCBI Gene Expression Omnibus (GEO) database; *panx1a*$^{-/-}$/*panx1b*$^{-/-}$, data deposit at GSE is pending on

submission of the manuscript) found a total of 58,616 RNAs in each sample (n=3/ genotype). Setting thresholds at an FDR<0.05 and *p*-value<0.001, 1213 downregulated, and 746 upregulated RNAs were detected. Using the ZFIN database, the deregulated genes were matched with the genes expressed in the CNS and visual system. One hundred twenty-five upregulated genes and 219 downregulated genes matched genes expressed in the central nervous system (***Fig. 5.2.a***, left panel). Furthermore, 97 upregulated genes and 171 downregulated genes matched genes expressed in the visual system (***Fig. 5.2.a***, right panel).

A Gene Ontology (GO) analysis (http://amigo.geneontology.org/amigo/landing) revealed that upregulated genes were enriched in biological processes related to photoperiodism and the regulation of transcription by RNA polymerase II (***Fig. 5.2.b***, green bubbles; ***Supplementary Tables 5.1***). Downregulated genes clustered in biological processes related to the interaction between DNA and proteins, such as nucleosome assembly, regulation of gene expression, mRNA processing, negative regulation of nitrogen compound, and G-protein coupled receptors (***Fig. 5.2.b***, purple bubbles; ***Supplementary Tables 5.2***). While no Reactome pathways could be assigned to the upregulated genes, the downregulated genes were concentrated in transcriptional regulation by small RNAs and DNA damage/telomere stress-induced senescence pathways (***Supplementary Tables 5.3***).

5.3. DKO larvae locomote normally in different light conditions

Both *panx1a* and *panx1b* single mutants demonstrated difficulty navigating in a dark environment. The peak response to dark stimuli as well as visual acuity was compromised. These primary findings, in addition to the transcriptome data showing

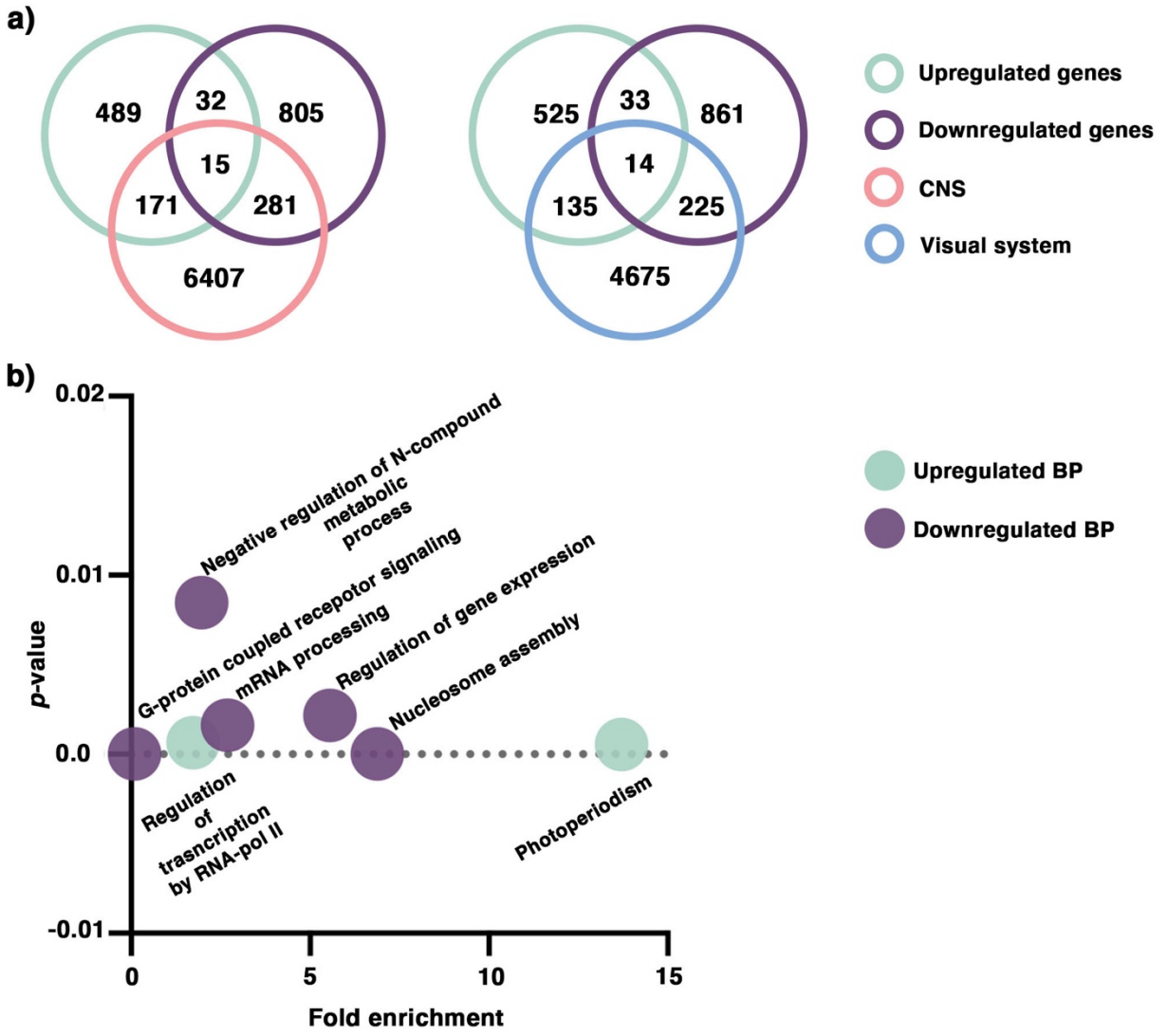

Figure 5.2. RNA-seq analysis of 6dpf DKO larvae. *a) Comparison of deregulated genes against two categories: central nervous system (CNS) and the visual system. b) GO annotation of RNA-seq data in terms of biological process (BP): the upregulated genes were enriched in photoperiodism and the regulation transcription by RNA polymerase(pol) II processes, whereas the downregulated genes were annotated for nucleosome assembly, regulation of gene expression, mRNA processing, negative regulation of nitrogen (N) compounds metabolism, and G-protein coupled receptor signaling.*

upregulation of genes functioning in photoperiodism in DKO larvae, advocated for analyzing the visual performance in the DKO genotype.

DKO larvae had comparable locomotor activity as TL controls in light, similar to the single mutants. The average distance traveled ($t = 1.7689$, $df = 49.253$, p-value = 0.08311) and velocity ($t = 1.3672$, $df = 49.809$, p-value = 0.1777;) were not significantly different between groups (TL, n=30; DKO, n=24; ***Fig. 5.3.a***).

Surprisingly, DKO larvae showed no difficulties navigating during the Light-OFF period. Although slightly hyperactive, they swam similar distances ($t = 1.1227$, $df = 39.957$, p-value = 0.2683) with the same speed ($t = 0.4553$, $df = 47.191$, p-value = 0.651) as TL-controls (TL, n=30; DKO, n=24; ***Fig. 5.3.b***).

Next, larval reaction to the sudden changes of lighting condition was tested using the VMR assay. The mean activity plot over three trials of light onset (Light-ON) and offset (Light-OFF) is shown in ***Fig. 5.4.a***. Both groups displayed the same activity levels during Light-ON phases; DKO larvae were more active than TL controls during Light-OFF trials. A closer look at the immediate reactions after light switches revealed no significant differences between genotypes. Both DKO and TL larvae responded immediately and with the same intensity to either the Light-ON (0-1 sec; p-value<0.43; ***Fig. 5.4.b***) or the Light-OFF stimulus (0-1 sec; p-value<0.20; ***Fig. 5.4.c***).

These data suggested that regardless of lighting condition, DKO fish can perform normal locomotor behavior as TL controls.

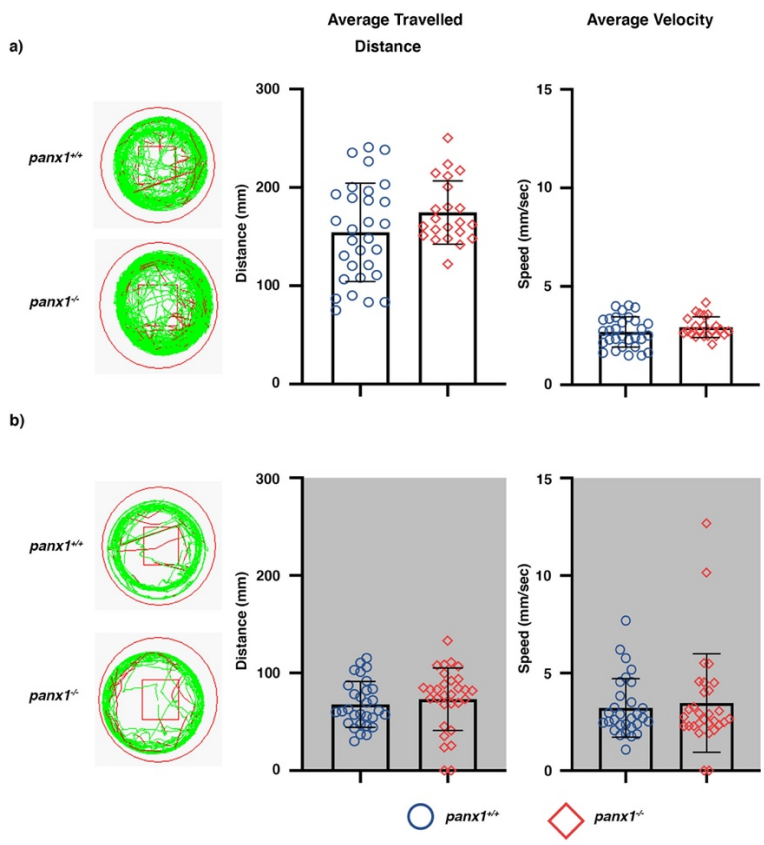

Figure 5.3. Locomotor activity in Light-Dark conditions

. Locomotion was video tracked for 60 min in a) Light-ON and b) Light-OFF conditions. The wells on the left show examples of TL control and DKO locomotion patterns. Medium (<20 mm/sec) or high-speed movements (>20 mm/sec) are visualized with green and red colors. Bar graphs show no significant differences between TL control and DKO larvae in terms of the average traveled distance (in mm) and velocity (mm/sec). TL, n=30; DKO, n=24. Significance: p-value<0.05.

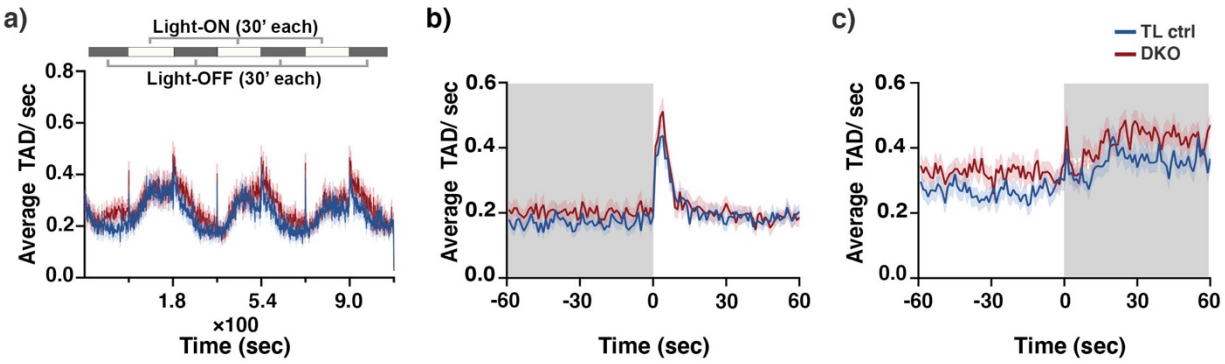

Figure 5.4. Visual-motor response (VMR) changes in DKO larvae. *a) The outline of the experimental paradigm is shown on top. The line graph shows the average TAD of DKO and TL control larvae from a representative test with n=40 larvae for each genotype. The activity was defined as the fraction of frames per second that a larva spent swimming. b, c) The results for average Light-ON and Light-OFF VMR are shown from 1 min before the light switch to 1 min after the light switch. The color ribbons surrounding the average activity line graph correspond to 1 SEM. The values are the average of the second trial from four independent tests with n=40 larvae for each genotype. The Light-ON and Light-OFF periods are indicated by white and black bars at the top of the panels. Significance: p-value<0.05. ctrl: control.*

5.4. Visual acuity declines in double knockout larvae

The visual acuity of DKO larvae was examined next. ***Fig. 5.5*** shows the average OMR values (depicted as the percentage of positive response; PPR) for 6dpf DKO and TL control larvae across three spatial frequencies (SF; 64, 128, 256 cycle/deg) paired with two velocities (72 and 144 deg/s) and two contrast levels (10 and 100%). As indicated by these plots, the visual acuity in doubly mutants was markedly impaired when presented with left-ward moving gratings. Similar to *panx1b*$^{-/-}$ single mutants, exposing larvae to left-ward moving strips at SF of 256 (cycle/deg), speed of 144, and a contrast level of 10% revealed a significant decline in the DKO's PPR compared to TL controls (*p*-value=0.003, TL n= 35, DKO n=40). The left-ward direction of motion when presented at high contrast condition, or the right-ward moving gratings (regardless of contrast conditions) yielded no significant PPR differences between groups. All the *p-value*s are given in ***Table 5.1***. This test's outcome revealed that the dependency of visual acuity on contrast level and spatial frequency in DKO larvae is similar to those identified by previous studies (Stiebel-Kalish *et al.*, 2012; Rainy *et al.*, 2016). It also provided the optimum combinations of direction, spatiotemporal frequency, and contrast level to elicit the significant OMR differences between *panx1* knockout and TL controls.

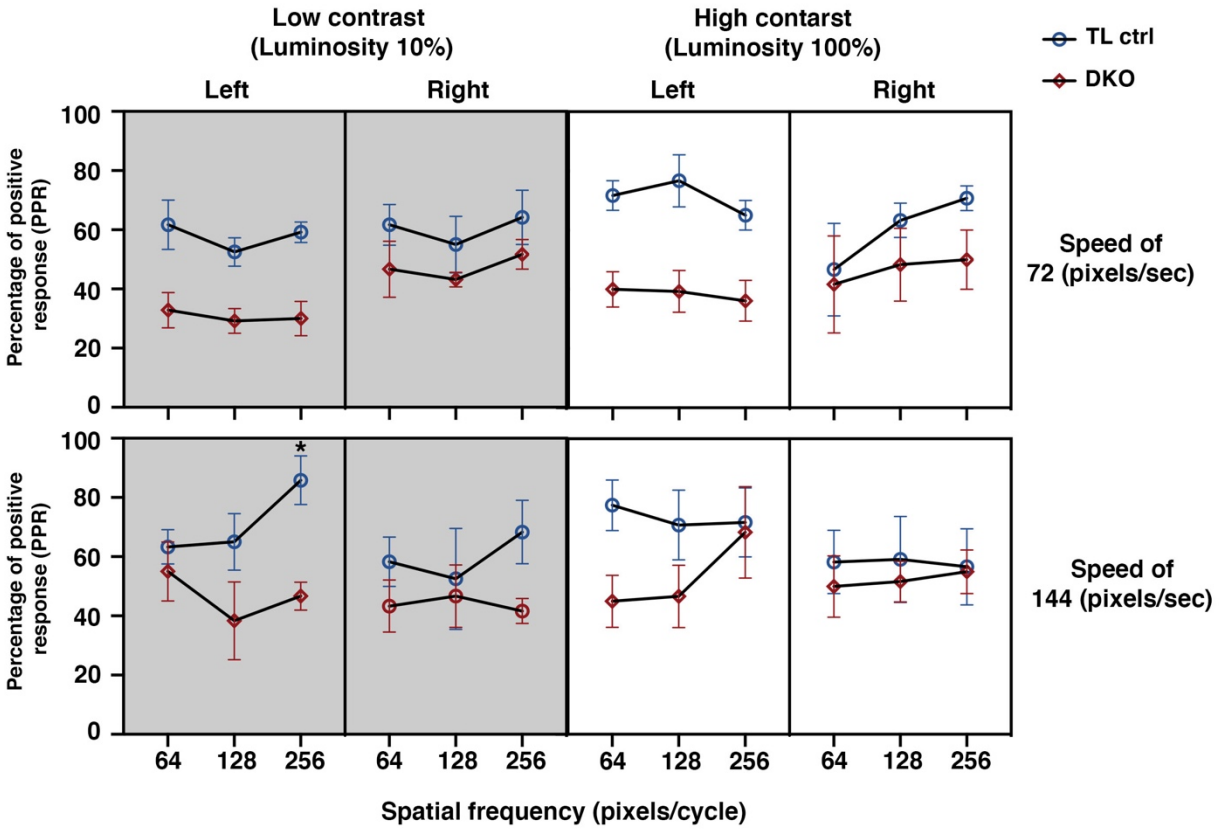

Figure 5.5. Lack of panx1 genes affects larval visual acuity. *Despite reduced response levels in the absence of both panx1a and panx1b copies, DKO larvae still accurately followed the direction of motion in all tested spatiotemporal frequencies. Though similar to the panx1b-/- group, the DKO's percentage of positive response (PPR) was significantly lower compared to TL controls for the left-ward motion at SF=256 (p/c), speed of 144 (p/s), and low contrast setting. The PPR values for each setting are the average of four tests ±SEM (n=40). Significance: p-value<0.05. Ctrl: control.*

Table 5.1. The multivariate comparisons of OMR between TL controls and DKO larvae.

Contrast levels		***Low (10%)***			***High (100%)***		
Speed (pixels/sec)	***Direction***	***Spatial Frequencies (pixels/cycles)***					
		64	***128***	***256***	***64***	***128***	***256***
72	***Leftward***	0.049	0.45	0.23	0.92	0.13	0.013
	Rightward	0.59	0.77	0.466	0.97	0.81	0.35
144	***Leftward***	0.133	0.35	0.003	0.52	0.26	0.68
	Rightward	0.899	0.8	0.51	0.87	0.99	0.77

5.5. Double knockout zebrafish discriminate colors normally

In the color preference test, DKO larvae (6dpf) normally discriminated colors, preferred blue color significantly more than other colors, and showed a similar color preference trend as single mutants. The color preference ranking order in DKO group was B> R> Y> G, which is different than that in TL control larvae (B>Y>R>G). Interestingly, the percentage of larvae choosing each subjective color was not significantly different between TL controls and DKO larvae (Blue: TL ctrl 69.43%, DKO 66.21%, *p*-value = 0.935; Green: TL ctrl 7.77%, DKO 6.42%, *p*-value = 0.671; Red: TL ctrl 10.85%, DKO 17.93%, *p*-value = 0.507; Yellow: TL ctrl 11.34%, DKO 7.09%, *p*-value = 0.825; TL ctrl, n=80, DKO, n=92; ***Fig. 5.6***).

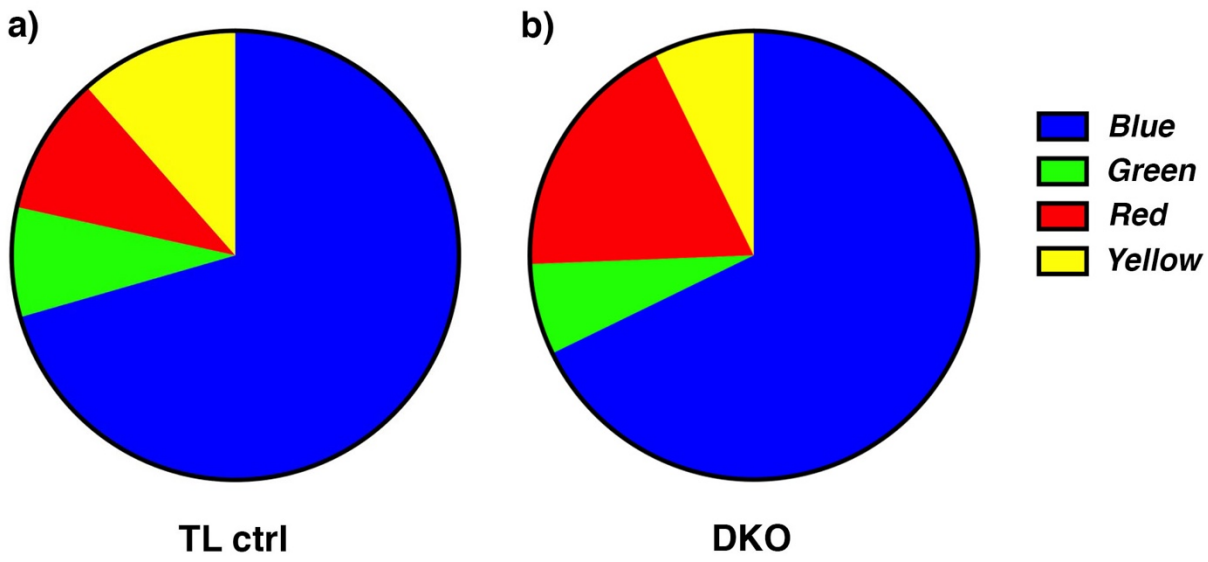

Figure 5.6. DKO larvae normally discriminate colors. *The color preference ranking pattern slightly differs in DKO larvae compared to TL controls. a) WT: B>>Y>R>G; b) DKO: B>>R>Y>G. The innate blue preference trait is preserved in double mutants. No differences were detected between mutants and TL controls in the tendency towards red, yellow, and green. Ctrl: control.*

5.6. Supplementary Tables

Supplementary Table 5.1. GO annotation for upregulated genes.

Biological Process	Danio rerio (REF) #	upload #	Fold Enrichment	p-value
Photoperiodism	25	9	13.71	0.000548
Regulation of transcription by RNA	2174	99	1.73	0.000626

Supplementary Table 5.2. GO annotation for downregulated genes.

Biological Process	Danio rerio (REF) #	Upload #	Fold Enrichment	p-value
Nucleosome assembly (GO:0006334)	65	18	6.88	0.00216
Regulation of gene expression, epigenetic (GO:0040029)	67	15	5.56	0.00216
mRNA processing (GO:0006397)	332	36	2.69	0.00161
negative regulation of nitrogen compound metabolic process (GO:0051172)	756	60	1.97	0.00847
G protein-coupled receptor signaling pathway (GO:0007186)	1134	4	0.09	$2.06e^{-11}$

Supplementary Table 5.3. Reactome pathways associated with downregulated genes.

Reactome pathways	Danio rerio (REF) #	upload #	Fold Enrichment	p-value
Transcriptional regulation by small RNAs	41	11	6.66	0.00597
DNA damage/Telomere stress induced senescence	43	11	6.35	0.00882

Chapter 6. Discussion

The two pannexin 1 (*panx1*) genes, *panx1a* and *panx1b*, originate from a third whole-genome duplication (R3 WGD) event implying that *panx1* copies emerged with ray-finned fishes and diverged thereafter (Bond et al., 2012). Since in mammals one Panx1 seems sufficient, a question raises about how zebrafish benefits from having two *Panx*1 proteins with distinct tissue distribution and properties, of which Panx1a expression pattern mimics the near ubiquity of mammalian Panx1, while Panx1b is highly enriched in the brain and eyes (Bond et al., 2012). Although some degree of functional specialization of both Panx1 proteins in the retina has been suggested (Kurtenbach et al., 2013), their roles at the system level and in behavioral studies remained elusive. This dissertation focused on characterizing the molecular and behavioral consequences of full genetic disruption of the pannexin 1 through deletion of both *panx1a* and *panx1b*. we utilized transcriptome analysis along with visual-motor behaviors to discover how ablation of either *panx1* gene would impact larval zebrafish vision and vision-related performance.

6.1. Establishing transgenic lines

The employed targeted gene knockout approach, transcription activator-like effector nucleases (TALEN), introduced small deletions in exon 4 of the *panx1a* and *panx1b* genes. Both mutations caused the generation of truncated proteins. The mutation in the *panx1a* gene was distinct from the previously reported *panx1a*$^{-/-}$ model in which the start codon was targeted (Cenedese et al., 2017), but better compared to the mouse knockout model with deletions of exons 3 and 4, which was used previously to investigate sensory processes and learning and memory (Prochnow et al., 2012; Dvoriantchikova et al.,

2018). The approaches used to generate *panx1b* and *panx1a*/*panx1b* (double) knockout zebrafish models in this study are synonymous to the previous report (Cenedese *et al.*, 2017). Similar to other rodents (Bargiotas et al., 2012; Hanstein et al., 2016) and the other zebrafish model (Cenedese et al., 2017), the *panx1a*$^{-/-}$, *panx1b*$^{-/-}$, and DKO zebrafish are viable and fertile, with no apparent anatomical abnormalities or morphologic changes to the eyes.

All investigations were performed at 6dpf when the subdivisions of the brain and sensory systems have formed, and excitatory glutamatergic neurons, inhibitory GABAergic interneurons, astrocytes, and microglia required for normal excitatory discharges within neuronal networks are functional (Guo et al., 1999; Holzschuh et al., 2001; Higashijima, Mandel and Fetcho, 2004).

6.2. Loss of function mutations in each panx1 gene affect transcriptome differently

The transcriptome analysis demonstrated that loss of *panx1a* effectively altered transcription of almost 20% of all expressed genes. The observed expression regulation was consistent with the known expression profile of *panx1a* across multiple organ systems (N. Prochnow et al., 2009; Bond et al., 2012; Kurtenbach et al., 2013). Vision-related processes and the development of the eye, or the transportome, a collective term referring to proteins facilitating transport to and across membranes, which includes ion channels, purinergic and neurotransmitter receptors, and solute carrier (SLC) transporters were affected (Huang et al., 2004). Furthermore, the regulation of genes known as primarily located in the pre and postsynaptic compartments of dopaminergic synapses provides for the first-time evidence that ablation of *panx1a* alters dopaminergic

signaling. These transcriptional changes are noteworthy and substantiate the role of *panx1a* as a significant molecular hub, which was proposed previously from interactome studies (Wicki-Stordeur and Swayne, 2014). Moving forward, the transcriptome study opens windows of opportunity to study the diverse mechanism dynamically regulating Panx1a channel function, such as elevated extracellular K^+ (Wang, Jackson and Dahl, 2018), or the interaction with purinergic (Iglesias et al., 2008; Boyce and Swayne, 2017), NMDA (Weilinger et al., 2016; Bialecki et al., 2020), or α1-adrenergic receptors (Chiu et al., 2017; DeLalio et al., 2019).

Transcriptome changes in the absence of *panx1b* were markedly different compared to *panx1a*$^{-/-}$ larvae. Approximately 3.5% of all genes, mainly involved in the regulation of metabolism, were deregulated. The upregulation of genes involved in the primary metabolic processes was accompanied by the downregulation of genes related to RNA processing and circadian rhythms in 6 dpf *panx1b*$^{-/-}$ larva. Evidently, the circadian clock system closely interacts with the metabolic pathways (Asher and Sassone-Corsi, 2015; Reinke and Asher, 2019). Also, most visual system functions, such as opsins genes expression, retinal neurotransmission, perception of light, and contrast sensitivity, display robust day-night rhythms (Foster et al., 1993; Argamaso et al., 1995; Bellingham and Foster, 2002; Green and Besharse, 2004; Tosini et al., 2008; McMahon, Iuvone and Tosini, 2014; Li, 2019). The observed disruption of the clock system in *panx1b*$^{-/-}$ larva revealed a novel nexus through which *panx1b* may affect vision. A major challenge remains in determining how these interactions between *panx1b* and circadian clock genes promote vision and visual behaviors. Because zebrafish maintain evolutionary proximity

to mammals (Li, 2019; Chen, 2020; Demin et al., 2020), the findings from zebrafish research may help better understand circadian mechanisms underlying vision in other vertebrate species, including humans.

Interestingly, in the absence of both *panx1* copies (i.e., *panx1a* and *panx1b*), a distinct pattern of gene expression alteration was detected. Unlike *panx1a*$^{-/-}$, no deregulations in either purinergic or dopaminergic pathways were identified in 6dpf DKO larva. However, a profound upregulation of circadian clock genes was present in double mutants, indicating that both the single *panx1b* and the interactions between the two *panx1* genes play an important role in the old game of photoperiodism. Since the clock system deregulation in *panx1b*$^{-/-}$ and DKO larvae shows inverse trends deciphering the underlying mechanisms of interaction between the two *panx1* genes seems necessary. Furthermore, DKO larvae displayed downregulation of DNA damage/telomere stress-induced senescence pathway, which indicates a potential instability in the cell-cycle arrest mechanisms (Hewitt et al., 2012). It is believed that senescence has an important role in vivo, on the one hand as a safeguard against cancer (Serrano et al., 1997) and on the other hand contributing to biological processes such as embryonic development (Muñoz-Espín et al., 2013; Storer et al., 2013), wound healing (Jun and Lau, 2010), tissue repair (Krizhanovsky et al., 2008) and organismal aging (Baker et al., 2008; Van Deursen, 2014). It's worth mentioning that Panx1 has so far been shown to be involved in adult neurogenesis (Wicki-Stordeur et al., 2012), which is important during both physiological brain development as well as brain repair during pathology and diseases (Berg et al., 2013), and in cornea wound healing (Mayo et al., 2008). Taken together, it seems the

crosstalk between *panx1a* and *panx1b* provides feedbacks to a multitude of signaling pathways involved in regulating the cell cycle. Therefore, a detailed comparative analysis of transcriptome profiles of all three mutant types (i.e., *panx1a*$^{-/-}$, *panx1b*$^{-/-}$ and DKO) may shed more light on the Panx1 nexus.

6.3. Panx1 channels are critically involved in visually guided locomotion in dark conditions

The deregulation of genes involved in dopaminergic signaling in *panx1a*$^{-/-}$ as well as the circadian clock system disruptions in *panx1b*$^{-/-}$ and DKO fish suggest consequential alterations in behavioral outcomes. Cellular effects driven by the loss of *panx1a* functions reduced larvae's navigational competence in a dark environment. In contrast, a markedly increased locomotion was observed in larvae null for *panx1b* and, DKO fish surprisingly performed similarly to the TL controls. The inverse impacts of ablation of either *panx1* gene on dark navigation competence emphasize distinct molecular mechanisms underlying each Panx1 function, which, along with double mutants' normal phenotype, suggests that Panx1a and Panx1b signalings might negate each other effects at least in some visual-motor circuits.

To further investigate larval dark vision, we utilized the visual-motor response (VMR) assay, which allows measuring the responsiveness of zebrafish larvae to changes in light intensities (Emran, Rihel and Dowling, 2008). This responsiveness requires an intact retina (Fernandes et al., 2012) and photoreceptor populations with distinct spectral properties (Burton et al., 2017). The advantage of this test compared to the optokinetic reflex test (OKR) is that it allows extracting behavioral responses caused by changes in

the retinal ON and OFF pathways. A limitation of the VMR test is that at 6dpf, it does not discriminate between rod and cone responses (Ganzen et al., 2017) since rod photoreceptors are not functional in zebrafish until 15dpf (Bilotta, Saszik and Sutherland, 2001; Morris and Fadool, 2005).

The significant reduction in larval response to the sudden darkness in both *panx1a*$^{-/-}$ and *panx1b*$^{-/-}$ groups reinforces a compromised dark vision in mutants. This phenotype was reproduced in TL control larvae through pharmacological activation of D1-/D2-like dopaminergic receptors and rescued in *panx1a*$^{-/-}$ larvae by treatment with the D2-like receptor antagonist Haloperidol and an adenosine receptors agonist, adenosine. These results suggest that the altered behavior of *panx1a*$^{-/-}$ larvae in a dark environment and during light/dark transitions is caused by Panx1a modulating visual inputs through D2-like dopaminergic receptors signaling. Moreover, the adenosine signaling seems to lie at the crossroad between Panx1a and the dopaminergic system. Beyond the visual system, a recent behavioral study in Panx1 knockout mice showed that loss of Panx1 induces difficulties in motor control and changes of the sleep-wakefulness cycle. The authors suggested that deficiencies in adenosine and other signaling pathways were causing the reported deficiency (Kovalzon et al., 2017).

However, in *panx1b*$^{-/-}$ larvae, the reduced immediate response to sudden darkness could not be associated with any changes in the dopaminergic and adenosine signaling pathways as observed in *panx1a*$^{-/-}$ larvae. Rather it seemed to result from disruptions in the inner nuclear layer (INL) and/ ganglion cell layer (GCL) circuits, where Panx1b proteins are prominently localized (Kurtenbach et al., 2013). In line with this proposal is a

recent study that reported Panx1 channel activity currents only in the OFF-type retinal ganglion cells (RGCs), the neurons responsible for detecting light decrement. Using pattern electroretinogram (PERG) recordings, it was shown that targeted ablation of the Panx1 gene in RGCs impairs the retina's electrical output in mice (Dvoriantchikova et al., 2018). Although the exact molecular mechanism underlying the role of Panx1b in the zebrafish inner retinal OFF pathways remains unclear, it could be speculated that diminished Light-OFF peak response in *panx1b*$^{-/-}$ larvae is due to considerable downregulation of several core clock genes (i.e., *cry 1*, *cry 5*, *bmal1a* and *1b*, and *clock 2*; as revealed by RNA-seq and qRT-PCR data) which have been shown to play an important role in regulating the zebrafish inner retina functions and adjusting visual sensitivity (Li and Dowling, 1998, 2000; Frøland Steindal et al., 2018). The circadian clock system's role in regulating visual sensitivity has been the subject of numerous studies. For example, using a behavioral assay, the luminance detectability of rats was shown to be influenced by a circadian clock; in rats maintained in constant darkness, visual sensitivity fluctuated by up to one log unit during a period of 24-hour (Rosenwasser et al., 1979). In zebrafish, the circadian rhythm of behavioral visual sensitivity was evaluated by measuring the minimum light intensities required to evoke the scape responses (Li and Dowling, 1998, 2000; Schmitt and Dowling, 1999; X. Li *et al.*, 2012). The experiments were performed under both cyclic and constant illumination. Under a normal light-dark (LD) cycle, the minimum light intensities required to evoke the escape were markedly higher in the early morning time than in the afternoon time. This suggests zebrafish are least sensitive to visual stimuli before light on (dawn) and most sensitive before light off

(dusk) over the period of 24 hours. This pattern of fluctuation persisted in constant darkness, suggesting the involvement of circadian clocks in the regulation of zebrafish behavioral visual sensitivity. In our VMR experiments, the dark and light cycle's length (30 min) was comparable to that in Li and Dowling (Li and Dowling, 1998) Scape Test (20 min). However, it should be noted that we always did the measurements in a fixed early afternoon time (between 1-4 pm), not throughout the entire 24-h period. It is possible that the clock-mediated heightened retinal sensitivity around afternoon time, which improves luminance detectability (Rosenwasser et al., 1979; Li and Dowling, 1998), fails to function properly in *panx1b*$^{-/-}$ larvae, leading to diminution of dark pulse response.

Lastly, the normal Light-OFF response in the DKO larvae provides further support for the possibility of an inverse correlation between Panx1a and Panx1b signaling cascades.

6.4. Color preference and perception is minimally affected in the absence of panx1s

Numerous studies in zebrafish have documented physiological responses of the different retinal cell types to colored (spectral) light stimuli, indicating a complex level of information processing and color vision in this species; for review, see (Meier, Nelson and Connaughton, 2018). This study examined the innate color preference of larval zebrafish to investigate the functional implications of either Panx1s proteins in the color recognition and address the subtle responses to monochromatic light in the daytime.

Our results showed a very distinct color preference ranking pattern among genotypes (TL: B>>Y>R>G; *panx1a*$^{-/-}$ B>>R>G>Y; *panx1b*$^{-/-}$ and DKO: B>>R>Y>G), with blue being the most preferred light, agreeing with previous studies (Risner et al., 2006; Oliveira et al., 2015; Park et al., 2016; Peeters, Moeskops and Veenvliet, 2016). First, these data

indicate that larval spectral detection ability and normal preference for blue light are not affected by ablating either of *panx1s* genes. Though, the secondary color choice was different between TL controls and mutants. The larvae null for *panx1s* (both single and doubly *panx1s* mutants) showed more preference for red light (after blue; in secondary order), whereas normal TLs preferred yellow. Previously, it was reported that both larval (Park et al., 2016) and adult (Avdesh et al., 2012; Bault, Peterson and Freeman, 2015; Siregar et al., 2020) zebrafish avoid yellow color. Since in our study, the color preference index was not significantly different among red, yellow, and green for normal TLs, *panx1a*$^{-/-}$, and DKO groups, these ranking pattern discrepancies can be neglected. However, the attraction of *panx1b*$^{-/-}$ larvae towards red light was significantly higher than that towards green, but not yellow. It was also higher compared to the red preference index in TL controls, which is confounding. An explanation for *panx1b*$^{-/-}$ larvae preferring red over green and yellow could be that the overexpression of opn1lw2 (a longwave/ red-sensitive opsin) gene in the absence of *panx1b*, as revealed by transcriptome data, drives that effect. Interestingly, other studies have also reported a higher preference for red light (Avdesh et al., 2012; Ahmad and Richardson, 2013). It was suggested that the red preference is due to the natural foraging behavior of zebrafish as their natural diet is rich in microcrustaceans (Spence et al., 2008) and carotenoids (Olson and Owens, 1998), which are red in color. However, the larvae subjected to color vision tests were not fed in this study. Though, whether the increased tendency towards red color in the absence of Panx1b functions results from changes in the spectral detection, transduction, and/ perception circuits needs further molecular and behavioral investigations.

6.5. Loss of Panx1b function impairs directional tuning of the optic flow

The optomotor response (OMR) test can be used to evaluate the spatial acuity in zebrafish, as fish will turn and swim in the direction of perceived motion when presented with a whole-field moving grating (Neuhauss et al., 1999; Orger et al., 2000). The OMR procedure offers the advantage that the fish can be tested without prior training and while they are head-fixed (Neuhauss et al., 1999; Orger et al., 2008; Portugues et al., 2015; Naumann et al., 2016) or freely moving (Maaswinkel and Li, 2003; Stiebel-Kalish et al., 2012; Rainy et al., 2016). However, a disadvantage might be that they are not perfectly swimming in a fixed depth and therefore, view the stripe patterns from variable distances. A complete grating sensitivity function takes approximately 30 minutes of testing in our setting, which enables relatively rapid screening for spatial vision in zebrafish.

Here we examined different spatial and temporal frequencies and contrast levels to determine how genetic disruption of the *panx1b* compromises larval vision. Our data confirmed that 6 dpf larvae could elicit OMR in line with the previous studies showing this response is present in fish as early as 5 dpf (Portugues and Engert, 2011; Stiebel-Kalish et al., 2012; Rainy et al., 2016). The exciting finding is the dependency of the optic flow's direction-selectivity to the Panx1b channel's function in low contrast conditions. The 6dpf *panx1b*$^{-/-}$ and DKO larvae failed to follow the left-ward direction of motion when tested with high spatiotemporal frequencies (i.e., SF of 256 pixels/cycle and speed of 144 pixels/s) at low contrast levels. In contrast, their responses to the same stimuli but in the right-ward direction or in high contrast conditions were similar to normal TL larvae. In zebrafish, as in humans (Wandell et al., 1999; Ruppertsberg, Wuerger and Bertamini,

2003), motion detection is dominated by a luminance channel, which pools red and green cone signals (Orger and Baier, 2005). These signals are input into direction-selective (DS) ganglion cells (DSGCs), which further process and encode the presence and the direction of motion (Taylor and Vaney, 2002; Briggman, Helmstaedter and Denk, 2011; Ding et al., 2016; Naumann et al., 2016). Although our transcriptome data revealed the opn1lw2 (a longwave/ red-sensitive opsin) gene expression alters in the absence of *panx1b*, it does not seem to drive any effects on the cone's motion detection function, as mutant larvae could elicit the OMR in all tested spatiotemporal frequencies. The left-ward OMR's profound defects revealed a novel role for Panx1b channels in the directional-coding retinal mechanisms. In the larval zebrafish, the direction of motion is encoded by three direction-selective (DS) subtypes of ganglion cells tuned to upward, downward, and caudal-to-rostral motion. Whether the head-to-tail moving gratings presented to larvae in our study revealed a deficiency in this specific population of DSGCs needs further anatomical and physiological studies. On top of that, the direction tuning of multiple subtypes of DSGCs has been shown to depend on light level (Tikidji-Hamburyan et al., 2015). For instance, superior preferring ON-OFF DSGCs are electrically coupled by gap junctions, while cells preferring the other directions are not coupled (Vaney, 1994; Trenholm et al., 2014). Coupling through gap junctions strikes a balance between improving the detection of motion in dimly lit conditions against a cost to the accuracy of direction estimation (Yao et al., 2018). Since the OMR deficiency in the absence of Panx1b occurred only with the left-ward motion at low light conditions, it is intriguing to understand if Panx1b channels play similar roles as connexins in broadening direction

tuning at low light levels in specific DSGCs types. Further structural and physiological studies will shed more light on the precise mechanisms underlying Panx1b channels' contribution to shaping the direction-selectivity of retinal outflow.

6.6. Larvae null for panx1b do not habituate to aversive visual stimuli

Larval zebrafish show a remarkable capacity for behavioral plasticity in response to visual stimuli, including habituation (Roberts et al., 2011; Wolman et al., 2011; Randlett et al., 2019), as evidenced by a progressive attenuation of responsiveness to the trained stimuli (Thompson and Spencer, 1966). Here, we developed a spaced training paradigm based on previous reports (Wolman et al., 2011; Randlett et al., 2019), which yielded a long-lasting response decrement up to 17 h post-training. This effect is consistent with habituation paradigms reported for other organisms (Beck and Rankin, 1995; Rose et al., 2002; Sullivan, Rose and Pfefferbaum, 2006; Cooke et al., 2015), as well as larval zebrafish (Wolman et al., 2011; Randlett et al., 2019). The space training paradigm was chosen since it was previously shown to efficiently induce longer-lasting habituation of behavior, lasting up to 24 h post-training, compared to the 1 hour when using massed training protocols (Wolman et al., 2011). In our experiment, the interstimulus interval (ISI) followed that reported by Randlett and co-workers (Randlett et al., 2019). We analyzed the duration of sudden bursts of hyperactivity (a component called "burdur" in viewpoint software) to report on the magnitude of startle responses. Other researchers had also used this kinematic parameter of movement to assess habituation in larval zebrafish going through the DF space training. The related memory was reported to last about 5 hours (Randlett et al., 2019). In comparison, our results indicated that longer retention of

memory, up to 17 hours, can occur. While the two experiments had different approaches of calculating the DF response duration, one must also consider the potential impacts of using different zebrafish strains (Toupfel long fin in our experiment vs. Tuebingen long-fin (TLF)). Different strains of zebrafish differ genetically, physiologically, and behaviourally (Wright et al., 2006; Oswald and Robison, 2008; Benner et al., 2010; Vital and Martins, 2011; Drew et al., 2012; Van Den Bos et al., 2019). For instance, Vignette and co-workers (Vignet et al., 2013) compared the exploratory behavior and color conditioning of two strains of zebrafish, AB and TU. They showed while TU fish recover swimming activity faster in T-maze or home base release in novel tank tests, AB fish scored better in the color learning test. Moreover, inhibitory avoidance in zebrafish was found to be rapidly acquired (Blank et al., 2009); though, some strains of zebrafish, such as AB strain, are unable to learn inhibitory avoidance (Gorissen et al., 2015). On the other hand, AB strain has appeared stronger in changing their locomotor activity levels in response to light-dark transitions and faster in habituation to acoustic/vibrational stimuli than TL strain (Van Den Bos et al., 2017). However, there is no study comparing the cognitive performances between TL and TLF strains so far. The present study was the first demonstration of visual memory retention beyond 17 hours after learning trials in the TL strain of zebrafish to the best of our knowledge.

Unlike normal TL larvae exhibiting an iterative reduction in response to a series of DF stimuli, which satisfies habituation's criteria, the larvae null for *panx1b* failed to show any learning. Instead, the persistent increment of responses over training blocks suggests a disruption of this non-associative learning (habituation) process in mutants. Behavioral

studies in animal models (Bert et al., 2002; Kofman et al., 2007; Küçük et al., 2008; Abuhamdah et al., 2016) along with human cases (Davidson, Jackson and Kalin, 2000; Grillon, 2002; McTeague et al., 2011; McTeague and Lang, 2012; Jackson et al., 2017) have revealed that increased tendency for heightened responding to aversive stimuli is linked to anxiety disorder. Although the mutant larvae displayed deficiencies in habituating to the visual stimuli, their DF responses in the Post-test block were significantly lower than naïve levels (those observed in trial 1) in both trained and untrained groups. This attenuation of locomotor activity the day after the initial exposure to the stimuli suggests that other mechanisms rather than memory recall drove this effect. Considering that circadian clock genes, which are significantly downregulated in the absence of *panx1b*, are implicated in the regulation of cognitive functions (Wulff et al., 2010; Krishnan and Lyons, 2015; Rawashdeh, Parsons and Maronde, 2018), it is rational to hypothesize that the misalignments of circadian oscillations are underlying this learning and memory deficit in the mutant larvae. The novel evidence of *panx1b* linkage to the well-established connections between the circadian clock system and cognition may have important translational approaches. For example, therapeutic compounds selectively targeting Panx1b might offer great molecular and behavior-modifying precision in clinical use for cognitive disorders.

6.7. Tracing Panx1b relevance to the clock-cognition nexus

Circadian genes are implicated in the regulation of cognition (Wulff et al., 2010), mood, and anxiety (Mansour et al., 2006; Kripke et al., 2009; Sipilä et al., 2010; Wulff et al., 2010; Logan and McClung, 2019) and, learning and memory (Gerstner and Yin, 2010;

Kondratova et al., 2010). For instance, gene expression analysis and behavioral assays in mice have shown that the genetic disruption of the circadian clock through disrupting the core genes cryptochrome 1 and 2 (*cry1* and *cry2*) results in elevated anxiety. Mice lacking *cry1* and *cry2* (*cry1*$^{-/-}$ and *cry2*$^{-/-}$) displayed attenuated dark phase and novelty-induced locomotor activity, along with an impaired recognition memory (De Bundel et al., 2013). In a separate study, the selective knockdown of the core clock gene *bmal1* was reported to cause an attenuation of circadian rhythms and the subsequent emergence of anxiety-like behaviors. Behaviors such as avoiding a potentially dangerous environment, increased latencies, or failures to escape with increased immobility times when exposed to startling stimuli were observed (Landgraf et al., 2016). Acquisition of certain types of memory, such as long-term emotional memory, has been linked to *clock2/npas2* genes, which regulate the neuronal expression of a battery of genes required for the consolidation of memory. *Npas2*-deficient mice were found to exhibit deficits in the long-term memory arm of the cued and contextual fear task (Garcia et al., 2000). Similar results were obtained in our *panx1b*$^{-/-}$ larvae displaying a significant downregulation of 5 core clock genes (i.e., *cry1*, *cry5*, *bmal1a*, *bmal1b*, *clock2*). In-depth analysis of locomotion patterns in the dark revealed that the reduced immediate response of *panx1b*$^{-/-}$ fish to sudden darkness is accompanied by being slower to escape, spending more time immobile during the first few seconds after the light switch and, subsequently, showing persistent hyperactivity during the entire dark phase. The persistent hyperactivity during habituation test's training trials provides another piece of evidence for a potential anxiety-like phenotype in mutant larvae. Suppose *panx1b* proves to function as part of a circadian

oscillator widespread throughout the eye and the brain; in that case, the behavioral deficits observed in the present study may reflect the importance of rhythmic gene expression on the execution of complex cognitive tasks. However, at present, the detailed molecular mechanisms connecting Panx1b and the circadian clock and the exact downstream cascade affecting visual and cognitive behaviors remain elusive. In the following section, the possible modulators connecting *panx1b* and the circadian clock system are discussed.

6.8. Mapping Panx1-mediated ATP signaling in outer and inner retinas

6.8.1. Panx1a and outer retinal pathways

The Panx1a channel has been implicated in visual information processing at the first retinal synapse, where horizontal cells (HC) inhibit photoreceptors. This inhibitory interaction generates the center/surround organization of bipolar cell receptive fields and is critical for adjusting the contrast sensitivity. It was explained that the acidification of synaptic clefts by phosphate groups and protons that are released via conversion of the extracellular ATP into AMP mediates this inhibitory effect (Vroman *et al.*, 2014). Our findings support the assumption that Panx1a exercises its regulatory effect on neuronal processing via an additional mechanism, which is adenosine mediated (***Fig. 6.1***).

Further hydrolysis of extracellular ATP released via Panx1a channels gives rise to adenosine molecules. In the outer retina, adenosine works with dopamine to coregulate the photoreceptor coupling through gap junctions (Li *et al.*, 2013). This coupling suppresses voltage noise (Lamb and Simon, 1976), facilitates the input of rod signals into cone pathways (Trümpler *et al.*, 2008), and improves contrast sensitivity and detection of

small stimuli (Lebedev, Byzov and Govardovskii, 1998; P. H. Li *et al.*, 2012). In all vertebrates, connexin 35/36 (gene homologs Cx36 in mammals, Cx35 in other vertebrates) is the major gap junction protein that mediates photoreceptor coupling (Li, Chuang and O'Brien, 2009). The light/dark adaptation, and circadian rhythms, dynamically control photoreceptor coupling such that it is minimal under light-adapted conditions and maximal at night in dark-adapted conditions (Li *et al.*, 2013).

Dopamine has long been implicated in the light-driven reduction in the coupling, and a circadian rhythm of dopamine secretion can account for the reduction of coupling in the subjective day. In light, dopamine synthesis and release by dopaminergic interplexiform neurons that ascend their dendrites to contact horizontal cells (HCs) and bipolar cells (BCs) in the outer plexiform layer (OPL) increases. Dopamine activates D2-type receptors on photoreceptors; this inhibits adenylyl cyclase, down-regulates cAMP and PKA activity, and leads to photoreceptor uncoupling, imposing the daytime/light condition (Doyle *et al.*, 2002; Doyle, McIvor and Menaker, 2002; Ribelayga, Wang and Mangel, 2004). A circadian rhythm of extracellular adenosine in the retina has the opposite phase as does dopamine, displaying an increased level in darkness and at night compared with illumination (Li *et al.*, 2013). High extracellular concentrations of adenosine at night provide an endogenous trigger for enhancing phosphorylation of connexin 35/36 in photoreceptors and, therefore, increasing photoreceptor coupling. The pathway involves an A_{2A} receptor-mediated PKA activity (Stella, Bryson and Thoreson, 2002; Ribelayga and Mangel, 2005). Interestingly, the Panx1a channel is maximally active in the darkness and releases ATP into the synaptic cleft. Thus, the trinary interaction between Panx1a,

adenosine, and dopamine might adjust the contrast sensitivity through co-regulating the photoreceptor coupling rate in the nighttime/darkness.

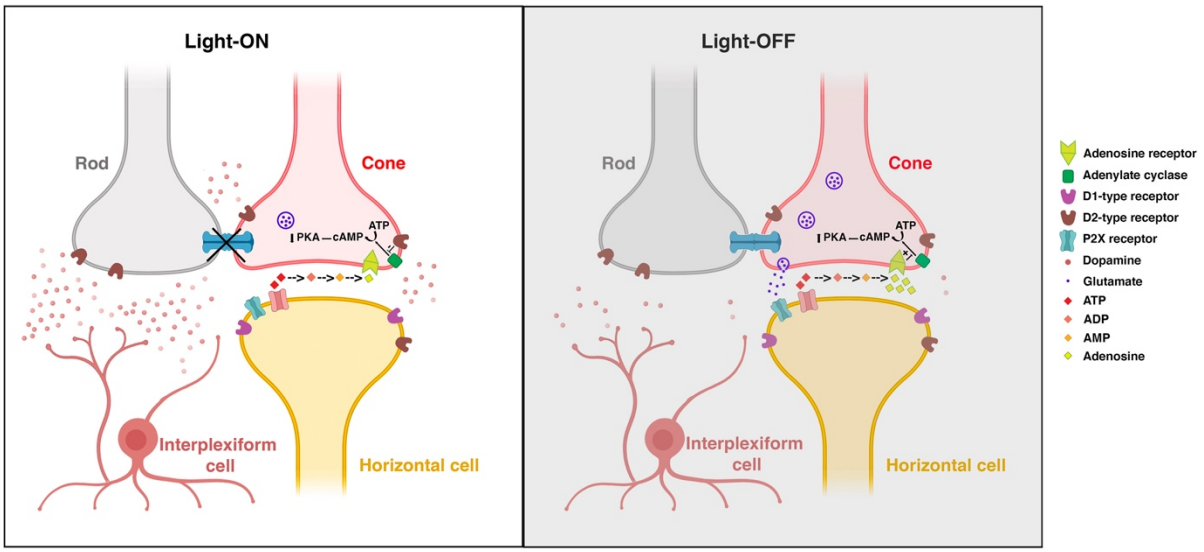

Figure 6.1. Schematic representation of photoreceptor coupling through Panx1a-adenosine-dopamine signaling in the outer retina. *In subjective light (Light-ON), the synthesis and release of dopamine by dopaminergic interplexiform cells are maximal. Dopamine activates D2-type receptors located on rods and cones and reduces photoreceptor coupling by down-regulating cAMP and PKA activity. During the subjective night (Light-OFF), the accumulation of the extracellular adenosine occurs via the conversion of ATP molecules released (in part) by the Panx1a channel. Adenosine signaling through A_{2A} receptors opposes the effects of dopamine by increasing cAMP and PKA activity and enhancing photoreceptor coupling. Thus, the Panx1a channel seems to be involved in the photoreceptor coupling through the nighttime/darkness signal adenosine. (Created by N.S.).*

6.8.2. Panx1b and inner retinal pathways

Our data revealed a profound linkage between the Panx1b channel and the circadian clock system. Although the underlying molecular mechanism associating with the two components is unclear, two hypotheses could currently be considered: a PH- and a calcium-dependent mechanism.

First, the circadian clock system might modulate the extracellular PH levels by regulating ATP release rate from Panx1b channels. It's now known that the hydrolysis of the extracellular ATP (released in part from Panx1b channels) generates AMP, phosphate

groups, and protons. The phosphate groups and protons were suggested to form a pH buffer with a pKa of 7.2, which keeps the pH in the retinal synaptic space relatively acidic (Vroman et al., 2014). Notably, the Panx1b channel function is sensitive to PH changes, such that further acidifications in the extracellular PH can lead to the closure of Panx1b channels (Kurtenbach et al., 2013). Electrophysiological recordings in fish and rabbits have demonstrated that a circadian clock regulates PH in the retina so that PH is lower during the night time (Light-OFF) compared to the daytime (Light-ON) (Dmitriev and Mangel, 2000, 2001). The clock system may maintain the acidic PH of the synaptic cleft by increasing the rate of Panx1b channels open state at night. Further analysis of the Panx1b channel opening/ closure rhythm can bring more insights.

The second hypothetical mechanism, however, involves intracellular Ca^{2+} signaling. The intracellular Ca^{2+} is an essential component of the cellular oscillation machinery. It plays a major role in regulating how and when clock genes, such as per1/2 (Akiyama et al., 2001), are turned on and off in response to environmental stimuli in nearly all systems, including the brain and eyes (Harrisingh et al., 2007; Hastings, Maywood and O'Neill, 2008; O'Neill and Reddy, 2012).

In the vertebrate's retina, glutamate is the major excitatory neurotransmitter released by photoreceptors and bipolar cells in response to light (Thoreson and Witkovsky, 1999). The glutamate released from bipolar cells stimulates ionotropic (such as NMDA and AMPA receptors) and metabotropic glutamate receptors (mGluRs) located on amacrine and ganglion cells in the inner retina (Akopian and Witkovsky, 2001). Both ionotropic and metabotropic glutamate receptors exert their effects through pathways that alter the

intracellular Ca^{2+} ($[Ca^{2+}]_i$) concentration (Gilbertson, Scobey and Wilson, 1991; Diamond and Copenhagen, 1993; Peng *et al.*, 1995). Light-induced depolarization causes Ca^{2+} influx by activating ionotropic glutamate receptors and voltage-dependent Ca^{2+} channels (VDCC). Besides, activation of mGluRs increases $[Ca^{2+}]_i$ by triggering the release of Ca^{2+} from intracellular stores. The elevated $[Ca^{2+}]_i$ consequently mediates alterations in the circadian clock genes expression rate (Tischkau *et al.*, 2003; O'Neill and Reddy, 2012). Interestingly, there is a potential for the Panx1b channel to be involved in intracellular Ca^{2+} signaling. It was previously shown that exogenously expressed Panx1b proteins can somehow remain in intracellular compartments near the perinuclear region (Kurtenbach et al., 2013). This localization was also reported with human Panx1 in over-expression systems. It was associated with forming Ca^{2+}-permeable channels in the endoplasmic reticulum (ER), leading to the Ca^{2+} leakage from ER into the cytosol (Vanden Abeele et al., 2006). ***Figure 6.2*** depicts the hypothetical pathway whereby the Panx1b channel might link to the circadian system via a Ca^{2+} signaling-mediated mechanism. However, further molecular and cellular studies are required to reveal whether the Panx1b channel function as an ER Ca^{2+} leak route (Kurtenbach et al., 2013), and if this proposed mechanism is accurate.

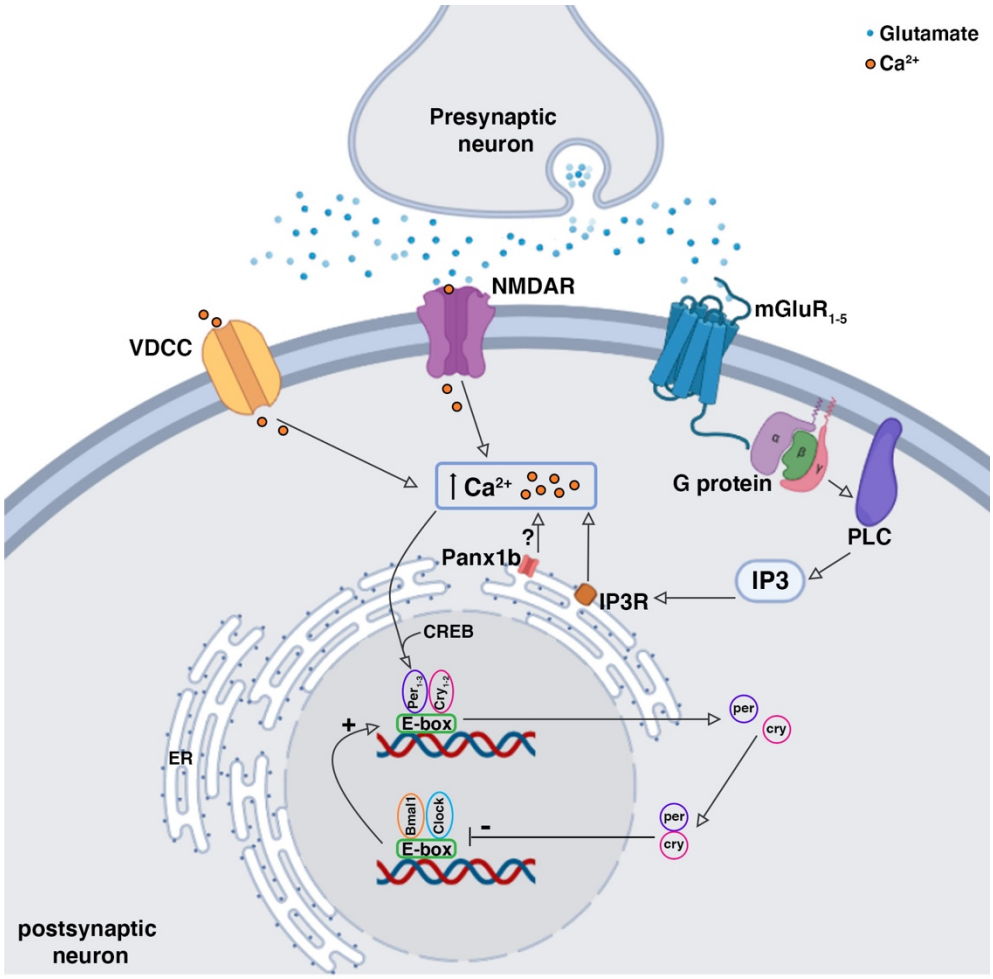

Figure 6.2. Panx1b linkage to the circadian clock system via Ca^{2+} signaling. *Light-induced glutamate release from bipolar cells triggers both ionotropic and metabotropic glutamate receptors on amacrine and ganglion cells. The Ca^{2+} influx through NMDAR and VDCC, along with the release of Ca^{2+} from the intracellular store, give rise to the elevated $[Ca^{2+}]_i$. Panx1b channels localized in the prenuclear region in overexpression systems were proposed to play a role in the Ca^{2+} leakage from ER into the cytosol. The elevated $[Ca^{2+}]_i$ works with cAMP response element-binding protein (CREB) to induce Per1-2 gene expression, thereby facilitating clock resetting according to the time of the day. ER, endoplasmic reticulum; IP3R: inositol triphosphate receptor; mGluR1-5, metabotropic glutamate receptor subtypes 1-5; NMDA, N-methyl-d-aspartate; PLC, phospholipase C; VDCC, voltage-dependent calcium channel. (Created by N.S.).*

6.9. Mysteries behind the crosstalk between Panx1a and Panx1b signaling pathways

A first step toward understanding the functional implications of carrying two *panx1* copies in molecular and behavioral terms was establishing a double *panx1a*$^{-/-}$/ *panx1b*$^{-/-}$ knockout (DKO) model. Our group previously showed that both Panx1 channels are engaged in ATP-release functions and are expressed in equal levels in the retina (Kurtenbach et al., 2013). The present study further demonstrated that *panx1a* copy, being expressed in the outer retina, engages in phototransduction and several signaling pathways strongly linked to eye development and visual processing. Whereas *panx1b* copy, being highly localized in the RGCs and inner retina, engages in more diverse signaling pathways centering around the circadian clock system. Surprisingly, the DKO larvae did not show similar transcriptome changes as single mutants; no significant alterations in pathways related to eye development and vision were found in this group. Moreover, the genes related to photoperiodism were upregulated in DKO larvae, opposing the trend observed in *panx1b*$^{-/-}$ fish. Besides, a behavioral inspection of DKO larvae led us to conclude that the two *panx1s* in question contribute to the pathways related to the detection of light decrements; though, they mediate their effects through different yet interacting signaling pathways. Locomotor activity and the peak response to dark stimuli were not different than controls in DKO larvae, contrary to single mutants phenotypes. Furthermore, DKO fish demonstrated normal color vision as TL controls. Interestingly, DKO larvae sized neither shorter (like *panx1a*$^{-/-}$) nor longer (like *panx1b*$^{-/-}$) than TL controls. They were morphologically normal, viable and fertile similar to their normal TL siblings. The only

pathology detected in the DKO group was declined visual acuity in low contrast conditions, similar to that observed in *panx1b*$^{-/-}$ larvae. Electroretinography studies could shed more light on the visual acuity deficiency of DKO larvae. Altogether, these data suggested that a compensatory mechanism might function to recover some of the effects resulting from each *panx1* gene's absence. Additional inferences concerning the interaction between Panx1a and 1b signaling pathways can be brought about by using high-throughput gene expression and protein-protein interaction (PPI) data. The most common technologies used to study PPI are two-dimensional sodium dodecyl sulfate polyacrylamide gel electrophoresis (2D SDS-PAGE) and mass spectrometry (MS). PPI data is a direct source of information about the structure of signaling pathways (Kabir *et al.*, 2018). Aside from experimental information, bioinformatic tools also provide sophisticated methods to predict protein–protein interactions. Several PPI databases such as the Database of Interacting Proteins (DIP), the General Repository for Interaction Datasets (GRID), the Bio-molecular Interaction Network Database (BIND), and the Human Protein Reference Database (HPRD) are available for human and model organisms such as zebrafish (von Mering *et al.*, 2003; Tang *et al.*, 2015; Kabir *et al.*, 2018).

SUMMARY

We studied the functional implications of the distinct retinal localization of Panx1a and Panx1b proteins in the zebrafish visual behaviors. Both Panx1 proteins contribute to the retinal OFF pathway functions, though through different signaling cascades. Panx1a channels, located in the outer retina (Kurtenbach et al., 2013), modulate light decrement detection through an adenosine-dopamine crosstalk mechanism. The proof of this mechanism is haloperidol and adenosine treatments that could rescue the Light-OFF phenotype in *panx1a*$^{-/-}$ larvae. In the absence of Panx1a channels, a fundamental route of ATP transport to the extracellular milieu is compromised; hence, a decline in the extracellular adenosine level can be expected. This notion receives further support from the *panx1a*$^{-/-}$ larvae transcriptome data showing a reduction of key enzymes involved in the ATP catabolism in the extracellular matrix (like ectonucleotidases and adenosine deaminase). This adenosine decline removes the inhibitory effects on the dopaminergic receptors, leading to an increase in the DA receptors' conductance; therefore, driving the observed Light-OFF phenotype in mutants. Ample neurochemical and pharmacological evidence indicates that adenosine and dopamine interact functionally in the CNS and that such interactions have pathophysiological and therapeutic implications (Salmi, Chergui and Fredholm, 2005). Two major adenosine-dopamine receptor interactions exist in the CNS: the antagonistic interaction between adenosine A1-dopamine D1 receptor and antagonistic interaction between adenosine A2A-dopamine D2 receptor (Fuxe et al., 2007). Further molecular, immunostaining, and electrophysiology studies can shed more

light on the details of the proposed interactions between Panx1a- A2A-dopamine D2 receptors in the retina.

The novel association between Panx1b channels, localized in the RGCs (Kurtenbach et al., 2013), and the circadian clock system suggests that the Panx1b signaling can regulate a wide spectrum of biological processes within the visual system. Our findings revealed that in the absence of functional Panx1b channels, a significant downregulation of core clock genes (i.e., *cry1*, *cry5*, *bmal1a* and *1b,* and *clock2*) occurs. Mutant larvae elicit visual impairment in responding to the dark stimulus, fail to correctly detect motion direction, and demonstrate cognitive dysfunction and anxiety-related behavior. Noteworthy, RGCs have several dozen types (based on anatomical, physiological, and molecular characteristics), each dedicated to encoding distinct features of visual information, such as luminosity, motion, direction, etc. (Barlow, Hill and Levick, 1964; Cleland and Levick, 1974; DeVries and Baylor, 1997; Baden et al., 2016). In addition, a small subset of retinal ganglion cells called intrinsically photosensitive retinal ganglion cells (ipRGCs) provide luminance information that plays a critical role in the synchronization of behavioral rhythms with the circadian light-dark cycle, sleep regulation, and mood (Güler et al., 2008; Altimus et al., 2010; Johnson et al., 2010; Detwiler, 2018; Nelson and Chbeir, 2018). Therefore, Panx1b channels seem to regulate the functions of a wide variety of RGC types. However, more detailed molecular and cellular data are required to better resolute this matter.

Finally, the interaction between two Panx1 proteins also modulates the output of retinal OFF pathways. The visual-motor deficiencies observed in single mutants indicate that

only one *panx1* copy is not sufficient to ensure the retinal OFF-pathways' normal output. Besides, as the dual deletion of *panx1a* and *1b* generated zebrafish that were phenotypically indistinguishable from the TL group, a contradictory interaction might exist between the two Panx1s' networks. Which and how components of these two proteins' networks crosstalk needs further molecular, immunostaining, and proteomic studies.

SIGNIFICANCE AND FUTURE DIRECTION

Panx1 research in the visual system has moved from early expression and localization to functional studies (Kurtenbach, Kurtenbach and Zoidl, 2014). Despite clinical relevance in many physiological and pathophysiological settings, Panx1 links to precise signaling pathways are largely unknown. A major caveat of this research has been the limited availability of animal models to conduct Panx1 studies, from genes to behavioral outcomes. Recently, zebrafish, a lower vertebrate, has emerged as a promising model for studying neuronal mechanisms of sensory perception and cognition and provide a complimentary model to rodents (Neuhauss, 2003, 2010; Orger and De Polavieja, 2017). In this thesis, we have identified Panx1 cellular mechanisms underlying visual behaviors. Data uncovers that in zebrafish, *panx1* genes converge onto a few major signaling pathways: dopaminergic pathway, circadian rhythm, transcriptional control, chromatin remodeling, and cellular metabolism. These novel findings may also fortify our understanding of how changes to this channel have the potential to impact diverse physiological functions by altering major signaling pathways. For instance, the adenosine-dopamine antagonism has represented a new way for the treatment of motor as well as nonmotor symptoms, such as reduced cognition, anxiety, and depression, in Parkinson's disease (PD) (Armentero *et al.*, 2011; Shook and Jackson, 2011; Jenner, 2014). So, the trinary association mapped between Panx1, adenosine and dopamine receptors highlights Panx1 therapeutic potential for neurodegenerative disorders such as PD. Furthermore, the association with the circadian clock system opens up new avenues to study the role of Panx1 in a diverse array of biological processes from sleep/wakefulness

to metabolism. Indeed, more works are required to unravel more details of Panx1 signaling pathways and discover how changes to this channel can impact physiological functions by altering major signaling pathways.

The next step perhaps could be the in-depth analysis of gene expression and PPI data for predicting functional associations between two Panx1s. A machine learning system can be trained to recognize interactions based on primary structure and associated physiological properties. The bioinformatics tools provide the possibility of proceeding directly from the automated identification of a cell's gene products to inference of the protein interaction pairs, facilitating protein function and cellular signaling pathway identification. Also, given the efficiency of neurogenesis and repair mechanisms in the zebrafish (Zambusi A, 2020), it would also be worth assessing the visual performance of adult *panx1* knockout zebrafish to configure if the phenotypes are restricted to an specific phase of development early in the larval stage or not.

BIBLIOGRAPHY

A. Weisman, G. *et al.* (2012) 'P2Y Receptors in the Mammalian Nervous System: Pharmacology, Ligands and Therapeutic Potential', *CNS & Neurological Disorders - Drug Targets*. doi: 10.2174/187152712803581047.

Abbracchio, M. P. *et al.* (2006) 'International Union of Pharmacology LVIII: Update on the P2Y G protein-coupled nucleotide receptors: From molecular mechanisms and pathophysiology to therapy', *Pharmacological Reviews*. doi: 10.1124/pr.58.3.3.

Vanden Abeele, F. *et al.* (2006) 'Functional implications of calcium permeability of the channel formed by pannexin 1', *Journal of Cell Biology*. doi: 10.1083/jcb.200601115.

Abuhamdah, R. M. *et al.* (2016) 'Pre-training in a radial arm maze abolished anxiety and impaired habituation in C57BL6/J mice treated with dizocilpine', *Physiology and Behavior*. doi: 10.1016/j.physbeh.2016.06.017.

Ahmad, F. and Richardson, M. K. (2013) 'Exploratory behaviour in the open field test adapted for larval zebrafish: Impact of environmental complexity', *Behavioural Processes*. doi: 10.1016/j.beproc.2012.10.014.

Akiyama, M. *et al.* (2001) 'Calcium and pituitary adenylate cyclase-activating polypeptide induced expression of circadian clock gene mPer1 in the mouse cerebellar granule cell culture', *Journal of Neurochemistry*. doi: 10.1046/j.1471-4159.2001.00452.x.

Akopian, A. and Witkovsky, P. (2001) 'Intracellular calcium reduces light-induced excitatory post-synaptic responses in salamander retinal ganglion cells', *Journal of Physiology*. doi: 10.1111/j.1469-7793.2001.0043g.x.

Allison, W. T. *et al.* (2004) 'Visual pigment composition in zebrafish: Evidence for a rhodopsin-porphyropsin interchange system', *Visual Neuroscience*. doi: 10.1017/S0952523804216145.

Altimus, C. M. *et al.* (2010) 'Rod photoreceptors drive circadian photoentrainment across a wide range of light intensities', *Nature Neuroscience*. doi: 10.1038/nn.2617.

Ambrosi, C. *et al.* (2010) 'Pannexin1 and pannexin2 channels show quaternary similarities to connexons and different oligomerization numbers from each other', *Journal of Biological Chemistry*. doi: 10.1074/jbc.M110.115444.

Antonioli, L. *et al.* (2019) 'Adenosine signaling and the immune system: When a lot could be too much', *Immunology Letters*. doi: 10.1016/j.imlet.2018.04.006.

Arden, G. B. and Jacobson, J. J. (1978) 'A simple grating test for contrast sensitivity: Preliminary results indicate value in screening for glaucoma', *Investigative Ophthalmology and Visual Science*.

Argamaso, S. M. *et al.* (1995) 'Photopigments and circadian systems of vertebrates', *Biophysical Chemistry*. doi: 10.1016/0301-4622(95)00009-M.

Armentero, M. T. *et al.* (2011) 'Past, present and future of A2A adenosine receptor antagonists in the therapy of Parkinson's disease', *Pharmacology and Therapeutics*. doi: 10.1016/j.pharmthera.2011.07.004.

Asher, G. and Sassone-Corsi, P. (2015) 'Time for food: The intimate interplay between nutrition, metabolism, and the circadian clock', *Cell*. doi: 10.1016/j.cell.2015.03.015.

Avdesh, A. *et al.* (2012) 'Evaluation of color preference in zebrafish for learning and memory', *Journal of Alzheimer's Disease*. doi: 10.3233/JAD-2011-110704.

Baba, K. *et al.* (2009) 'Melatonin modulates visual function and cell viability in the mouse retina via the MT1 melatonin receptor', *Proceedings of the National Academy of Sciences of the United States of America*. doi: 10.1073/pnas.0904400106.

Baden, T. *et al.* (2016) 'The functional diversity of retinal ganglion cells in the mouse', *Nature*. doi: 10.1038/nature16468.

Baden, T. and Osorio, D. (2019) 'The Retinal Basis of Vertebrate Color Vision', *Annual Review of Vision Science*. doi: 10.1146/annurev-vision-091718-014926.

Bahl, A. and Engert, F. (2020) 'Neural circuits for evidence accumulation and decision making in larval zebrafish', *Nature Neuroscience*. doi: 10.1038/s41593-019-0534-9.

Baier, M. L. *et al.* (2005) 'Low-contrast letter acuity testing captures visual dysfunction in patients with multiple sclerosis', *Neurology*. doi: 10.1212/01.WNL.0000154521.40686.63.

Baker, D. J. *et al.* (2008) 'Opposing roles for p16Ink4a and p19Arf in senescence and ageing caused by BubR1 insufficiency', *Nature Cell Biology*. doi: 10.1038/ncb1744.

Balcer, L. J. *et al.* (2003) 'Contrast letter acuity as a visual component for the Multiple Sclerosis Functional Composite', *Neurology*. doi: 10.1212/01.WNL.0000094315.19931.90.

Bao, L., Locovei, S. and Dahl, G. (2004) 'Pannexin membrane channels are mechanosensitive conduits for ATP', *FEBS Letters*. doi: 10.1016/j.febslet.2004.07.009.

Baranova, A. *et al.* (2004) 'The mammalian pannexin family is homologous to the invertebrate innexin gap junction proteins', *Genomics*. doi: 10.1016/j.ygeno.2003.09.025.

Bargiotas, P. *et al.* (2012) 'Functional outcome of pannexin-deficient mice after cerebral ischemia', *Channels*. doi: 10.4161/chan.22315.

Barlow, H. B., Hill, R. M. and Levick, W. R. (1964) 'Retinal ganglion cells responding selectively to direction and speed of image motion in the rabbit', *The Journal of Physiology*. doi: 10.1113/jphysiol.1964.sp007463.

Baroja-Mazo, A., Barberà-Cremades, M. and Pelegrín, P. (2013) 'The participation of plasma membrane hemichannels to purinergic signaling', *Biochimica et Biophysica Acta - Biomembranes*. doi: 10.1016/j.bbamem.2012.01.002.

Bass, J. and Takahashi, J. S. (2010) 'Circadian integration of metabolism and energetics', *Science*. doi: 10.1126/science.1195027.

Bault, Z. A., Peterson, S. M. and Freeman, J. L. (2015) 'Directional and color preference in adult zebrafish: Implications in behavioral and learning assays in neurotoxicology studies', *Journal of Applied Toxicology*. doi: 10.1002/jat.3169.

Beck, C. D. and Rankin, C. H. (1995) 'Heat shock disrupts long-term memory consolidation in Caenorhabditis elegans.', *Learning & memory (Cold Spring Harbor, N.Y.)*. doi: 10.1101/lm.2.3-4.161.

Bedell, V. M. *et al.* (2012) 'In vivo genome editing using a high-efficiency TALEN system', *Nature*. doi: 10.1038/nature11537.

Begandt, D. *et al.* (2017) 'Pannexin channel and connexin hemichannel expression in vascular function and inflammation', *BMC Cell Biology*. doi: 10.1186/s12860-016-0119-3.

Bellingham, J. and Foster, R. G. (2002) 'Opsins and mammalian photoentrainment', *Cell and*

Tissue Research. doi: 10.1007/s00441-002-0573-4.

Bellmann, C. *et al.* (2003) 'Visual acuity and contrast sensitivity in patients with neovascular age-related macular degeneration. Results from the radiation therapy for age-related macular degeneration (RAD-) study', *Graefe's Archive for Clinical and Experimental Ophthalmology*. doi: 10.1007/s00417-003-0689-6.

Benner, M. J. *et al.* (2010) 'Zebrafish (Danio rerio) vary by strain and sex in their behavioral and transcriptional responses to selenium supplementation', *Comparative Biochemistry and Physiology - A Molecular and Integrative Physiology*. doi: 10.1016/j.cbpa.2010.07.016.

Berg, D. A. *et al.* (2013) 'Neurotransmitter-mediated control of neurogenesis in the adult vertebrate brain', *Development (Cambridge)*. doi: 10.1242/dev.088005.

Berson, D. M., Dunn, F. A. and Takao, M. (2002) 'Phototransduction by retinal ganglion cells that set the circadian clock', *Science*. doi: 10.1126/science.1067262.

Bert, B. *et al.* (2002) 'Fischer 344 and Wistar rats differ in anxiety and habituation but not in water maze performance', *Neurobiology of Learning and Memory*. doi: 10.1006/nlme.2001.4040.

Best, J. D. and Alderton, W. K. (2008) 'Zebrafish: An in vivo model for the study of neurological diseases', *Neuropsychiatric Disease and Treatment*. doi: 10.2147/ndt.s2056.

Bialecki, J. *et al.* (2020) 'Suppression of presynaptic glutamate release by postsynaptic metabotropic NMDA receptor signalling to pannexin-1', *Journal of Neuroscience*. doi: 10.1523/JNEUROSCI.0257-19.2019.

Bilotta, J., Saszik, S. and Sutherland, S. E. (2001) 'Rod contributions to the electroretinogram of the dark-adapted developing zebrafish', *Developmental Dynamics*. doi: 10.1002/dvdy.1188.

Blank, M. *et al.* (2009) 'A one-trial inhibitory avoidance task to zebrafish: Rapid acquisition of an NMDA-dependent long-term memory', *Neurobiology of Learning and Memory*. doi: 10.1016/j.nlm.2009.07.001.

Boassa, D. *et al.* (2007) 'Pannexin1 channels contain a glycosylation site that targets the hexamer to the plasma membrane', *Journal of Biological Chemistry*. doi: 10.1074/jbc.M702422200.

De Bock, M. *et al.* (2014) 'The dual face of connexin-based astroglial Ca2+ communication: A key player in brain physiology and a prime target in pathology', *Biochimica et Biophysica Acta - Molecular Cell Research*. doi: 10.1016/j.bbamcr.2014.04.016.

Bollmann, J. H. (2019) 'The Zebrafish Visual System: From Circuits to Behavior', *Annual Review of Vision Science*. doi: 10.1146/annurev-vision-091718-014723.

Bond, S. R. *et al.* (2012) 'Pannexin 1 ohnologs in the teleost lineage', *Journal of Membrane Biology*. doi: 10.1007/s00232-012-9497-4.

Bonner, J. T. (2013a) *Randomness in evolution*, *Randomness in Evolution*. doi: 10.5860/choice.51-0262.

Bonner, J. T. (2013b) 'Time, Size, and Complexity', in *Randomness in Evolution*. doi: 10.23943/princeton/9780691157016.003.0002.

Bonner, J. T. (2019) 'The evolution of evolution', *Journal of Experimental Zoology Part B: Molecular and Developmental Evolution*. doi: 10.1002/jez.b.22859.

Van Den Bos, R. *et al.* (2017) 'Further characterisation of differences between TL and AB Zebrafish (Danio rerio): Gene expression, physiology and behaviour at day 5 of the larval stage', *PLoS ONE*. doi: 10.1371/journal.pone.0175420.

Van Den Bos, R. *et al.* (2019) 'Early life exposure to cortisol in zebrafish (Danio rerio): Similarities and differences in behaviour and physiology between larvae of the AB and TL strains', *Behavioural Pharmacology*. doi: 10.1097/FBP.0000000000000470.

Boyce, A. K. J. *et al.* (2014) 'Pore positioning: Current concepts in Pannexin channel trafficking', *Channels*. doi: 10.4161/chan.27287.

Boyce, A. K. J. *et al.* (2015) 'ATP stimulates pannexin 1 internalization to endosomal compartments', *Biochemical Journal*. doi: 10.1042/BJ20141551.

Boyce, A. K. J. *et al.* (2018) 'Transcriptional and post-translational regulation of pannexins', *Biochimica et Biophysica Acta - Biomembranes*. doi: 10.1016/j.bbamem.2017.03.004.

Boyce, A. K. J. and Swayne, L. A. (2017) 'P2X7 receptor cross-Talk regulates ATP-induced pannexin 1 internalization', *Biochemical Journal*. doi: 10.1042/BCJ20170257.

Brand, M., M. G. and Nüsslein-Vollhard, C. (2002) 'Keeping and raising zebrafish, in Zebrafish: A practical approach', *Oxford University Press*. doi: 10.1017/S0016672303216384.

Briggman, K. L., Helmstaedter, M. and Denk, W. (2011) 'Wiring specificity in the direction-selectivity circuit of the retina', *Nature*. doi: 10.1038/nature09818.

Brosius, J. (1991) 'Retroposons - Seeds of evolution', *Science*. doi: 10.1126/science.1990437.

Bruzzone, R. *et al.* (2003) 'Pannexins, a family of gap junction proteins expressed in brain', *Proceedings of the National Academy of Sciences of the United States of America*. doi: 10.1073/pnas.2233464100.

Buhr, E. D. and Takahashi, J. S. (2013a) 'Molecular components of the mammalian circadian clock', *Handbook of Experimental Pharmacology*. doi: 10.1007/978-3-642-25950-0-1.

Buhr, E. D. and Takahashi, J. S. (2013b) 'Molecular Components of the Mammalian Circadian Clock', in. doi: 10.1007/978-3-642-25950-0_1.

De Bundel, D. *et al.* (2013) 'Cognitive dysfunction, elevated anxiety, and reduced cocaine response in circadian clock-deficient cryptochrome knockout mice', *Frontiers in Behavioral Neuroscience*. doi: 10.3389/fnbeh.2013.00152.

Bunse, S. *et al.* (2009) 'The potassium channel subunit Kvβ3 interacts with pannexin 1 and attenuates its sensitivity to changes in redox potentials', *FEBS Journal*. doi: 10.1111/j.1742-4658.2009.07334.x.

Bunse, S. *et al.* (2011) 'Single cysteines in the extracellular and transmembrane regions modulate Pannexin 1 channel function', *Journal of Membrane Biology*. doi: 10.1007/s00232-011-9393-3.

Burnstock, G. *et al.* (2010) 'The birth and postnatal development of purinergic signalling', *Acta Physiologica*. doi: 10.1111/j.1748-1716.2010.02114.x.

Burnstock, G. and Knight, G. E. (2004) 'Cellular distribution and functions of P2 receptor subtypes in different systems', *International Review of Cytology*. doi: 10.1016/S0074-7696(04)40002-3.

Burton, C. E. *et al.* (2017) 'Spectral properties of the zebrafish visual motor response', *Neuroscience Letters*. doi: 10.1016/j.neulet.2017.03.002.

Cahill, G. M. (2002) 'Clock mechanisms in zebrafish', *Cell and Tissue Research*. doi: 10.1007/s00441-002-0570-7.

Cahill, G. M. and Besharse, J. C. (1995) 'Circadian rhythmicity in vertebrate retinas: Regulation by a photoreceptor oscillator', *Progress in Retinal and Eye Research*. doi: 10.1016/1350-9462(94)00001-Y.

van Calker, D. *et al.* (2019) 'The role of adenosine receptors in mood and anxiety disorders', *Journal of Neurochemistry*. doi: 10.1111/jnc.14841.

Cameron, M. A. *et al.* (2008) 'Electroretinography of wild-type and Cry mutant mice reveals circadian tuning of photopic and mesopic retinal responses', *Journal of Biological Rhythms*. doi: 10.1177/0748730408325874.

Camici, M., Garcia-Gil, M. and Tozzi, M. G. (2018) 'The inside story of adenosine', *International Journal of Molecular Sciences*. doi: 10.3390/ijms19030784.

Carman, A. J. *et al.* (2011) 'Adenosine receptor signaling modulates permeability of the blood-brain barrier', *Journal of Neuroscience*. doi: 10.1523/JNEUROSCI.3337-11.2011.

Cattell, R. B. (1978) *The Scientific Use of Factor Analysis in Behavioral and Life Sciences*, *The Scientific Use of Factor Analysis in Behavioral and Life Sciences*. doi: 10.1007/978-1-4684-2262-7.

Cenedese, V. *et al.* (2017) 'Pannexin 1 is critically involved in feedback from horizontal cells to cones', *Frontiers in Molecular Neuroscience*. doi: 10.3389/fnmol.2017.00403.

Cermak, T. *et al.* (2011) 'Efficient design and assembly of custom TALEN and other TAL effector-based constructs for DNA targeting', *Nucleic Acids Research*. doi: 10.1093/nar/gkr218.

Cermakian, N. and Boivin, D. B. (2009) 'The regulation of central and peripheral circadian clocks in humans', *Obesity Reviews*. doi: 10.1111/j.1467-789X.2009.00660.x.

Chekeni, F. B. *et al.* (2010) 'Pannexin 1 channels mediate "find-me" signal release and membrane permeability during apoptosis', *Nature*. doi: 10.1038/nature09413.

Chen, A. *et al.* (2000) 'Nitric oxide influences injury-induced microglial migration and accumulation in the leech CNS', *Journal of Neuroscience*. doi: 10.1523/jneurosci.20-03-01036.2000.

Chen, L. (2020) 'Visual system: An understudied target of aquatic toxicology', *Aquatic Toxicology*. doi: 10.1016/j.aquatox.2020.105542.

Cheung, G., Chever, O. and Rouach, N. (2014) 'Connexons and pannexons: Newcomers in neurophysiology', *Frontiers in Cellular Neuroscience*. doi: 10.3389/fncel.2014.00348.

Chiu, Y. H. *et al.* (2017) 'A quantized mechanism for activation of pannexin channels', *Nature Communications*. doi: 10.1038/ncomms14324.

Chiu, Y. H. *et al.* (2018) 'Revisiting multimodal activation and channel properties of Pannexin 1', *Journal of General Physiology*. doi: 10.1085/jgp.201711888.

Christou, M. *et al.* (2020) 'DMSO effects larval zebrafish (Danio rerio) behavior, with additive and interaction effects when combined with positive controls', *Science of the Total Environment*. doi: 10.1016/j.scitotenv.2019.134490.

Ciruela, F. *et al.* (2006) 'Heterodimeric adenosine receptors: A device to regulate neurotransmitter release', *Cellular and Molecular Life Sciences*. doi: 10.1007/s00018-006-6216-2.

Cleland, B. G. and Levick, W. R. (1974) 'Brisk and sluggish concentrically organized ganglion cells in the cat's retina', *The Journal of Physiology*. doi: 10.1113/jphysiol.1974.sp010617.

Coddou, C. *et al.* (2011) 'Activation and regulation of purinergic P2X receptor channels', *Pharmacological Reviews*. doi: 10.1124/pr.110.003129.

Collins, L. E. *et al.* (2010) 'Interactions between adenosine and dopamine receptor antagonists with different selectivity profiles: Effects on locomotor activity', *Behavioural Brain Research*. doi: 10.1016/j.bbr.2010.03.003.

Colwill, R. M. *et al.* (2005) 'Visual discrimination learning in zebrafish (Danio rerio)', *Behavioural Processes*. doi: 10.1016/j.beproc.2005.03.001.

Cooke, S. F. *et al.* (2015) 'Visual recognition memory, manifested as long-term habituation, requires synaptic plasticity in V1', *Nature Neuroscience*. doi: 10.1038/nn.3920.

Cristóvão-Ferreira, S. *et al.* (2013) 'A1R-A2AR heteromers coupled to Gs and Gi/0 proteins modulate GABA transport into astrocytes', *Purinergic Signalling*. doi: 10.1007/s11302-013-9364-5.

Czeisler, C. A. and Gooley, J. J. (2007) 'Sleep and circadian rhythms in humans', in *Cold Spring Harbor Symposia on Quantitative Biology*. doi: 10.1101/sqb.2007.72.064.

D'hondt, C. *et al.* (2013) 'Regulation of connexin- and pannexin-based channels by post-translational modifications', *Biology of the Cell*. doi: 10.1111/boc.201200096.

Dahl, G. (2015) 'ATP release through pannexon channels', *Philosophical Transactions of the Royal Society B: Biological Sciences*. doi: 10.1098/rstb.2014.0191.

Dahl, G. (2018) 'The Pannexin1 membrane channel: distinct conformations and functions', *FEBS Letters*. doi: 10.1002/1873-3468.13115.

Dahl, G. and Locovei, S. (2006) 'Pannexin: To gap or not to gap, is that a question?', *IUBMB Life*. doi: 10.1080/15216540600794526.

Davidson, R. J., Jackson, D. C. and Kalin, N. H. (2000) 'Emotion, plasticity, context, and regulation: Perspectives from affective neuroscience', *Psychological Bulletin*. doi: 10.1037/0033-2909.126.6.890.

Debertin, G. *et al.* (2015) 'Tyrosine hydroxylase positive perisomatic rings are formed around various amacrine cell types in the mammalian retina', *Journal of Neurochemistry*. doi: 10.1111/jnc.13144.

Decrock, E. *et al.* (2015) 'Connexin and pannexin signaling pathways, an architectural blueprint for CNS physiology and pathology?', *Cellular and Molecular Life Sciences*. doi: 10.1007/s00018-015-1962-7.

DeLalio, L. J. *et al.* (2019) 'Constitutive SRC-mediated phosphorylation of pannexin 1 at tyrosine 198 occurs at the plasma membrane', *Journal of Biological Chemistry*. doi: 10.1074/jbc.RA118.006982.

Demin, K. A. *et al.* (2020) 'Cross-species Analyses of Intra-species Behavioral Differences in Mammals and Fish', *Neuroscience*. doi: 10.1016/j.neuroscience.2019.12.035.

Deng, Z. *et al.* (2020) 'Cryo-EM structures of the ATP release channel pannexin 1', *Nature Structural and Molecular Biology*. doi: 10.1038/s41594-020-0401-0.

Detwiler, P. B. (2018) 'Phototransduction in retinal ganglion cells', *Yale Journal of Biology and Medicine*.

Van Deursen, J. M. (2014) 'The role of senescent cells in ageing', *Nature*. doi: 10.1038/nature13193.

DeVries, S. H. and Baylor, D. A. (1997) 'Mosaic arrangement of ganglion cell receptive fields in rabbit retina', *Journal of Neurophysiology*. doi: 10.1152/jn.1997.78.4.2048.

Diamond, J. S. and Copenhagen, D. R. (1993) 'The contribution of NMDA and Non-NMDA receptors to the light-evoked input-output characteristics of retinal ganglion cells', *Neuron*. doi: 10.1016/0896-6273(93)90082-3.

Ding, H. *et al.* (2016) 'Species-specific wiring for direction selectivity in the mammalian retina', *Nature*. doi: 10.1038/nature18609.

Dmitriev, A. V. and Mangel, S. C. (2000) 'A circadian clock regulates the pH of the fish retina', *Journal of Physiology*. doi: 10.1111/j.1469-7793.2000.0077m.x.

Dmitriev, A. V. and Mangel, S. C. (2001) 'Circadian clock regulation of pH in the rabbit retina', *Journal of Neuroscience*. doi: 10.1523/jneurosci.21-08-02897.2001.

Dougherty, R. P. (2005) 'Extensions of DAMAS and benefits and limitations of deconvolution in beamforming', in *Collection of Technical Papers - 11th AIAA/CEAS Aeroacoustics Conference*. doi: 10.2514/6.2005-2961.

Doyle, S. E. *et al.* (2002) 'Circadian rhythms of dopamine in mouse retina: The role of melatonin', *Visual Neuroscience*. doi: 10.1017/S0952523802195058.

Doyle, S. E., McIvor, W. E. and Menaker, M. (2002) 'Circadian rhythmicity in dopamine content of mammalian retina: Role of the photoreceptors', *Journal of Neurochemistry*. doi: 10.1046/j.1471-4159.2002.01149.x.

Drew, R. E. *et al.* (2012) 'Brain transcriptome variation among behaviorally distinct strains of zebrafish (Danio rerio)', *BMC Genomics*. doi: 10.1186/1471-2164-13-323.

Dvoriantchikova, G. *et al.* (2006) 'Expression of pannexin family of proteins in the retina', *FEBS Letters*. doi: 10.1016/j.febslet.2006.03.026.

Dvoriantchikova, G. *et al.* (2018) 'Pannexin 1 sustains the electrophysiological responsiveness of retinal ganglion cells', *Scientific Reports*. doi: 10.1038/s41598-018-23894-2.

Easter, S. S. and Nicola, G. N. (1996) 'The development of vision in the zebrafish (Danio rerio)', *Developmental Biology*. doi: 10.1006/dbio.1996.0335.

Emran, F., Rihel, J. and Dowling, J. E. (2008) 'A behavioral assay to measure responsiveness of Zebrafish to changes in light intensities', *Journal of Visualized Experiments*. doi: 10.3791/923.

Engelhardt, K. *et al.* (2015) 'Effects on Channel Properties and Induction of Cell Death Induced by C-terminal Truncations of Pannexin1 Depend on Domain Length', *Journal of Membrane Biology*. doi: 10.1007/s00232-014-9767-4.

Enger, C., Alexander, M. F. and Fine, S. L. (1988) 'Contrast Sensitivity in Age-Related Macular Degeneration', *Archives of Ophthalmology*. doi: 10.1001/archopht.1988.01060130061028.

Erb, L. *et al.* (2006) 'P2 receptors: Intracellular signaling', *Pflugers Archiv European Journal of Physiology*. doi: 10.1007/s00424-006-0069-2.

Fernandes, A. M. *et al.* (2012) 'Deep brain photoreceptors control light-seeking behavior in zebrafish larvae', *Current Biology*. doi: 10.1016/j.cub.2012.08.016.

Ferré, S. *et al.* (1992) 'Adenosine-dopamine interactions in the brain', *Neuroscience*. doi: 10.1016/0306-4522(92)90291-9.

Feschotte, C. and Pritham, E. J. (2007) 'DNA Transposons and the Evolution of Eukaryotic Genomes', *Annual Review of Genetics*. doi: 10.1146/annurev.genet.40.110405.090448.

Fields, C., Bischof, J. and Levin, M. (2020) 'Morphological coordination: A common ancestral function unifying neural and non-neural signaling', *Physiology*. doi: 10.1152/physiol.00027.2019.

Finger, A. M., Dibner, C. and Kramer, A. (2020) 'Coupled network of the circadian clocks: a driving force of rhythmic physiology', *FEBS Letters*. doi: 10.1002/1873-3468.13898.

Fischer, W. and Krugel, U. (2007) 'P2Y Receptors: Focus on Structural, Pharmacological and Functional Aspects in the Brain', *Current Medicinal Chemistry*. doi: 10.2174/092986707782023695.

Fleisch, V. C. and Neuhauss, S. C. F. (2006) 'Visual behavior in zebrafish', *Zebrafish*. doi: 10.1089/zeb.2006.3.191.

Foster, R. G. *et al.* (1993) 'Photoreceptors regulating circadian behavior: a mouse model.', *Journal of biological rhythms*. doi: 10.21236/ada264881.

Foster, R. G. and Kreitzman, L. (2014) 'The rhythms of life: What your body clock means to you!', *Experimental Physiology*. doi: 10.1113/expphysiol.2012.071118.

Freedman, M. S. *et al.* (1999) 'Regulation of mammalian circadian behavior by non-rod, non-cone, ocular photoreceptors', *Science*. doi: 10.1126/science.284.5413.502.

Frøland Steindal, I. A. *et al.* (2018) 'Development of the Astyanax mexicanus circadian clock and non-visual light responses', *Developmental Biology*. doi: 10.1016/j.ydbio.2018.06.008.

Fushiki, D. *et al.* (2010) 'Phylogenetic and bioinformatic analysis of gap junction-related proteins, innexins, pannexins and connexins', *Biomedical Research*. doi: 10.2220/biomedres.31.133.

Fuxe, K. *et al.* (2007) 'Adenosine receptor-dopamine receptor interactions in the basal ganglia and their relevance for brain function', *Physiology and Behavior*. doi: 10.1016/j.physbeh.2007.05.034.

Fuxe, K. *et al.* (2010) 'Adenosine-dopamine interactions in the pathophysiology and treatment of cns disorders', *CNS Neuroscience and Therapeutics*. doi: 10.1111/j.1755-5949.2009.00126.x.

Fuxe, K., Agnati, L. F. and Borroto-Escuela, D. O. (2014) 'The impact of receptor-receptor interactions in heteroreceptor complexes on brain plasticity', *Expert Review of Neurotherapeutics*. doi: 10.1586/14737175.2014.922878.

Ganzen, L. *et al.* (2017) 'Utilizing zebrafish visual behaviors in drug screening for retinal degeneration', *International Journal of Molecular Sciences*. doi: 10.3390/ijms18061185.

Garcia, J. A. *et al.* (2000) 'Impaired cued and contextual memory in NPAS2-deficient mice', *Science*. doi: 10.1126/science.288.5474.2226.

Gerevich, Z. and Illes, P. (2004) 'P2Y receptors and pain transmission', *Purinergic Signalling*. doi: 10.1007/s11302-004-4740-9.

Gerstner, J. R. and Yin, J. C. P. (2010) 'Circadian rhythms and memory formation', *Nature Reviews Neuroscience*. doi: 10.1038/nrn2881.

Gilbertson, T. A., Scobey, R. and Wilson, M. (1991) 'Permeation of calcium ions through non-NMDA glutamate channels in retinal bipolar cells', *Science*. doi: 10.1126/science.1849316.

Gomes, C. V. *et al.* (2011) 'Adenosine receptors and brain diseases: Neuroprotection and neurodegeneration', *Biochimica et Biophysica Acta - Biomembranes*. doi: 10.1016/j.bbamem.2010.12.001.

Gorissen, M. *et al.* (2015) 'Differences in inhibitory avoidance, cortisol and brain gene expression in TL and AB zebrafish', *Genes, Brain and Behavior*. doi: 10.1111/gbb.12220.

Göz, D. *et al.* (2008) 'Targeted destruction of photosensitive retinal ganglion cells with a saporin conjugate alters the effects of light on mouse circadian rhythms', *PLoS ONE*. doi: 10.1371/journal.pone.0003153.

Green, C. B. and Besharse, J. C. (2004) 'Retinal Circadian Clocks and Control of Retinal

Physiology', *Journal of Biological Rhythms*. doi: 10.1177/0748730404263002.

Grillon, C. (2002) 'Startle reactivity and anxiety disorders: Aversive conditioning, context, and neurobiology', *Biological Psychiatry*. doi: 10.1016/S0006-3223(02)01665-7.

Guillaumond, F. *et al.* (2005) 'Differential control of Bmal1 circadian transcription by REV-ERB and ROR nuclear receptors', *Journal of Biological Rhythms*. doi: 10.1177/0748730405277232.

Güler, A. D. *et al.* (2008) 'Melanopsin cells are the principal conduits for rod-cone input to non-image-forming vision', *Nature*. doi: 10.1038/nature06829.

Guo, S. *et al.* (1999) 'Mutations in the zebrafish unmask shared regulatory pathways controlling the development of catecholaminergic neurons', *Developmental Biology*. doi: 10.1006/dbio.1999.9204.

Guo, S. (2004) 'Linking genes to brain, behavior and neurological diseases: What can we learn from zebrafish?', *Genes, Brain and Behavior*. doi: 10.1046/j.1601-183X.2003.00053.x.

Guthrie, P. B. *et al.* (1999) 'ATP released from astrocytes mediates glial calcium waves', *Journal of Neuroscience*. doi: 10.1523/JNEUROSCI.19-02-00520.1999.

Guzman, S. J. and Gerevich, Z. (2016) 'P2Y Receptors in Synaptic Transmission and Plasticity: Therapeutic Potential in Cognitive Dysfunction', *Neural Plasticity*. doi: 10.1155/2016/1207393.

Hagins, W. A., Penn, R. D. and Yoshikami, S. (1970) 'Dark Current and Photocurrent in Retinal Rods', *Biophysical Journal*. doi: 10.1016/S0006-3495(70)86308-1.

Hahn, M. W. (2009) 'Distinguishing among evolutionary models for the maintenance of gene duplicates', *Journal of Heredity*. doi: 10.1093/jhered/esp047.

Hanstein, R. *et al.* (2016) 'Glial pannexin1 contributes to tactile hypersensitivity in a mouse model of orofacial pain', *Scientific Reports*. doi: 10.1038/srep38266.

Harrisingh, M. C. *et al.* (2007) 'Intracellular Ca2+ regulates free-running circadian clock oscillation in vivo', *Journal of Neuroscience*. doi: 10.1523/JNEUROSCI.3680-07.2007.

Hastings, M. H., Maywood, E. S. and O'Neill, J. S. (2008) 'Cellular Circadian Pacemaking and the Role of Cytosolic Rhythms', *Current Biology*. doi: 10.1016/j.cub.2008.07.021.

Hatori, M. *et al.* (2008) 'Inducible ablation of melanopsin-expressing retinal ganglion cells reveals their central role in non-image forming visual responses', *PLoS ONE*. doi: 10.1371/journal.pone.0002451.

Hattar, S. *et al.* (2002) 'Melanopsin-containing retinal ganglion cells: Architecture, projections, and intrinsic photosensitivity', *Science*. doi: 10.1126/science.1069609.

Hawkins, A. S. *et al.* (2003) 'Comparison of contrast sensitivity, visual acuity, and Humphrey visual field testing in patients with glaucoma', *Journal of Glaucoma*. doi: 10.1097/00061198-200304000-00008.

Hawkins, B. T. and Davis, T. P. (2005) 'The blood-brain barrier/neurovascular unit in health and disease', *Pharmacological Reviews*. doi: 10.1124/pr.57.2.4.

Hewitt, G. *et al.* (2012) 'Telomeres are favoured targets of a persistent DNA damage response in ageing and stress-induced senescence', *Nature Communications*. doi: 10.1038/ncomms1708.

Higashijima, S. I., Mandel, G. and Fetcho, J. R. (2004) 'Distribution of prospective glutamatergic, glycinergic, and gabaergic neurons in embryonic and larval zebrafish', *Journal of Comparative Neurology*. doi: 10.1002/cne.20278.

Holzschuh, J. *et al.* (2001) 'Dopamine transporter expression distinguishes dopaminergic neurons from other catecholaminergic neurons in the developing zebrafish embryo', *Mechanisms of Development*. doi: 10.1016/S0925-4773(01)00287-8.

Honda, S. *et al.* (2001) 'Extracellular ATP or ADP induce chemotaxis of cultured microglia through Gi/o-coupled P2Y receptors', *Journal of Neuroscience*. doi: 10.1523/jneurosci.21-06-01975.2001.

Huang, Y. *et al.* (2004) 'Membrane transporters and channels: Role of the transportome in cancer chemosensitivity and chemoresistance', *Cancer Research*. doi: 10.1158/0008-5472.CAN-03-3884.

Huang, Y. J. *et al.* (2007) 'The role of pannexin 1 hemichannels in ATP release and cell-cell communication in mouse taste buds', *Proceedings of the National Academy of Sciences of the United States of America*. doi: 10.1073/pnas.0611280104.

Hyman, S. L., Shores, A. and North, K. N. (2005) 'The nature and frequency of cognitive deficits in children with neurofibromatosis type 1', *Neurology*. doi: 10.1212/01.wnl.0000179303.72345.ce.

Idzko, M., Ferrari, D. and Eltzschig, H. K. (2014) 'Nucleotide signalling during inflammation', *Nature*. doi: 10.1038/nature13085.

Iglesias, R. *et al.* (2008) 'P2X7 receptor-Pannexin1 complex: Pharmacology and signaling', *American Journal of Physiology - Cell Physiology*. doi: 10.1152/ajpcell.00228.2008.

Iglesias, R. *et al.* (2009) 'Pannexin 1: The molecular substrate of astrocyte "hemichannels"', *Journal of Neuroscience*. doi: 10.1523/JNEUROSCI.6062-08.2009.

Ikegami, K. *et al.* (2019) 'Interconnection between circadian clocks and thyroid function', *Nature Reviews Endocrinology*. doi: 10.1038/s41574-019-0237-z.

Isenberg, J. C. *et al.* (2013) 'Attention skills in children with neurofibromatosis type 1', *Journal of Child Neurology*. doi: 10.1177/0883073812439435.

Iuvone, P. M. *et al.* (1991) 'Effects of apomorphine, a dopamine receptor agonist, on ocular refraction and axial elongation in a primate model of myopia', *Investigative Ophthalmology and Visual Science*.

Jackson, F. *et al.* (2017) 'Pubertal development and anxiety risk independently relate to startle habituation during fear conditioning in 8–14 year-old females', *Developmental Psychobiology*. doi: 10.1002/dev.21506.

Jatllon, O. *et al.* (2004) 'Genome duplication in the teleost fish Tetraodon nigroviridis reveals the early vertebrate proto-karyotype', *Nature*. doi: 10.1038/nature03025.

Jenner, P. (2014) 'An Overview of adenosine A2A receptor antagonists in Parkinson's disease', in *International Review of Neurobiology*. doi: 10.1016/B978-0-12-801022-8.00003-9.

Johnson, J. *et al.* (2010) 'Melanopsin-dependent light avoidance in neonatal mice', *Proceedings of the National Academy of Sciences of the United States of America*. doi: 10.1073/pnas.1008533107.

Jun, J. Il and Lau, L. F. (2010) 'The matricellular protein CCN1 induces fibroblast senescence and restricts fibrosis in cutaneous wound healing', *Nature Cell Biology*. doi: 10.1038/ncb2070.

Kabir, M. H. *et al.* (2018) 'Identification of active signaling pathways by integrating gene expression and protein interaction data', *BMC Systems Biology*. doi: 10.1186/s12918-018-0655-x.

Kawamura, M., Ruskin, D. N. and Masino, S. A. (2010) 'Metabolic autocrine regulation of neurons

involves cooperation among pannexin hemichannels, adenosine receptors, and KATP channels', *Journal of Neuroscience*. doi: 10.1523/JNEUROSCI.0055-10.2010.

Khakh, B. S. and North, R. A. (2012) 'Neuromodulation by Extracellular ATP and P2X Receptors in the CNS', *Neuron*. doi: 10.1016/j.neuron.2012.09.024.

Kist, A. M. and Portugues, R. (2019) 'Optomotor Swimming in Larval Zebrafish Is Driven by Global Whole-Field Visual Motion and Local Light-Dark Transitions', *Cell Reports*. doi: 10.1016/j.celrep.2019.09.024.

Kofman, O. *et al.* (2007) 'Habituation, discrimination and anxiety in transgenic mice overexpressing acetylcholinesterase splice variants', *Brain Research*. doi: 10.1016/j.brainres.2007.09.018.

Kondratova, A. A. *et al.* (2010) 'Circadian clock proteins control adaptation to novel environment and memory formation', *Aging*. doi: 10.18632/aging.100142.

Kovalzon, V. M. *et al.* (2017) 'Sleep-wakefulness cycle and behavior in pannexin1 knockout mice', *Behavioural Brain Research*. doi: 10.1016/j.bbr.2016.10.015.

Kranz, K. *et al.* (2013) 'Expression of Pannexin1 in the outer plexiform layer of the mouse retina and physiological impact of its knockout', *Journal of Comparative Neurology*. doi: 10.1002/cne.23223.

Kripke, D. F. *et al.* (2009) 'Circadian polymorphisms associated with affective disorders', *Journal of Circadian Rhythms*. doi: 10.1186/1740-3391-7-2.

Krishnan, H. C. and Lyons, L. C. (2015) 'Synchrony and desynchrony in circadian clocks: Impacts on learning and memory', *Learning and Memory*. doi: 10.1101/lm.038877.115.

Krizhanovsky, V. *et al.* (2008) 'Senescence of Activated Stellate Cells Limits Liver Fibrosis', *Cell*. doi: 10.1016/j.cell.2008.06.049.

Kuboyama, K. *et al.* (2011) 'Astrocytic P2Y1 receptor is involved in the regulation of cytokine/chemokine transcription and cerebral damage in a rat model of cerebral ischemia', *Journal of Cerebral Blood Flow and Metabolism*. doi: 10.1038/jcbfm.2011.49.

Küçük, A. *et al.* (2008) 'Effects of age and anxiety on learning and memory', *Behavioural Brain Research*. doi: 10.1016/j.bbr.2008.05.023.

von Kugelgen, I. and Harden, T. K. (2011) 'Molecular Pharmacology, Physiology, and Structure of the P2Y Receptors', in *Advances in Pharmacology*. doi: 10.1016/B978-0-12-385526-8.00012-6.

Kurtenbach, Sarah *et al.* (2013) 'Pannexin1 Channel Proteins in the Zebrafish Retina Have Shared and Unique Properties', *PLoS ONE*. doi: 10.1371/journal.pone.0077722.

Kurtenbach, Sarah, Kurtenbach, Stefan and Zoidl, G. (2014) 'Emerging functions of pannexin 1 in the eye', *Frontiers in Cellular Neuroscience*. doi: 10.3389/fncel.2014.00263.

Lamb, T. D. and Simon, E. J. (1976) 'The relation between intercellular coupling and electrical noise in turtle photoreceptors.', *The Journal of Physiology*. doi: 10.1113/jphysiol.1976.sp011631.

Landgraf, D. *et al.* (2016) 'Genetic Disruption of Circadian Rhythms in the Suprachiasmatic Nucleus Causes Helplessness, Behavioral Despair, and Anxiety-like Behavior in Mice', *Biological Psychiatry*. doi: 10.1016/j.biopsych.2016.03.1050.

Lazzerini Ospri, L., Prusky, G. and Hattar, S. (2017) 'Mood, the Circadian System, and Melanopsin Retinal Ganglion Cells', *Annual Review of Neuroscience*. doi: 10.1146/annurev-

neuro-072116-031324.

Lebedev, D. S., Byzov, A. L. and Govardovskii, V. I. (1998) 'Photoreceptor coupling and boundary detection', *Vision Research*. doi: 10.1016/S0042-6989(98)00017-0.

Levine, T. M. *et al.* (2006) 'Cognitive Profile of Neurofibromatosis Type 1', *Seminars in Pediatric Neurology*. doi: 10.1016/j.spen.2006.01.006.

Li, H. *et al.* (2013) 'Adenosine and dopamine receptors coregulate photoreceptor coupling via gap junction phosphorylation in mouse retina', *Journal of Neuroscience*. doi: 10.1523/JNEUROSCI.2807-12.2013.

Li, H., Chuang, A. Z. and O'Brien, J. (2009) 'Photoreceptor coupling is controlled by connexin 35 phosphorylation in zebrafish retina', *Journal of Neuroscience*. doi: 10.1523/JNEUROSCI.3517-09.2009.

Li, L. (2019) 'Circadian Vision in Zebrafish: From Molecule to Cell and from Neural Network to Behavior', *Journal of Biological Rhythms*. doi: 10.1177/0748730419863917.

Li, L. and Dowling, J. E. (1998) 'Zebrafish visual sensitivity is regulated by a circadian clock', *Visual Neuroscience*. doi: 10.1017/S0952523898155050.

Li, L. and Dowling, J. E. (2000) 'Effects of dopamine depletion on visual sensitivity of zebrafish', *Journal of Neuroscience*. doi: 10.1523/jneurosci.20-05-01893.2000.

Li, P. H. *et al.* (2012) 'Gap-junctional coupling of mammalian rod photoreceptors and its effect on visual detection', *Journal of Neuroscience*. doi: 10.1523/JNEUROSCI.2144-11.2012.

Li, S., Tomić, M. and Stojilkovic, S. S. (2011) 'Characterization of novel Pannexin 1 isoforms from rat pituitary cells and their association with ATP-gated P2X channels', *General and Comparative Endocrinology*. doi: 10.1016/j.ygcen.2011.08.019.

Li, X. *et al.* (2012) 'Pineal photoreceptor cells are required for maintaining the circadian rhythms of behavioral visual sensitivity in zebrafish', *PLoS ONE*. doi: 10.1371/journal.pone.0040508.

Lindsey, B. W. *et al.* (2018) 'A whole brain staining, embedding, and clearing pipeline for adult zebrafish to visualize cell proliferation and morphology in 3-dimensions', *Frontiers in Neuroscience*. doi: 10.3389/fnins.2017.00750.

Liu, Y. J. *et al.* (2019) 'Research progress on adenosine in central nervous system diseases', *CNS Neuroscience and Therapeutics*. doi: 10.1111/cns.13190.

Livingstone, M. S. and Hubel, D. H. (1987) 'Psychophysical evidence for separate channels for the perception of form, color, movement, and depth', *Journal of Neuroscience*. doi: 10.1523/jneurosci.07-11-03416.1987.

Locovei, S. *et al.* (2007) 'Pannexin1 is part of the pore forming unit of the P2X7 receptor death complex', *FEBS Letters*. doi: 10.1016/j.febslet.2006.12.056.

Locovei, S., Wang, J. and Dahl, G. (2006) 'Activation of pannexin 1 channels by ATP through P2Y receptors and by cytoplasmic calcium', *FEBS Letters*. doi: 10.1016/j.febslet.2005.12.004.

Logan, R. W. and McClung, C. A. (2019) 'Rhythms of life: circadian disruption and brain disorders across the lifespan', *Nature Reviews Neuroscience*. doi: 10.1038/s41583-018-0088-y.

Lohman, A. W. *et al.* (2012) 'S-nitrosylation inhibits pannexin 1 channel function', *Journal of Biological Chemistry*. doi: 10.1074/jbc.M112.397976.

Lohman, A. W. *et al.* (2015) 'Pannexin 1 channels regulate leukocyte emigration through the venous endothelium during acute inflammation', *Nature Communications*. doi:

10.1038/ncomms8965.

Ma, A. C. *et al.* (2013) 'High Efficiency In Vivo Genome Engineering with a Simplified 15-RVD GoldyTALEN Design', *PLoS ONE*. doi: 10.1371/journal.pone.0065259.

Ma, A. C. H. *et al.* (2016) 'TALEN-Mediated mutagenesis and genome editing', in *Methods in Molecular Biology*. doi: 10.1007/978-1-4939-3771-4_2.

Ma, W. *et al.* (2009) 'Pharmacological characterization of pannexin-1 currents expressed in mammalian cells', *Journal of Pharmacology and Experimental Therapeutics*. doi: 10.1124/jpet.108.146365.

Ma, W. *et al.* (2012) 'Pannexin 1 forms an anion-selective channel', *Pflugers Archiv European Journal of Physiology*. doi: 10.1007/s00424-012-1077-z.

Maaswinkel, H. and Li, L. (2003) 'Spatio-temporal frequency characteristics of the optomotor response in zebrafish', *Vision Research*. doi: 10.1016/S0042-6989(02)00395-4.

MacPhail, R. C. *et al.* (2009) 'Locomotion in larval zebrafish: Influence of time of day, lighting and ethanol', *NeuroToxicology*. doi: 10.1016/j.neuro.2008.09.011.

MacVicar, B. A. and Thompson, R. J. (2010) 'Non-junction functions of pannexin-1 channels', *Trends in Neurosciences*. doi: 10.1016/j.tins.2009.11.007.

Magadum, S. *et al.* (2013) 'Gene duplication as a major force in evolution', *Journal of Genetics*. doi: 10.1007/s12041-013-0212-8.

Malicki, J. *et al.* (1996) 'Mutations affecting development of the zebrafish retina', *Development*. doi: 10.5167/uzh-224.

Mansour, H. A. *et al.* (2006) 'Association study of eight circadian genes with bipolar I disorder, schizoaffective disorder and schizophrenia', *Genes, Brain and Behavior*. doi: 10.1111/j.1601-183X.2005.00147.x.

Marijuán, P. C., del Moral, R. and Navarro, J. (2013) 'On eukaryotic intelligence: Signaling system's guidance in the evolution of multicellular organization', *BioSystems*. doi: 10.1016/j.biosystems.2013.06.005.

Matsui, H. and Sugie, A. (2017) 'An optimized method for counting dopaminergic neurons in zebrafish', *PLoS ONE*. doi: 10.1371/journal.pone.0184363.

Mattis, J. and Sehgal, A. (2016) 'Circadian Rhythms, Sleep, and Disorders of Aging', *Trends in Endocrinology and Metabolism*. doi: 10.1016/j.tem.2016.02.003.

Mattson, M. P. and Bruce-Keller, A. J. (1999) 'Compartmentalization of signaling in neurons: Evolution and deployment', *Journal of Neuroscience Research*. doi: 10.1002/(SICI)1097-4547(19991001)58:1<2::AID-JNR2>3.0.CO;2-T.

Mayo, C. *et al.* (2008) 'Regulation by P2X7: Epithelial migration and stromal organization in the cornea', *Investigative Ophthalmology and Visual Science*. doi: 10.1167/iovs.08-1688.

McMahon, D. G., Iuvone, P. M. and Tosini, G. (2014) 'Circadian organization of the mammalian retina: From gene regulation to physiology and diseases', *Progress in Retinal and Eye Research*. doi: 10.1016/j.preteyeres.2013.12.001.

McTeague, L. M. *et al.* (2011) 'Aversive imagery in panic disorder: Agoraphobia severity, comorbidity, and defensive physiology', *Biological Psychiatry*. doi: 10.1016/j.biopsych.2011.03.005.

McTeague, L. M. and Lang, P. J. (2012) 'The anxiety spectrum and the reflex physiology of

defense: From circumscribed fear to broad distress', in *Depression and Anxiety*. doi: 10.1002/da.21891.

Meeker, N. D. *et al.* (2007) 'Method for isolation of PCR-ready genomic DNA from zebrafish tissues', *BioTechniques*. doi: 10.2144/000112619.

Meier, A., Nelson, R. and Connaughton, V. P. (2018) 'Color processing in zebrafish retina', *Frontiers in Cellular Neuroscience*. doi: 10.3389/fncel.2018.00327.

von Mering, C. *et al.* (2003) 'STRING: A database of predicted functional associations between proteins', *Nucleic Acids Research*. doi: 10.1093/nar/gkg034.

Michalski, K., Syrjanen, Johanna L., *et al.* (2020) 'The Cryo-EM structure of a pannexin 1 reveals unique motifs for ion selection and inhibition', *eLife*. doi: 10.7554/eLife.54670.

Michalski, K., Syrjanen, Johanna L, *et al.* (2020) 'The Cryo-EM structure of pannexin 1 reveals unique motifs for ion selection and inhibition', *eLife*. doi: 10.7554/elife.54670.

Milhiet, V. *et al.* (2011) 'Circadian biomarkers, circadian genes and bipolar disorders', *Journal of Physiology Paris*. doi: 10.1016/j.jphysparis.2011.07.002.

Morin, L. P., Blanchard, J. H. and Provencio, I. (2003) 'Retinal ganglion cell projections to the hamster suprachiasmatic nucleus, intergeniculate leaflet, and visual midbrain: Bifurcation and melanopsin immunoreactivity', *Journal of Comparative Neurology*. doi: 10.1002/cne.10881.

Morris, A. C. and Fadool, J. M. (2005) 'Studying rod photoreceptor development in zebrafish', *Physiology and Behavior*. doi: 10.1016/j.physbeh.2005.08.020.

Moustafa, A. (2020) 'Effect of Light-Dark Cycle Misalignment on the Hypothalamic-Pituitary-Gonadal Axis, Testicular Oxidative Stress, and Expression of Clock Genes in Adult Male Rats', *International Journal of Endocrinology*. doi: 10.1155/2020/1426846.

Muñoz-Espín, D. *et al.* (2013) 'XProgrammed cell senescence during mammalian embryonic development', *Cell*. doi: 10.1016/j.cell.2013.10.019.

Musiek, E. S. *et al.* (2013) 'Circadian clock proteins regulate neuronal redox homeostasis and neurodegeneration', *Journal of Clinical Investigation*. doi: 10.1172/JCI70317.

Naumann, E. A. *et al.* (2016) 'From Whole-Brain Data to Functional Circuit Models: The Zebrafish Optomotor Response', *Cell*. doi: 10.1016/j.cell.2016.10.019.

Neff, K. L. *et al.* (2013) 'Mojo Hand, a TALEN design tool for genome editing applications', *BMC Bioinformatics*. doi: 10.1186/1471-2105-14-1.

Nelson, R. J. and Chbeir, S. (2018) 'Dark matters: Effects of light at night on metabolism', in *Proceedings of the Nutrition Society*. doi: 10.1017/S0029665118000198.

Neuhauss, S. C. F. *et al.* (1999) 'Genetic disorders of vision revealed by a behavioral screen of 400 essential loci in zebrafish', *Journal of Neuroscience*. doi: 10.1523/jneurosci.19-19-08603.1999.

Neuhauss, S. C. F. (2003) 'Behavioral genetic approaches to visual system development and function in zebrafish', *Journal of Neurobiology*. doi: 10.1002/neu.10165.

Neuhauss, S. C. F. (2010) 'Zebrafish Vision: Structure and Function of the Zebrafish Visual System', in *Fish Physiology - Zebrafish: Volume 29*. doi: 10.1016/S1546-5098(10)02903-1.

Nguyen, T. D. *et al.* (2001) 'P2Y11, a purinergic receptor acting via cAMP, mediates secretion by pancreatic duct epithelial cells', *American Journal of Physiology - Gastrointestinal and Liver Physiology*. doi: 10.1152/ajpgi.2001.280.5.g795.

Nir, I., Haque, R. and Iuvone, P. M. (2000) 'Diurnal metabolism of dopamine in the mouse retina', *Brain Research*. doi: 10.1016/S0006-8993(00)02409-4.

O'Neill, J. S. and Reddy, A. B. (2012) 'The essential role of cAMP/Ca 2+ signalling in mammalian circadian timekeeping', *Biochemical Society Transactions*. doi: 10.1042/BST20110691.

Oliveira, J. *et al.* (2015) 'The zebrafish world of colors and shapes: Preference and discrimination', *Zebrafish*. doi: 10.1089/zeb.2014.1019.

Olivier, E. *et al.* (2016) 'P2X7-pannexin-1 and amyloid β-induced oxysterol input in human retinal cell: Role in age-related macular degeneration?', *Biochimie*. doi: 10.1016/j.biochi.2016.04.014.

Olson, V. A. and Owens, I. P. F. (1998) 'Costly sexual signals: Are carotenoids rare, risky or required?', *Trends in Ecology and Evolution*. doi: 10.1016/S0169-5347(98)01484-0.

Organisciak, D. T. *et al.* (2000) 'Circadian-dependent retinal light damage in rats', *Investigative Ophthalmology and Visual Science*.

Orger, M. B. *et al.* (2000) 'Perception of Fourier and non-Fourier motion by larval zebrafish', *Nature Neuroscience*. doi: 10.1038/80649.

Orger, M. B. *et al.* (2008) 'Control of visually guided behavior by distinct populations of spinal projection neurons', *Nature Neuroscience*. doi: 10.1038/nn2048.

Orger, M. B. and Baier, H. (2005) 'Channeling of red and green cone inputs to the zebrafish optomotor response', *Visual Neuroscience*. doi: 10.1017/S0952523805223039.

Orger, M. B. and De Polavieja, G. G. (2017) 'Zebrafish Behavior: Opportunities and Challenges', *Annual Review of Neuroscience*. doi: 10.1146/annurev-neuro-071714-033857.

Oster, H. (2020) 'The interplay between stress, circadian clocks, and energy metabolism', *Journal of Endocrinology*. doi: 10.1530/JOE-20-0124.

Oswald, M. and Robison, B. D. (2008) 'Strain-specific alteration of zebrafish feeding behavior in response to aversive stimuli', *Canadian Journal of Zoology*. doi: 10.1139/Z08-085.

Ota, T. *et al.* (2012) 'Circadian clock signals in the adrenal cortex', *Molecular and Cellular Endocrinology*. doi: 10.1016/j.mce.2011.08.010.

Panchin, Y. V. (2005) 'Evolution of gap junction proteins - The pannexin alternative', *Journal of Experimental Biology*. doi: 10.1242/jeb.01547.

Panchina, Y. *et al.* (2000) 'A ubiquitous family of putative gap junction molecules [2]', *Current Biology*. doi: 10.1016/S0960-9822(00)00576-5.

Panda, S. *et al.* (2005) 'Illumination of the melanopsin signaling pathway', *Science*. doi: 10.1126/science.1105121.

Panda, S. (2016) 'Circadian physiology of metabolism', *Science*. doi: 10.1126/science.aah4967.

Pando, M. P. and Sassone-Corsi, P. (2002) 'Unraveling the mechanisms of the vertebrate circadian clock: Zebrafish may light the way', *BioEssays*. doi: 10.1002/bies.10091.

Panula, P. *et al.* (2010) 'The comparative neuroanatomy and neurochemistry of zebrafish CNS systems of relevance to human neuropsychiatric diseases', *Neurobiology of Disease*. doi: 10.1016/j.nbd.2010.05.010.

Park, J. S. *et al.* (2016) 'Innate color preference of zebrafish and its use in behavioral analyses', *Molecules and Cells*. doi: 10.14348/molcells.2016.0173.

Partch, C. L., Green, C. B. and Takahashi, J. S. (2014) 'Molecular architecture of the mammalian

circadian clock', *Trends in Cell Biology*. doi: 10.1016/j.tcb.2013.07.002.

Peeters, B. W. M. M., Moeskops, M. and Veenvliet, A. R. J. (2016) 'Color Preference in Danio rerio: Effects of Age and Anxiolytic Treatments', *Zebrafish*. doi: 10.1089/zeb.2015.1150.

Peichl, L. and Gonzalez-Soriano, J. (1993) 'Unexpected presence of neurofilaments in axon-bearing horizontal cells of the mammalian retina', *Journal of Neuroscience*. doi: 10.1523/jneurosci.13-09-04091.1993.

Pelegrin, P. and Surprenant, A. (2006) 'Pannexin-1 mediates large pore formation and interleukin-1β release by the ATP-gated P2X7 receptor', *EMBO Journal*. doi: 10.1038/sj.emboj.7601378.

Pelegrin, P. and Surprenant, A. (2009) 'The P2X7 receptor - Pannexin connection to dye uptake and IL-1β release', *Purinergic Signalling*. doi: 10.1007/s11302-009-9141-7.

Peng, Y. W. *et al.* (1995) 'Distribution of glutamate receptor subtypes in the vertebrate retina', *Neuroscience*. doi: 10.1016/0306-4522(94)00569-Q.

Penn, R. D. and Hagins, W. A. (1972) 'Kinetics of the Photocurrent of Retinal Rods', *Biophysical Journal*. doi: 10.1016/S0006-3495(72)86145-9.

Penuela, S. *et al.* (2007) 'Pannexin 1 and pannexin 3 are glycoproteins that exhibit many distinct characteristics from the connexin family of gap junction proteins', *Journal of Cell Science*. doi: 10.1242/jcs.009514.

Penuela, S. *et al.* (2008) 'Diverse subcellular distribution profiles of pannexin1 and pannexin3', *Cell Communication and Adhesion*. doi: 10.1080/15419060802014115.

Penuela, S. *et al.* (2009) 'Glycosylation regulates pannexin intermixing and cellular localization', *Molecular Biology of the Cell*. doi: 10.1091/mbc.E09-01-0067.

Penuela, S., Gehi, R. and Laird, D. W. (2013) 'The biochemistry and function of pannexin channels', *Biochimica et Biophysica Acta - Biomembranes*. doi: 10.1016/j.bbamem.2012.01.017.

Penuela, S. and Laird, D. W. (2012) 'The cellular life of pannexins', *Wiley Interdisciplinary Reviews: Membrane Transport and Signaling*. doi: 10.1002/wmts.63.

Penuela, S., Simek, J. and Thompson, R. J. (2014) 'Regulation of pannexin channels by post-translational modifications', in *FEBS Letters*. doi: 10.1016/j.febslet.2014.01.028.

Pfaffl, M. W. (2002) 'Relative expression software tool (REST(C)) for group-wise comparison and statistical analysis of relative expression results in real-time PCR', *Nucleic Acids Research*. doi: 10.1093/nar/30.9.e36.

Plesner, L. (1995) 'Ecto-ATPases: Identities and Functions', *International Review of Cytology*. doi: 10.1016/S0074-7696(08)62487-0.

Poornima, V. *et al.* (2012) 'P2X 7 receptor-pannexin 1 hemichannel association: Effect of extracellular calcium on membrane permeabilization', *Journal of Molecular Neuroscience*. doi: 10.1007/s12031-011-9646-8.

Portugues, R. *et al.* (2015) 'Whole-field visual motion drives swimming in larval zebrafish via a stochastic process', *Journal of Experimental Biology*. doi: 10.1242/jeb.118299.

Portugues, R. and Engert, F. (2011) 'Adaptive locomotor behavior in larval zebrafsh', *Frontiers in Systems Neuroscience*. doi: 10.3389/fnsys.2011.00072.

Potolicchio, I. *et al.* (2012) 'Connexin-dependent signaling in neuro-hormonal systems', *Biochimica et Biophysica Acta - Biomembranes*. doi: 10.1016/j.bbamem.2011.09.022.

Preitner, N. *et al.* (2002) 'The orphan nuclear receptor REV-ERBα controls circadian transcription within the positive limb of the mammalian circadian oscillator', *Cell*. doi: 10.1016/S0092-8674(02)00825-5.

Prochnow, N. *et al.* (2009) 'Pannexin1 in the outer retina of the zebrafish, Danio rerio', *Neuroscience*. doi: 10.1016/j.neuroscience.2009.04.064.

Prochnow, Nora *et al.* (2009) 'Replacement of a single cysteine in the fourth transmembrane region of zebrafish pannexin1 alters hemichannel gating behavior', *Experimental Brain Research*. doi: 10.1007/s00221-009-1957-4.

Prochnow, N. *et al.* (2012) 'Pannexin1 Stabilizes Synaptic Plasticity and Is Needed for Learning', *PLoS ONE*. doi: 10.1371/journal.pone.0051767.

Qu, R. *et al.* (2020) 'Cryo-EM structure of human heptameric Pannexin 1 channel', *Cell Research*. doi: 10.1038/s41422-020-0298-5.

Rainy, N. *et al.* (2016) 'Knockdown of unc119c results in visual impairment and early-onset retinal dystrophy in zebrafish', *Biochemical and Biophysical Research Communications*. doi: 10.1016/j.bbrc.2016.04.041.

Randlett, O. *et al.* (2019) 'Distributed Plasticity Drives Visual Habituation Learning in Larval Zebrafish', *Current Biology*. doi: 10.1016/j.cub.2019.02.039.

Rawashdeh, O., Parsons, R. and Maronde, E. (2018) 'Clocking In Time to Gate Memory Processes: The Circadian Clock Is Part of the Ins and Outs of Memory', *Neural plasticity*. doi: 10.1155/2018/6238989.

Ray, A. *et al.* (2005) 'Site-specific and developmental expression of pannexin1 in the mouse nervous system', *European Journal of Neuroscience*. doi: 10.1111/j.1460-9568.2005.04139.x.

Regan, D. and Neima, D. (1984) 'Low-contrast letter charts in early diabetic retinopathy, ocular hypertension, glaucoma, and Parkinson's disease', *British Journal of Ophthalmology*. doi: 10.1136/bjo.68.12.885.

Reinke, H. and Asher, G. (2019) 'Crosstalk between metabolism and circadian clocks', *Nature Reviews Molecular Cell Biology*. doi: 10.1038/s41580-018-0096-9.

Resta, V. *et al.* (2005) 'Neuronal death induced by endogenous extracellular ATP in retinal cholinergic neuron density control', *Development*. doi: 10.1242/dev.01855.

Ribelayga, C. and Mangel, S. C. (2005) 'A circadian clock and light/dark adaptation differentially regulate adenosine in the mammalian retina', *Journal of Neuroscience*. doi: 10.1523/JNEUROSCI.3138-04.2005.

Ribelayga, C., Wang, Y. and Mangel, S. C. (2004) 'A circadian clock in the fish retina regulates dopamine release via activation of melatonin receptors', *Journal of Physiology*. doi: 10.1113/jphysiol.2003.053710.

Riordan-Eva, P. (2004) 'Clinical assessment of optic nerve disorders', *Eye*. doi: 10.1038/sj.eye.6701575.

Risner, M. L. *et al.* (2006) 'Behavioral spectral sensitivity of the zebrafish (Danio rerio)', *Vision Research*. doi: 10.1016/j.visres.2005.12.014.

Roberts, A. C. *et al.* (2011) 'Habituation of the C-start response in larval zebrafish exhibits several distinct phases and sensitivity to NMDA receptor Blockade', *PLoS ONE*. doi: 10.1371/journal.pone.0029132.

Robson, J. G. and Frishman, L. J. (2014) 'The rod-driven a-wave of the dark-adapted mammalian electroretinogram', *Progress in Retinal and Eye Research*. doi: 10.1016/j.preteyeres.2013.12.003.

Romanov, R. A. *et al.* (2007) 'Afferent neurotransmission mediated by hemichannels in mammalian taste cells', *EMBO Journal*. doi: 10.1038/sj.emboj.7601526.

Rose, E. *et al.* (2002) 'A comparative study of two mandibular advancement appliances for the treatment of obstructive sleep apnoea', *European Journal of Orthodontics*. doi: 10.1093/ejo/24.2.191.

Rosenwasser, A. M. *et al.* (1979) 'Circadian rhythm of luminance detectability in the rat', *Physiology and Behavior*. doi: 10.1016/0031-9384(79)90115-X.

Ross, J. E., Bron, A. J. and Clarke, D. D. (1984) 'Contrast sensitivity and visual disability in chronic simple glaucoma', *British Journal of Ophthalmology*. doi: 10.1136/bjo.68.11.821.

Ruan, G. X. *et al.* (2006) 'Circadian organization of the mammalian retina', *Proceedings of the National Academy of Sciences of the United States of America*. doi: 10.1073/pnas.0601940103.

Ruan, Z. *et al.* (2020) 'Structures of human pannexin 1 reveal ion pathways and mechanism of gating', *Nature*. doi: 10.1038/s41586-020-2357-y.

Ruppertsberg, A. I., Wuerger, S. M. and Bertamini, M. (2003) 'The chromatic input to global motion perception', *Visual Neuroscience*. doi: 10.1017/S0952523803204077.

Rutter, J., Reick, M. and McKnight, S. L. (2002) 'Metabolism and the control of circadian rhythms', *Annual Review of Biochemistry*. doi: 10.1146/annurev.biochem.71.090501.142857.

Sager, J. J., Bai, Q. and Burton, E. A. (2010) 'Transgenic zebrafish models of neurodegenerative diseases', *Brain Structure and Function*. doi: 10.1007/s00429-009-0237-1.

Sahu, G., Sukumaran, S. and Bera, A. K. (2014) 'Pannexins form gap junctions with electrophysiological and pharmacological properties distinct from connexins', *Scientific Reports*. doi: 10.1038/srep04955.

Salmi, P., Chergui, K. and Fredholm, B. B. (2005) 'Adenosine-dopamine interactions revealed in knockout mice', in *Journal of Molecular Neuroscience*. doi: 10.1385/JMN:26:2-3:239.

Sandilos, J. K. *et al.* (2012) 'Pannexin 1, an ATP release channel, is activated by caspase cleavage of its pore-associated C-terminal autoinhibitory region', *Journal of Biological Chemistry*. doi: 10.1074/jbc.M111.323378.

Schindelin, J. *et al.* (2012) 'Fiji: An open-source platform for biological-image analysis', *Nature Methods*. doi: 10.1038/nmeth.2019.

Schipke, C. G. *et al.* (2002) 'Astrocyte Ca2+ waves trigger responses in microglial cells in brain slices.', *The FASEB journal : official publication of the Federation of American Societies for Experimental Biology*. doi: 10.1096/fj.01-0514fje.

Schmidt, C. *et al.* (2007) 'A time to think: Circadian rhythms in human cognition', *Cognitive Neuropsychology*. doi: 10.1080/02643290701754158.

Schmitt, E. A. and Dowling, J. E. (1999) 'Early retinal development in the Zebrafish, Danio rerio: Light and electron microscopic analyses', *Journal of Comparative Neurology*. doi: 10.1002/(SICI)1096-9861(19990222)404:4<515::AID-CNE8>3.0.CO;2-A.

Serrano, M. *et al.* (1997) 'Oncogenic ras provokes premature cell senescence associated with accumulation of p53 and p16(INK4a)', *Cell*. doi: 10.1016/S0092-8674(00)81902-9.

Shook, B. C. and Jackson, P. F. (2011) 'Adenosine A2A receptor antagonists and Parkinson's disease', *ACS Chemical Neuroscience*. doi: 10.1021/cn2000537.

Silva, C. C. and Domínguez, R. (2020) 'Clock control of mammalian reproductive cycles: Looking beyond the pre-ovulatory surge of gonadotropins', *Reviews in Endocrine and Metabolic Disorders*. doi: 10.1007/s11154-019-09525-9.

Sinturel, F. *et al.* (2019) 'Cellular circadian period length inversely correlates with HbA1c levels in individuals with type 2 diabetes', *Diabetologia*. doi: 10.1007/s00125-019-4907-0.

Sipilä, T. *et al.* (2010) 'An Association Analysis of Circadian Genes in Anxiety Disorders', *Biological Psychiatry*. doi: 10.1016/j.biopsych.2009.12.011.

Siregar, P. *et al.* (2020) 'Method standardization for conducting innate color preference studies in different Zebrafish strains', *Biomedicines*. doi: 10.3390/BIOMEDICINES8080271.

Sollars, P. J. *et al.* (2003) 'Melanopsin and non-melanopsin expressing retinal ganglion cells innervate the hypothalamic suprachiasmatic nucleus', *Visual Neuroscience*. doi: 10.1017/S0952523803206027.

Sosinsky, G. E. *et al.* (2011) 'Pannexin channels are not gap junction hemichannels', *Channels*. doi: 10.4161/chan.5.3.15765.

Spagnol, G., Sorgen, P. L. and Spray, D. C. (2014) 'Structural order in Pannexin 1 cytoplasmic domains', *Channels*. doi: 10.4161/chan.28854.

Spence, R. *et al.* (2008) 'The behaviour and ecology of the zebrafish, Danio rerio', *Biological Reviews*. doi: 10.1111/j.1469-185X.2007.00030.x.

Stangos, N. *et al.* (1995) 'Contrast sensitivity evaluation in eyes predisposed to age-related macular degeneration and presenting normal visual acuity', *Ophthalmologica*. doi: 10.1159/000310612.

Stella, S. L., Bryson, E. J. and Thoreson, W. B. (2002) 'A2 adenosine receptors inhibit calcium influx through L-type calcium channels in rod photoreceptors of the salamander retina', *Journal of Neurophysiology*. doi: 10.1152/jn.00010.2001.

Stiebel-Kalish, H. *et al.* (2012) 'Gucy2f zebrafish knockdown-a model for Gucy2d-related leber congenital amaurosis', *European Journal of Human Genetics*. doi: 10.1038/ejhg.2012.10.

Stockton, R. A. and Slaughter, M. M. (1989) 'B-wave of the electroretinogram: A Reflection of ON bipolar cell activity', *Journal of General Physiology*. doi: 10.1085/jgp.93.1.101.

Storch, K. F. *et al.* (2007) 'Intrinsic Circadian Clock of the Mammalian Retina: Importance for Retinal Processing of Visual Information', *Cell*. doi: 10.1016/j.cell.2007.06.045.

Storer, M. *et al.* (2013) 'XSenescence is a developmental mechanism that contributes to embryonic growth and patterning', *Cell*. doi: 10.1016/j.cell.2013.10.041.

Sullivan, E. V., Rose, J. and Pfefferbaum, A. (2006) 'Effect of vision, touch and stance on cerebellar vermian-related sway and tremor: A quantitative physiological and MRI study', *Cerebral Cortex*. doi: 10.1093/cercor/bhj048.

Surprenant, A. *et al.* (1996) 'The cytolytic P2Z receptor for extracellular ATP identified as a P2X receptor (P2X7)', *Science*. doi: 10.1126/science.272.5262.735.

Tang, H. L. *et al.* (2015) 'PathPPI: an integrated dataset of human pathways and protein-protein interactions', *Science China Life Sciences*. doi: 10.1007/s11427-014-4766-3.

Tang, W. *et al.* (2008) 'Pannexins are new molecular candidates for assembling gap junctions in

the cochlea', *NeuroReport*. doi: 10.1097/WNR.0b013e32830891f5.

Taylor, W. R. and Vaney, D. I. (2002) 'Diverse synaptic mechanisms generate direction selectivity in the rabbit retina', *Journal of Neuroscience*. doi: 10.1523/jneurosci.22-17-07712.2002.

Thompson, R. F. and Spencer, W. A. (1966) 'Habituation: A model phenomenon for the study of neuronal substrates of behavior', *Psychological Review*. doi: 10.1037/h0022681.

Thoreson, W. B. and Witkovsky, P. (1999) 'Glutamate receptors and circuits in the vertebrate retina', *Progress in Retinal and Eye Research*. doi: 10.1016/S1350-9462(98)00031-7.

Tikidji-Hamburyan, A. *et al.* (2015) 'Retinal output changes qualitatively with every change in ambient illuminance', *Nature Neuroscience*. doi: 10.1038/nn.3891.

Timonina, K., Kotova, A. and Zoidl, G. (2020) 'Role of an aromatic–aromatic interaction in the assembly and trafficking of the zebrafish panx1a membrane channel', *Biomolecules*. doi: 10.3390/biom10020272.

Tischkau, S. A. *et al.* (2003) 'Ca2+/cAMP response element-binding protein (CREB)-dependent activation of Per1 is required for light-induced signaling in the suprachiasmatic nucleus circadian clock', *Journal of Biological Chemistry*. doi: 10.1074/jbc.M209241200.

Tosini, G. *et al.* (2008) 'The circadian clock system in the mammalian retina', *BioEssays*. doi: 10.1002/bies.20777.

Tosini, G. and Menaker, M. (1996) 'Circadian rhythms in cultured mammalian retina', *Science*. doi: 10.1126/science.272.5260.419.

Tosini, G. and Menaker, M. (1998) 'The clock in the mouse retina: Melatonin synthesis and photoreceptor degeneration', *Brain Research*. doi: 10.1016/S0006-8993(97)01446-7.

Trenholm, S. *et al.* (2014) 'Nonlinear dendritic integration of electrical and chemical synaptic inputs drives fine-scale correlations', *Nature Neuroscience*. doi: 10.1038/nn.3851.

Trümpler, J. *et al.* (2008) 'Rod and cone contributions to horizontal cell light responses in the mouse retina', *Journal of Neuroscience*. doi: 10.1523/JNEUROSCI.1564-08.2008.

Vaney, D. I. (1994) 'Territorial organization of direction-selective ganglion cells in rabbit retina', *Journal of Neuroscience*. doi: 10.1523/jneurosci.14-11-06301.1994.

VÄRINEN, L., LAURINEN, P. and ROVAMO, J. (1983) 'CONTRAST SENSITIVITY IN EVALUATION OF VISUAL IMPAIRMENT DUE TO MACULAR DEGENERATION AND OPTIC NERVE LESIONS', *Acta Ophthalmologica*. doi: 10.1111/j.1755-3768.1983.tb01409.x.

Velasquez, S. and Eugenin, E. A. (2014) 'Role of Pannexin-1 hemichannels and purinergic receptors in the pathogenesis of human diseases', *Frontiers in Physiology*. doi: 10.3389/fphys.2014.00096.

Vignet, C. *et al.* (2013) 'Systematic screening of behavioral responses in two zebrafish strains', *Zebrafish*. doi: 10.1089/zeb.2013.0871.

Vital, C. and Martins, E. P. (2011) 'Strain differences in zebrafish (Danio rerio) social roles and their impact on group task performance', *Journal of Comparative Psychology*. doi: 10.1037/a0023906.

Volkers, A. C. W. *et al.* (1987) 'Spatial contrast sensitivity and the diagnosis of amblyopia', *British Journal of Ophthalmology*. doi: 10.1136/bjo.71.1.58.

Vroman, R. *et al.* (2014) 'Extracellular ATP Hydrolysis Inhibits Synaptic Transmission by Increasing pH Buffering in the Synaptic Cleft', *PLoS Biology*. doi: 10.1371/journal.pbio.1001864.

Wandell, B. A. *et al.* (1999) 'Color signals in human motion-selective cortex', *Neuron*. doi: 10.1016/S0896-6273(00)81037-5.

Wang, J., Jackson, D. G. and Dahl, G. (2018) 'Cationic control of panx1 channel function', *American Journal of Physiology - Cell Physiology*. doi: 10.1152/ajpcell.00303.2017.

Wang, X. H. *et al.* (2009) 'Identification and characterization of pannexin expression in the mammalian cochlea', *Journal of Comparative Neurology*. doi: 10.1002/cne.21898.

Ward, M. E. *et al.* (2018) 'Reduced contrast sensitivity among older women is associated with increased risk of cognitive impairment', *Annals of Neurology*. doi: 10.1002/ana.25196.

Warren, E. J. *et al.* (2003) 'Intrinsic light responses of retinal ganglion cells projecting to the circadian system', *European Journal of Neuroscience*. doi: 10.1046/j.1460-9568.2003.02594.x.

Weickert, S. *et al.* (2005) 'Expression of neural connexins and pannexin1 in the hippocampus and inferior olive: A quantitative approach', *Molecular Brain Research*. doi: 10.1016/j.molbrainres.2004.09.026.

Weil, R. S. *et al.* (2016) 'Visual dysfunction in Parkinson's disease', *Brain*. doi: 10.1093/brain/aww175.

Weilinger, N. L. *et al.* (2016) 'Metabotropic NMDA receptor signaling couples Src family kinases to pannexin-1 during excitotoxicity', *Nature Neuroscience*. doi: 10.1038/nn.4236.

Whyte-Fagundes, P. and Zoidl, G. (2018) 'Mechanisms of pannexin1 channel gating and regulation', *Biochimica et Biophysica Acta - Biomembranes*. doi: 10.1016/j.bbamem.2017.07.009.

Wicki-Stordeur, L. E. *et al.* (2012) 'Pannexin 1 regulates postnatal neural stem and progenitor cell proliferation', *Neural Development*. doi: 10.1186/1749-8104-7-11.

Wicki-Stordeur, L. E. and Swayne, L. A. (2014) 'The emerging Pannexin 1 signalome: A new nexus revealed?', *Frontiers in Cellular Neuroscience*. doi: 10.3389/fncel.2013.00287.

Wildberger, H. (1984) 'Neuropathies of the optic nerve and visual evoked potentials with special reference to color vision and differential light threshold measured with the computer perimeter OCTOPUS', *Documenta Ophthalmologica*. doi: 10.1007/BF00165761.

Wolman, M. A. *et al.* (2011) 'Chemical modulation of memory formation in larval zebrafish', *Proceedings of the National Academy of Sciences of the United States of America*. doi: 10.1073/pnas.1107156108.

Wolman, M. A. *et al.* (2014) 'Modulation of cAMP and Ras Signaling Pathways Improves Distinct Behavioral Deficits in a Zebrafish Model of Neurofibromatosis Type 1', *Cell Reports*. doi: 10.1016/j.celrep.2014.07.054.

Wright, D. *et al.* (2006) 'QTL analysis of behavioral and morphological differentiation between wild and laboratory zebrafish (Danio rerio)', *Behavior Genetics*. doi: 10.1007/s10519-005-9029-4.

Wulff, K. *et al.* (2010) 'Sleep and circadian rhythm disruption in psychiatric and neurodegenerative disease', *Nature Reviews Neuroscience*. doi: 10.1038/nrn2868.

Xin, D. and Bloomfield, S. A. (1999) 'Dark- and light-induced changes in coupling between horizontal cells in mammalian retina', *Journal of Comparative Neurology*. doi: 10.1002/(SICI)1096-9861(19990301)405:1<75::AID-CNE6>3.0.CO;2-D.

Yao, X. *et al.* (2018) 'Gap Junctions Contribute to Differential Light Adaptation across Direction-Selective Retinal Ganglion Cells', *Neuron*. doi: 10.1016/j.neuron.2018.08.021.

Yegutkin, G. G. (2008) 'Nucleotide- and nucleoside-converting ectoenzymes: Important

modulators of purinergic signalling cascade', *Biochimica et Biophysica Acta - Molecular Cell Research*. doi: 10.1016/j.bbamcr.2008.01.024.

Yen, M. R. and Saier, M. H. (2007) 'Gap junctional proteins of animals: The innexin/pannexin superfamily', *Progress in Biophysics and Molecular Biology*. doi: 10.1016/j.pbiomolbio.2007.03.006.

Yeung, A. K., Patil, C. S. and Jackson, M. F. (2020) 'Pannexin-1 in the CNS: Emerging concepts in health and disease', *Journal of Neurochemistry*. doi: 10.1111/jnc.15004.

Zambusi A, N. J. (2020) 'Regeneration of the central nervous system-principles from brain regeneration in adult zebrafish.', *World journal of stem cells.*, Jan 26(12(1)), pp. 8–24. doi: 10.4252/wjsc.v12.i1.8.

Zappalà, A. *et al.* (2006) 'Expression of pannexin1 in the cns of adult mouse: Cellular localization and effect of 4-aminopyridine-induced seizures', *Neuroscience*. doi: 10.1016/j.neuroscience.2006.03.053.

Zhang, H., Chen, Y. and Zhang, C. (2012) 'Patterns of heterogeneous expression of pannexin 1 and pannexin 2 transcripts in the olfactory epithelium and olfactory bulb', *Journal of Molecular Histology*. doi: 10.1007/s10735-012-9443-x.

Zhang, J. (2003) 'Evolution by gene duplication: An update', *Trends in Ecology and Evolution*. doi: 10.1016/S0169-5347(03)00033-8.

Zhang, L. *et al.* (2008) 'Role for nitric oxide in permeability of hippocampal neuronal hemichannels during oxygen glucose deprivation', *Journal of Neuroscience Research*. doi: 10.1002/jnr.21675.

Zhang, M. *et al.* (2012) 'P2Y2 receptor activation opens pannexin-1 channels in rat carotid body type II cells: Potential role in amplifying the neurotransmitter ATP', *Journal of Physiology*. doi: 10.1113/jphysiol.2012.236265.

Zimmermann, H. (1992) '5'-Nucleotidase: Molecular structure and functional aspects', *Biochemical Journal*. doi: 10.1042/bj2850345.

Zoidl, G. *et al.* (2007) 'Localization of the pannexin1 protein at postsynaptic sites in the cerebral cortex and hippocampus', *Neuroscience*. doi: 10.1016/j.neuroscience.2007.01.061.

Zoidl, G. *et al.* (2008) 'Molecular diversity of connexin and pannexin genes in the retina of the zebrafish danio rerioc', *Cell Communication and Adhesion*. doi: 10.1080/15419060802014081.

APPENDICES

Appendix A: Egg water (used for raising young embryos).

Stock salts solution:

Instant Ocean Salt	40 grams
Distilled Water	1 Litre

Working salts solution:

Add 1.5 ml of stock salts solution to 1 litre of distilled water to reach to a final concentration of 60 μg/ml. Methylene blue (10-5%; Sigma Aldrich) was added as a mold inhibitor.